Lúcia Raquel Brandão

Polymeric catalytic membrane reactors: Application to propylene and propyne hydrogenations

Dissertation presented for the degree of
DOCTOR IN CHEMICAL ENGINEERING
by
PORTO UNIVERSITY

SUPERVISORS:
Adélio Miguel M. Mendes, PhD (DEQ-FEUP)
Luís Miguel P. Madeira, PhD (DEQ-FEUP)

Universidade do Porto
Faculdade de Engenharia
FEUP

LEPAE,
Chemical Engineering Department

August 2007

Acknowledgments

I am grateful to the Portuguese Foundation for Science and Technology (FCT) for the PhD grant, reference SFRH/BD/3383/2000.

Prof. Adélio Mendes and Prof. Miguel Madeira, my supervisors, are thanked for giving me the opportunity to carry out my doctoral studies at LEPAE; and for the careful revision and scientific contribution to this thesis.

Doctor Detlev Fritsch, from GKSS - Research Centre, Geesthacht-Germany, for his helpful discussions and support during my stays at GKSS.

I would like to acknowledge my lab doctoral colleagues: Doctor João Santos and Doctor Paulo Cruz for their support; Doctor José Sousa for his valuable suggestions and Eng. Pedro Taveira for the time-lag experimental set-up; Sarah and Rosa, which beyond their careful help during this big journey, are also acknowledged for their good friendship.

Also, to all the colleagues that in one way or another worked at same time with me in the lab, thank you for the good environment created.

The Chemical Engineering Department at FEUP and its staff, that kindly helped me when I requested, are also recognized. A special thanks to D. Fátima Faustino, Sr. Sousa Vale, MSc. Luís Carlos Matos, Sr. José Meireles, D. Rosa Ramos, Prof. Lúcia Santos and Prof. Fernão Magalhães.

Financial support from FCT, through the project POCTI/32452/EQU/2000, is also acknowledged.

Thanks to all my friends and family, especially Zé Luís, my husband, for his unconditional support in all aspects.

Preface

This thesis was carried out at LEPAE (Laboratório de Engenharia de Processos, Ambiente e Energia) in the Chemical Engineering Department of the Faculty of Engineering - University of Porto (FEUP) between 2001 and 2006, under the framework of the project POCTI/32452/EQU/ 2000. This work results from the compilation of different papers published or accepted for publication while the doctoral studies were performed.

Relevance and Motivation

This work has its infancy in 1995, with the publication of the synthesis of a catalytic membrane loaded with catalyst nanoparticles (J. Membr. Sci. 99 (1995) 29), where a dense polymeric membrane was used to occlude palladium nanoclusters. However, the exact potentialities of this new material were not clear and, therefore, modelling the performance of a continuous reactor using such dense polymeric catalytic membrane was seen as being very important for the understanding of these reactors.

Actually, it was this lack of knowledge that provided the need of the present work. There are very few studies covering the simulation of these specific type of reactors. Moreover, the experimental validation of the mathematical models describing a membrane reactor when using a dense polymeric catalytic membrane is not described in the open literature for gas phase reactions, at the best knowledge of the author. The present study aims then to overcome this gap.

Objective and Outline

The main objective of this thesis is to improve the knowledge regarding the catalytic membrane technology in which the membrane is a dense one. This thesis aims also to contribute for the experimental validation of the phenomenological model of a polymeric catalytic membrane

reactor (pCMR). The system chosen considers the hydrogenation of propylene to propane and of propyne to propylene and propane in a poly(dimethylsiloxane) (PDMS) membrane loaded with 5 wt. % of Pd-nanoclusters.

This work is organized in five parts. Part I considers a general introduction focused on the membrane reactor concept and describes the main features and potentialities of this technology. It is included a very short overview concerning the use of polymeric catalytic membrane reactors.

In Part II, the use of palladium nanoclusters as catalysts in propylene and propyne hydrogenations is considered. Apart from the fact that selective hydrogenations are the most important reactions studied on the gas phase membrane reactors, it is worthy to mention that propyne partial hydrogenation is an important reaction in the petrochemical industry. The kinetic parameters for propylene and propyne hydrogenations over palladium particles were obtained, in a batch reactor, using nanoclusters of this metal stabilized on a surfactant, which showed no mass transport resistances.

Part III is devoted to the study of mass transport across the polymeric membrane where PDMS was used to prepare the catalytic membranes. The time-lag and sorption methods were used to obtain the kinetic and equilibrium relevant parameters for characterizing the mass transport through PDMS membranes, filled or not with palladium nanoclusters.

Following, Part IV is focused on propylene and propyne hydrogenations, performed in the continuous pCMR, under different operating conditions. Part IV also provides the experimental validation for the developed model, where a comparison of the simulated values (based on the kinetic and mass transport data determined in the previous chapters) with the results obtained from the experimental pCMR is performed, for both hydrogenations.

Finally, in Part V the main conclusions are summarized and future work is proposed.

Contents

Figure captions

Table captions

Abstract

The present dissertation deals with the study of the propylene and propyne hydrogenation reactions in an isothermal polymeric catalytic membrane reactor (pCMR). A poly(dimethylsiloxane) (PDMS) dense membrane, embedding the palladium nanoclusters catalyst, was used.

The work starts with the determination of the reaction kinetics of propylene and propyne hydrogenations in a closed reactor and of the transport properties of these reactants and reaction products in the dense catalytic membrane. The research work ends with the study of both hydrogenations in an open pCMR. A mathematical model was developed for describing the pCMR which is compared critically with the experimental results. Such model is an important tool for understanding the catalytic membrane reactors operating with a dense membrane.

Thus, surfactant-stabilized palladium nanoclusters were first used to catalyze the propylene hydrogenation in a batch reactor at 308 K. The method of initial rates was employed to propose a reaction mechanism and a rate equation was derived. Although the method adopted did not exclude other reaction schemes, it was shown that a Langmuir-Hinshelwood (L-H) rate equation represents well the reaction data. The proposed mechanism involves competitive adsorption of the reagents, with dissociation of hydrogen on the catalyst surface, and where surface reaction is the limiting step.

The kinetics of propyne hydrogenation over surfactant-stabilized palladium nanoclusters was also studied in the same reactor and at the same temperature. The reaction mechanism proposed was also obtained using the method of initial rates. It was found that experimental rate data agree well with a L-H mechanism involving non-competitive adsorption between propyne

and hydrogen for the catalyst surface, where hydrogen addition in the surface reaction(s) is the limiting step. The reaction rate is also well fitted using a power-law equation. Apparent kinetic orders of -0.02 and 1.09 for propyne and hydrogen partial pressures, respectively, were obtained.

Concerning the mass transport characterization, two different methods were employed: the so-called sorption and time-lag methods. Sorption, diffusion and permeability coefficients of argon, hydrogen, propane, propylene and propyne were determined at 308 K for a plain PDMS membrane and for a composite one, filled with palladium nanoclusters (5 wt. %), both with ca. 300 μm thickness.

For steady-state permeation, the relevant transport parameters are the sorption and diffusion coefficients in the polymeric phase (which are not affected by the presence of the catalyst nanoclusters), the catalyst volume content and the tortuosity factor. The presence of the palladium nanoclusters modifies the mass transport mainly during the transient regime, not only due to tortuosity but also because the nanoclusters can act as adsorption wells (mainly in the case of hydrogen).

The polymeric catalytic membrane used was ca. 4-μm thick and also loaded with 5 wt. % nano-sized Pd clusters. Results indicated that higher hydrocarbon conversions are obtained for feed hydrogen/hydrocarbon molar ratios that assure nearly maximum reaction rate conditions at catalyst surface. Validation of the mathematical model developed was then performed, and for that the relevant kinetic and mass transport parameters concerning propyne and propylene hydrogenations were inserted in the phenomenological model of the pCMR and results compared with the experimental ones obtained at 308 K. However, it was concluded that the surfactant used to stabilize the nanoclusters during the batch experiments affects the reaction kinetics, mainly

hydrocarbons adsorption. For that reason, the parameters related with these reactants were obtained by fitting the pCMR experimental results.

Finally, it was concluded that the model proposed predicts quite well the experimental data regarding the flow rates and mixture compositions in both retentate and permeate chambers as well the general performance of the pCMR.

Sumário

Neste trabalho estudou-se a hidrogenação do propeno e do propino num reactor de membrana catalítica polimérica em condições isotérmicas. A membrana utilizada é de polidimetilsiloxano (PDMS) com nanopartículas de catalisador de paládio dispersas na fase polimérica.

O estudo começa com a determinação das cinéticas de hidrogenação do propeno e do propino em reactor fechado e com a determinação das propriedades de transporte dos reagentes e produtos de reacção na membrana catalítica. O trabalho termina com o estudo das reacções de hidrogenação num reactor aberto de membrana catalítica polimérica. Desenvolveu-se um modelo matemático do reactor de membrana que foi validado experimentalmente. Este modelo é uma ferramenta importante para uma melhor compreensão da operação de reactores de membrana catalítica polimérica densa.

Primeiramente utilizaram-se nanopartículas de paládio estabilizadas num tensioactivo para conduzir a hidrogenação do propeno em reactor fechado a 308 K, tendo-se usado o método das velocidades iniciais com o intuito de se obter o mecanismo da reacção e a respectiva equação de velocidades. Verificou-se que os dados experimentais obtidos são bem representados por uma equação de velocidades do tipo Langmuir-Hinshelwood (L-H), cujo mecanismo envolve a adsorção competitiva dos reagentes, com dissociação do hidrogénio na superfície do catalisador, onde o passo limitante é a reacção superficial.

Seguidamente, estudou-se a cinética de hidrogenação do propino, também em reactor fechado a 308 K, tendo-se utilizado as mesmas nanopartículas de paládio estabilizadas num tensioactivo. O mecanismo reaccional proposto foi também determinado utilizando o método das velocidades iniciais. Os dados experimentais são coerentes com um mecanismo do tipo L-H, o

qual envolve adsorção não-competitiva entre o propino e o hidrogénio à superfície do catalisador, onde a(s) reacção(ões) superficial(is) é(são) o passo limitante. A equação de velocidades mostrou ainda ser correctamente descrita por uma lei de potências, obtendo-se ordens de reacção aparentes de -0,02 e 1,09 para as pressões parciais do propino e hidrogénio, respectivamente.

Relativamente à caracterização do transporte de massa, adoptaram-se os métodos de sorção e de *time-lag*. Os coeficientes de sorção, difusão e permeabilidade do árgon, hidrogénio, propino, propeno e propano nas membranas de PDMS, com e sem nanopartículas de paládio (5 % m/m), foram então determinados a 308 K em membranas com cerca de 300 μm de espessura.

Em estado estacionário, os parâmetros de transporte de massa relevantes são os coeficientes de sorção e difusão no polímero (que não são afectados pela presença das nanopartículas de catalisador), a fracção volúmica de catalisador e a tortuosidade. A presença das nanopartículas de paládio modifica principalmente o transporte de massa durante o regime transiente, pois além de aumentarem a tortuosidade, podem actuar como um poderoso poço de adsorção (principalmente no caso do hidrogénio).

A membrana catalítica de PDMS utilizada no reactor de membrana tem uma espessura de cerca de 4 μm e uma fracção mássica de catalisador de 5 %. Os resultados dos ensaios efectuados indicam que são obtidas conversões mais elevadas de hidrocarboneto para razões molares de hidrogénio/hidrocarboneto na corrente de alimentação que assegurem velocidades de reacção próximas das velocidades máximas na superfície do catalisador. Efectuou-se então uma validação experimental do modelo matemático proposto para descrever o reactor de membrana catalítica polimérica densa. Deste modo, os parâmetros cinéticos e de transporte de massa relevantes para a hidrogenação do propeno e do propino foram inseridos no modelo matemático e os resultados da simulação comparados com os experimentais, obtidos a 308 K. Concluiu-se, no entanto, que o

tensioactivo utilizado para estabilizar as nanopartículas de paládio, durante os ensaios em reactor fechado, afecta a cinética da reacção, nomeadamente a adsorção dos hidrocarbonetos. Deste modo, os parâmetros relacionados com estes reagentes foram obtidos através de ajuste aos resultados experimentais do reactor contínuo de membrana catalítica polimérica.

Finalmente, concluiu-se que o modelo matemático proposto para o reactor contínuo de membrana prevê correctamente os resultados experimentais, nomeadamente os caudais e as composições das correntes gasosas nas câmaras do retido e permeado, bem como o desempenho geral do reactor contínuo de membrana catalítica polimérica densa.

Sommaire

Le présent travail se propose d'étudier l'utilisation d'un réacteur de membrane catalytique polymérique dans des conditions isothermes dans l'hydrogénation du propène et du propine. La membrane utilisée est constituée de poly(diméthylsiloxane) (PDMS) avec des nanoparticules de palladium dispersées dans la phase polymérique.

L'étude commence par la détermination des cinétiques de l'hydrogénation du propène et du propine dans un réacteur fermé ainsi que par la détermination des propriétés de transport des réactifs et des produits de réaction dans la membrane catalytique. Le travail termine sur l'étude des réactions de l'hydrogénation dans un réacteur ouvert de membrane catalytique polymérique. On a développé un modèle mathématique du réacteur de membrane qui a été validé expérimentalement. Le modèle est un élément important pour une meilleure compréhension de l'opération de réacteurs de membrane catalytique polymérique dense.

On a utilisé des nanoparticules de palladium stabilisées avec un agent tensioactif pour conduire l'hydrogénation du propène en réacteur fermé à 308 K. On a utilisé la méthode des vitesses initiales avec l'intention d'établir le mécanisme de la réaction et l´équation respective des vitesses. Les données expérimentales obtenues sont bien représentées par une équation des vitesses du type Langmuir-Hinshelwood (L-H). Le mécanisme proposé englobe l'adsorption compétitive des réactifs avec dissociation de l'hydrogène à la surface du catalyseur où l'étape limitative est la réaction superficielle.

Ensuite, on a étudié la cinétique de hydrogénation du propine également en réacteur fermé à 308 K, en utilisant les mêmes nanoparticules de palladium stabilisées pour un agent tensioactif. Le mécanisme réactionnel proposé a été aussi déterminé par l'utilisation de la méthode des

vitesses initiales. Les données expérimentales correspondent au mécanisme de type L-H lequel développe une adsorption non-compétitive entre le propine et l'hydrogène à la surface du catalyseur où la réaction superficielle est l'étape limitative. L'équation des vitesses a démontré encore qu'elle était correctement décrite par une loi de puissances, on obtient ainsi des ordres de réaction évidents de -0,02 et 1,09 pour les pressions partielles du propine et de l'hydrogène respectivement.

Relativement à la caractérisation du transport de masse, on a adopté des méthodes de sorption et de *time-lag*. Les coefficients de sorption, diffusion et perméabilité de l'argon, de l'hydrogène, du propine, du propène et du propane dans les membranes de PDMS, avec et sans nanoparticules de palladium (5 % m/m), ont été fixés à 308 K sur des membranes de 300 μm à peu près.

Pour une pénétration à l'état stationnaire, les paramètres de transport importants sont: les coefficients de sorption et de diffusion dans le polymère (qui ne sont pas affectés par la présence des nanoparticules de catalyseur), la fraction volumique de catalyseur et la tortuosité. La présence de nanoparticules de palladium modifie, en particulier, le transport de masse pendant le régime non-stationnaire car non seulement ils augmentent la tortuosité comme ils agissent comme un adsorbant puissant (principalement dans le cas de l'hydrogène).

La membrane catalytique de PDMS utilisée dans le réacteur de membrane a une épaisseur de 4 μm et une fraction de masse de catalyseur de 5 %. Les résultats des essais réalisés indiquent que des conversions plus élevées d'hydrocarbure sont liées de l'hydrogène/hydrocarbure dans le courant d'alimentation qui garantit des vitesses de réactions maximales à la surface du catalyseur. Ainsi, la validité expérimentale du modèle mathématique alors développé pour décrire le réacteur de membrane catalytique polymère a été effectuée. Les paramètres cinétiques et de transport

d'importance pour l'hydrogénation du propène et du propine ont été insérés dans le modèle mathématique développé, et les résultats comparés aux donnés expérimentales obtenues à 308 K. On en a conclu, néanmoins, que l'agent tensioactif utilisé pour stabiliser les nanoparticules de palladium, pendant les essais en réacteur fermé, affecte la cinétique de la réaction, notamment dans l'adsorption des hydrocarbures. De cette façon, les paramètres qui sont en relation avec ces réactifs ont été obtenus au moyen d'un ajustement des résultats expérimentaux du réacteur de membrane catalytique polymérique.

Enfin, on a conclu que le modèle mathématique proposé pour le réacteur de membrane prévoit avec exactitude les compositions des mélanges gazeux dans les chambres de retenu et perméat, ainsi que la performance générale du réacteur de membrane catalytique polymérique dense.

Part I

1. Introduction

1.1 Membrane reactors

The study of catalytic membrane reactors is a multidisciplinary activity, which in recent years has attracted the attention of scientists in a number of disciplines, including materials science, chemistry and chemical engineering. Membrane-based reactive separation processes, which seek to combine two distinct functions, i.e. reaction and separation, have been a concept used since the early stages of the membrane field itself, but have only attracted substantial technical interest the last decade or so [1]. Although some small industrial units already exist, the concept has yet to find larger scale applications where the more important obstacles for further commercial development of membrane reactors are the membrane themselves, which still need to undergo optimization [1]. The membranes used in the membrane reactors can be very distinct with regard to their nature. They can be inert or catalytically active, dense or porous and can be made from polymers, metals, carbon, glass or ceramics. They can also be uniform in composition or be composite, with homogeneous or asymmetric porous structure.

The potentialities of membrane reactors reside in the fact that membranes, when coupled with reactors, can bring some advantages according to the scale at which they work, and this feature can be divided into three main groups [2]. The first group is at the process level (a), where the main advantage comes from the decreasing number of process units. The integration of a separation function into the reactor is particularly attractive if a reduction in investment and an increase in the economical viability are obtained by such compact process plant. Moreover, an improved efficiency would save energy costs and raw materials. However, the reaction

conditions should be compatible with the ones for the membrane separation in order to obtain a synergic coupling of these two functions.

At the reactor level (b), the ability of a membrane to transport material in a reactor can be explored to improve the efficiency of the combined process. One approach is to use the membrane to remove selectively a product from the reactor which resulted from an equilibrium-restricted reaction, in order to gain yield relatively to conventional reactors. Such membrane reactor can be called extractor [3, 4] and is represented in Fig. 1.1A. Another feature is the possibility to implement dosing concepts, such as distributed feeding of one reactant along the reactor, through a controlled permeation across the membrane. This type of membrane reactor can be called distributor [3, 4] (Fig. 1.1B), and one of the immediate benefits with this strategy is the establishment of uniform concentrations of the dosed species along the reactor, resulting in a higher selectivity and/or in an improved safety of the process. Also, the membrane can be used to set the reaction zone, with an active material incorporated into the membrane. This type of membrane reactor is called contactor [3, 4] (Fig. 1.1C). The incorporation of the active material can be done uniformly throughout all the membrane thickness or only in a certain region, as, for example, in a surface layer. With such a membrane reactor, the reactant streams can be passed along the different sides of the membrane and transported by diffusion to the catalytic zone (interfacial contactor), or the reactive mixture could be forced to flow through the active membrane (flow-through contactor). In this type of configuration, a porous membrane with a solid active material impregnated in its pore walls can be used, or the porous structure of a membrane can be filled with a liquid holding a dissolved homogeneous catalyst, or even a dense polymeric catalytic membrane can promote the reaction between reactants from immiscible phases (organic and aqueous, for example). In any case, it is possible to favour the contact

between the catalyst and the reactant in comparison with conventional reactors (e.g. gas in gas–liquid–solid processes, hydrophobic reactant with hydrophilic catalyst, etc.).

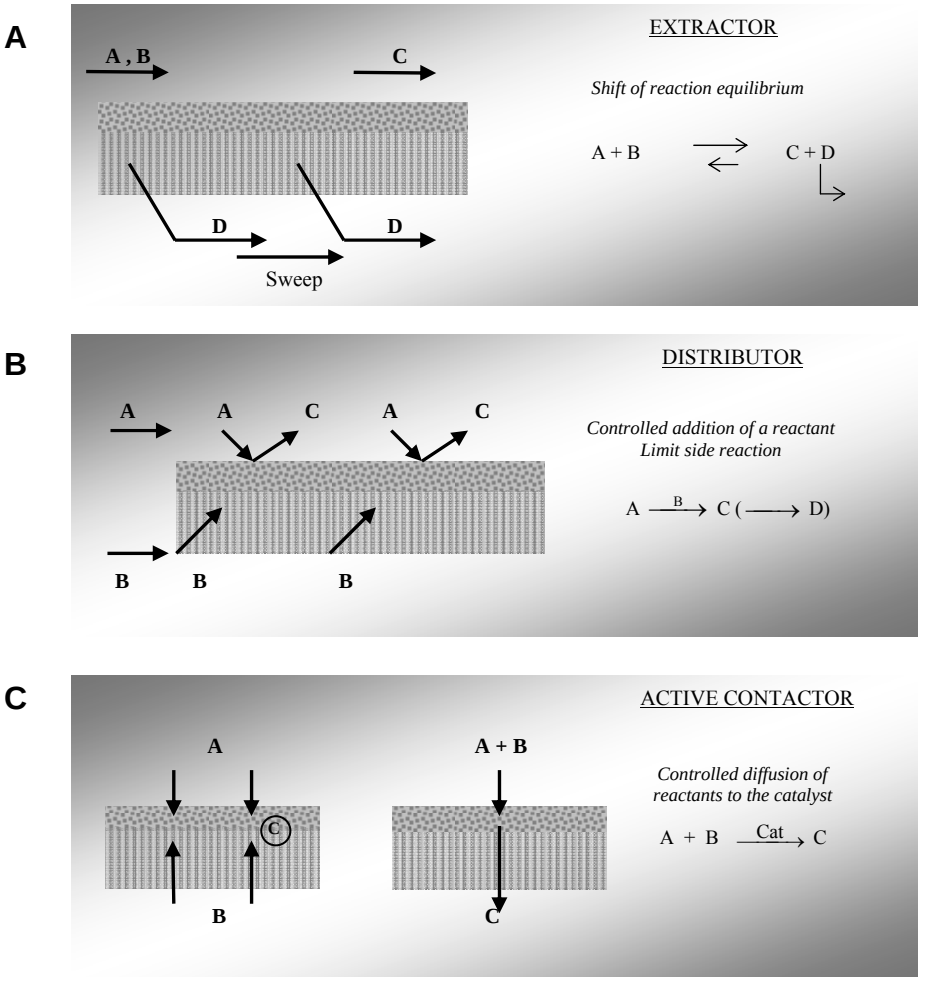

Fig. 1.1 The tree main membrane functions, at the reactor level, in a membrane reactor (adapted from [3].

Finally, at the catalyst level (c), the membrane may supply one of the reactants in a special form that is more active or selective for the reaction than in its molecular form. An example is the ceramic oxide ion conducting membranes, which can supply the reactant oxygen to a reaction

medium in the form of oxide ions, much more reactive than molecular oxygen from the reactant gas phase. Other examples include silver and palladium-based membranes (Pd or its alloys), which selectively permeate atomic oxygen and hydrogen, respectively. Polymeric proton exchange membranes, known from low temperature fuel cells, represent another class of membranes that could be used for such purposes.

1.1.1 Considerations on polymeric membranes

A great variety of polymeric membranes is available to select properly the most appropriate one to use in membrane-based reactor processes [5]. In fact, polymeric membranes showing versatile diffusivities and sorption capacities [6] have found a wide range of industrial applications in gas separations.

Dense polymeric membranes can be based on rubbery or glassy polymers. Rubbery polymers usually have high permeabilities towards vapours and gases, but relatively low selectivities, while glassy polymers have high selectivities but lower permeabilities. Apart from that, usually only the rubbery polymers are used to incorporate catalysts because stresses may occur in the less flexible glassy chains, which may result in cracks. Dense polymeric membranes can additionally take part in an active manner in the reaction because the diffusivity of reagents and products are very important parameters; if the products are quickly drained from the reaction medium the reaction progresses till a higher extension (for equilibrium-limited reactions) and more selectively (for consecutive reactions).

Porous catalytic membranes can also be used in polymeric membrane reactors but the choice of the polymer is of less importance as permeation does not take place through the polymer matrix [5]. The only impact of the membrane polymer is on the stability and surface

properties, such as wettability and fouling. Depending on the pore and molecule size, molecules are transported through porous membranes via viscous flow, knudsen diffusion, molecular diffusion, surface diffusion or capillary condensation [5].

Polymeric membranes used in membrane reactors can have some advantages over the expensive inorganic membranes, namely lower production costs, crack-free thin membranes and large scale production [7]. As a matter of fact, some polymer membrane-based reactors have been blessed with some commercial success, mainly in the biotechnological area [8, 9].

Nowadays, polymeric membrane reactors are mostly used in processes where most of the reactions occur under mild chemical conditions and at moderate temperatures (room temperature up to 150 ºC), because polymeric membranes show low resistance to high temperatures, aggressive solvents or oxidative conditions [5]. But these limitations are relative: Nafion® and poly(dimethylsiloxane) (PDMS), the two most widely used catalytic polymeric membranes [7, 8], proved to remain stable even under rather harsh conditions, showing an excellent thermal, mechanical and chemical resistance [5]. Moreover, PDMS is cheap, easy to prepare and its flexible chains provide a fast mass transfer across the membrane, which is important to allow that neither the supply of reagents nor the removal of the products become reaction rate limiting [5].

1.1.2 Polymeric membrane reactors applications

In the following, some examples of applications as well as modelling on polymeric membrane reactors are briefly referred. Out of this scope stay the biological, the pervaporation and the fuel cell processes.

Excellent reviews on polymeric membrane reactors have been reported recently [1, 2]. The brief discussion presented here is an extract of some of the important discussions presented in

these works; in addition, some more recent polymeric membrane reactors applications as well as modelling are also referred. These applications (divided according to the type of reaction studied) occur in gas phase or in liquid/gas or liquid/liquid systems, using dense or porous polymeric membranes.

1.1.2.1 Hydrogenation and dehydrogenation reactions

Mostly hydrogenation reactions are discussed in this review and Table 1.1 summarizes the works that are referred in this text for this type of reactions. Such reactions have been largely studied, particularly the partial hydrogenation of multiple-unsaturated hydrocarbons and the hydrogenation of contaminants in water. The first case is an important process in the petrochemical industry while the presence of contaminants in water has become a serious problem nowadays.

The hydrogenation of cyclopentadiene was studied over poly(phenylene oxide) (PPO) and polysulfone (PSF) membranes incorporating transition metal catalysts where the membrane function was only to support the catalyst [10] (Table 1.1). In addition, they also studied the selective hydrogenation of cyclopentadiene, isoprene or butadiene using polymer-anchored Pd catalysts deposited on the inner wall of hollow fibres made from different polymers (Table 1.1) that were inserted in a membrane reactor of a conctactor type. Table 1.2 shows some of the results obtained for the selective hydrogenation of cyclopentadiene in the catalytic hollow fibres reactor [11]. From both sets of studies, they concluded that most of these catalytic polymeric materials are considerably active for the studied hydrogenation reactions, though with different extensions. Moreover, the hollow fibre support and the polymer-anchored palladium complex also strongly influence the hydrogenation performance of these catalytic hollow fibres.

Table 1.1 Some studied hydrogenation reactions using polymeric catalytic membranes.

Hydrogenated reagent	Catalyst	Support	Phases	Operation mode	Ref.
Cyclopentadiene	Pd, Co, Cu, Ni	Poly(phenylene oxide) (PPO) and polysulfone (PSF)	Liquid/gas	Batch reactor, 40 °C	[10]
Cyclopentadiene, isoprene, butadiene	Pd	Polyvinylpyrrolidone (PVP), ethyl-cellulose (EC), melamine -formaldehyde (AR)	Gas	Membrane contactor, 40 ºC	[11]
Propadiene and propyne	Pd	Polyvinylpyrrolidone (PVP)	Gas	Membrane contactor, 40 ºC	[12]
Butadiene	Pd	Polyvinylpyrrolidone (PVP), ethyl-cellulose (EC), melamine-formaldehyde (AR)	Gas	Membrane contactor, 40 ºC	[13]
Cyclopentadiene	Pd-Co, Pd	Polyvinylpyrrolidone (PVP), ethyl-cellulose (EC), melamine-formaldehyde (AR)	Gas	Membrane contactor, 40 ºC	[14]
Ethylene, propylene and 1,3-butadiene	Pd	Diblock copolymers	Gas	Batch reactor, room temperature or 120 ºC	[15, 16]
Propylene	Pd	Poly(dimethylsiloxane) (PDMS)	Gas	Membrane contactor, 30 ºC	[17]
Propylene and propyne	Pd	Polyamideimide (PAI)	Gas	Membrane contactor, 30 ºC	[18]
Nitrate	Pd-Cu	Polyetherimide (PEI)	Liquid	Membrane contactor	[19]
Nitrate	Pd-Cu	Polyamide	Liquid	Membrane contactor, 25 ºC	[20]
Chlorobenzene	Pd	Poly(dimethylsiloxane) (PDMS)	Liquid/gas	Membrane contactor, 21 ºC	[21]
Oxygen	Pd	Polypropylene (PP)	Liquid/gas	Membrane contactor, room temperature	[22]
Oxygen	Pd, Pt	Poly(vinylidene fluoride) (PVDF)	Liquid/gas	Membrane contactor, room temperature	[23]

Table 1.2 Selective hydrogenation of cyclopentadiene in different catalytic hollow fibres reactors (40 ºC) (adapted from [11]).

Reactor	Supported Pd complex	Original fibre	Pd content / mg	TOF* / $mol_{H_2} mol_{Pd}^{-1} min^{-1}$	Conversion / %	Selectivity / %
CMR-1	PVP-Pd	CA	1.13	5.9	91.0	91.0
CMR-2	PVP-Pd	PSF	4.63	1.0	68.7	96.4
CMR-3	PVP-Pd	PAN	5.27	1.3	99.0	93.4
CMR-4	EC-Pd	CA	1.46	3.3	60.0	78.0
CMR-5	AR-Pd	CA	1.19	0.9	13.2	78.3

* Turnover frequency
Polyvinylpyrrolidone (PVP); ethyl-cellulose (EC); melamine-formaldehyde (AR); cellulose acetate (CA); polysulfone (PSF); polyacrylonitrile (PAN).

Following, the selective hydrogenation of propadiene and propyne in propene was performed in a membrane reactor using catalytic membranes made of PVP-Pd/CA [12] (Table 1.1). The contents of propadiene and propyne reduced from 1.2 % and 1.3 % (wt. %) to less than 10 and 5 ppm, respectively, and a high selectivity in the conversion of such components to propene (97.8 %) showed that this membrane reactor was very effective to conduct these reactions, provided the appropriated hollow fibres and operation conditions. The same group [13] also studied the selective hydrogenation of butadiene to 1-butene, by impregnating PVP-Pd, EC-Pd and AR-Pd on the inner wall of CA or PSF hollow fibres (Table 1.1). The authors found that all the membrane reactors were active for the selective hydrogenations, though with a strongly dependent efficiency on both the hollow fibre support and the polymer-anchored monometallic palladium complex.

The selective hydrogenation of cyclopentadiene to cyclopentene was yet reported by the same authors [14] but, this time, mono- (Pd) and bimetallic (Pd-Co) catalysts anchored in a polymer (PVP, EC and AR) were impregnated on the inner wall of the CA hollow fibres (Table 1.1). Two different reducing solutions were considered ($NaBH_4$ and NH_2NH_2). Table 1.3 presents the comparison of the mono and bimetallic membrane reactor's performances. A significant synergetic effect of palladium and cobalt reduced by $NaBH_4$ is observed. The authors also found that both mono- and bimetallic palladium catalytic membrane reactors were active for the selective hydrogenation, though with a strongly dependent efficiency on both the polymer-anchored palladium complex and the reducing agent.

Table 1.3 Selective hydrogenation of cyclopentadiene with different mono- and bimetallic catalytic hollow fibre reactors (40 ºC) (adapted from [14]).

Reactor	Catalytic fibres	Reducing agent	Pd content / mg	Conversion / %	Selectivity / %
R-1	PVP-Pd/CA	NH_2NH_2	1.13	91.0	91.0
R-2	PVP-Pd/CA	$NaBH_4$	1.15	92.7	93.4
R-7	PVP-Pd-0.5Co$(OAc)_2$/CA	NH_2NH_2	1.19	91.4	91.2
R-8	PVP-Pd-0.5Co$(OAc)_2$/CA	$NaBH_4$	1.10	97.5	98.4

The hydrogenations of ethylene [15], propylene [15] and 1,3-butadiene [16] using palladium nanoclusters within diblock copolymers, with a palladium content of 14 wt. %, were tested by Ciebien et al. (Table 1.1). The catalysts exhibited good selectivities for butenes over butane, at high temperatures and low partial pressures of hydrogen [16], but the activity was a complex function of the sorption and diffusion coefficients of the reactants in the polymeric

phase, sorption of reactants on the palladium clusters surface, molecular size of reactants, size of clusters and temperature. Moreover, the polymer was able to stabilize the clusters against large aggregation, but could not prevent some increase in cluster size [15, 16].

The catalytic activity of a dense PDMS membrane loaded with Pd nanoclusters (0-15 wt. % metal content) was studied by Theis et al. [17]. They selected the hydrogenation of propylene to propane as a test reaction, and the experiments were conducted in a membrane reactor operating in a flow-through contactor mode (Table 1.1). Atmospheric pressure in the retentate side and variable permeate pressures (up to 500 mbar) were tested. It is noteworthy that a 99 % molar fraction of propane in the permeate chamber was reached once provided the right combination of catalytic membrane, feed flow rate and permeate pressure. The same reaction was studied by these authors but using an ultra filtration porous membrane made of PAI loaded with Pd nanoclusters [18] (Table 1.1). The membrane surface was impregnated with an inorganic TiO_2 layer (up to 40 wt. %), and further activated by dispersing the nanosized Pd clusters. This way, the palladium catalyst was decoupled from the polymeric surface, contributing to increase the overall stability of the membranes which proved to be stable up to temperatures of 200 °C and for operation times up to 50 h. The experiments were conducted in a flow-through contactor (Table 1.1) with atmospheric pressure at the retentate side and 100 mbar at the permeate side. High conversions of propylene (up to 98.5 %) in the permeate chamber and high permeate fluxes were achieved. The same work [18] reports the selective hydrogenation of a stream containing 5 % of propyne in propylene using the same membranes, where a maximum selectivity of 99 % to propylene, based in the permeate composition, was achieved, with very low amounts of propyne present in the permeate chamber.

Regarding water contaminants, the presence of nitrates in drinking water is a serious problem because they are linked to a number of health hazards. The reduction of nitrate to nitrogen in aqueous solutions was studied by Ludtke et al. [19] using microporous PEI membranes incorporating bimetallic microsized clusters (4.45 wt. % Pd and 0.95 wt. % Co) coated on aluminium oxide (Table 1.1). The experiments were carried out in a hollow fibre membrane reactor and the effect of some reaction conditions was studied, namely pH and temperature. Ilinich et al. [20] also studied the same hydrogenation using mono- and bimetallic nanosized clusters of Pd and Co deposited on the macroporous structure of flat polyamide membranes (Table 1.1). The experiments were carried out in a flow-through contactor with forced flow and the main goal of the authors was to explain why the coupling of the Pd and Co catalysts, in the same membrane, gave rise to a multifold increase in the catalytic activity of aqueous nitrate ions reduction by hydrogen, comparatively to the values obtained with each of the catalysts individually impregnated in similar membranes.

Beyond water-contaminants such as nitrates, halogenated hydrocarbons are also important to eliminate, mainly in the ground water near some industrial areas. Fritsch et al. [21] selected the hydrodechlorination of chlorobenzene to test thin PDMS layers loaded with nanosized Pd clusters and supported on porous poly(acrylonitrile) (PAN). They used an interfacial flat membrane contactor (Table 1.1) where a hydrogen pressure of 1 bar was applied, together with recycling of the liquid phase. In this configuration, the catalyst was protected from the direct access of the aqueous phase (but allowing the permeation of the organic reactants) and also protected against poisoning by water ingredients (such as heavy metals and sulphur compounds other than sulphate). Moreover, the hydrophobic PDMS shows an excellent permeability towards

hydrogen. Besides, in such arrangement, the hydrogen supply from the gas phase to the catalyst through the membrane is not limited by its low solubility in water.

Still regarding water treatment, in certain ultra-pure water applications the dissolved oxygen is one of the major drawbacks and its catalytic reduction with hydrogen can be an attractive method. For that, Petrova et al. [22] developed an interfacial membrane contactor using a porous polypropylene (PP) hollow fibre with palladium placed in the external membrane surface (Table 1.1). The water circulated on the shell side and the hydrogen was fed to the bore. The measurements performed showed that the membranes kept the hydrophobicity and porosity of the original polymer in the internal pore system, indicating that such catalytic membranes were effective for the reduction of the dissolved oxygen content in the water. The hydrogenation of dissolved oxygen in water was also studied by Kim and Lee [23] using Pd- or Pt- doped porous PVDF membranes. The oxygen reduction was conducted in an interfacial flat membrane contactor with hydrogen introduced in the down-stream, while water saturated with dissolved oxygen was fed into up-stream. In such study, the influences of the doped catalysts and various operating conditions were tested. They concluded that the Pd-doped PVDF membranes showed higher dissolved oxygen removal efficiency than the counterparts doped with Pt. It was also found that such removal efficiency depends on the doped catalyst content and on the H_2 flow rate.

Regarding dehydrogenation reactions (namely of alkanes and ethylbenzene, for example), these are of great industrial importance because the respective products represent basic petrochemical building blocks for the manufacture of plastics, synthetic rubbers, etc. Also, cyclohexane has been considered as a chemical source of hydrogen (chemical hydride) [24], and

consequently its dehydrogenation to benzene has a potential significance for hydrogen storage and renewable energy applications [25].

High temperatures are usually necessary for conducting the dehydrogenation reactions, and because of that polymeric membrane reactors have been used only in some rare applications. For instance, Rezac et al. [26] described a membrane-assisted dehydrogenation process for n-butane. Such configuration consisted of two plug-flow reactors in series separated by a polyimide-ceramic composite membrane to remove hydrogen. Higher conversion enhancements, over the thermodynamic equilibrium value, were achieved at an operating temperature of 180 ºC. The overall process showed very low losses of butane in the permeate side and still keeping the selectivity to n-butene at the same level as in the non-membrane system. In the same topic, the dehydrogenation of cyclohexane to benzene was studied by Frisch et al. [27] using dense membranes prepared by blending polyethylacrylate with a 13X zeolite, which contained the dehydrogenation catalyst (Ti or Ni). Such study indicated that these catalytic membranes were active for that dehydrogenation at low temperatures (50 – 87 ºC).

1.1.2.2 Oxidation reactions

Polymeric catalytic membrane reactors have been also used to carry out oxidation reactions, mainly in the fine chemical synthesis, where mild conditions are usually used. In this case, a dense membrane can be applied to keep two immiscible reagent phases (organic and aqueous, mainly peroxide solutions) separated, eliminating the need of a solvent that complicates the separation of the products and also eliminates the need for the solid catalyst separation. The most used polymer for conducting oxidation reactions in membrane reactors has been the hydrophobic PDMS, which excludes excessive amounts of polar substances near to the active sites. This is

very important to minimize the peroxide decomposition, especially in the case of substrates with low reactivity, where the oxidant strongly competes for reaction sites.

The cyclohexane oxidation with the oxidant *t*-butylhydroperoxide, performed in an interfacial contactor at room temperature, was studied by Vankelecom and co-workers [28]. A PDMS membrane occluding the zeozyme FePcY (iron-phthalocyanine complex encapsulated in the cages of a zeolite Y, a mimic of the enzyme cytochrome P-450) was used. The same reaction was later investigated further, using a similar polymeric catalytic membrane reactor [29, 30]. A general increase in the catalytic activity was observed for cyclohexane oxidation as compared with non-embedded FePcY-zeolite system, which used acetone as solvent to homogenise the reaction mixture. In this case, acetone and water, from the peroxide solution, were adsorbed preferentially in the rather polar catalyst. As a consequence, the reagents, being more hydrophobic, were excluded from the catalyst. This way, the hydrophobic environment created by the PDMS matrix, after the catalyst occlusion, besides eliminating the presence of the solvent also excluded the water molecules, present in the peroxide phase, from the hydrophilic catalyst and a 6-fold increase in activity was observed.

The oxygenation of organic compounds such as hexane and the epoxidation of propylene with dilute (30 wt. %) aqueous hydrogen peroxide solution was studied by Kaliaguine and co-workers [31]. A liquid-liquid or gas-liquid catalytic interfacial contactor was patented, using a zeolite (titanium silicalite, TS-1) occluded in a polymeric matrix of pure or silane-modified PDMS. They observed no loss of activity for the oxygenation of hexane, compared with conventional bubble-slurry reactors, indicating that the membrane does not impose a rate limiting mass transfer of the reactants. In the case of the propylene epoxidation, repression of the secondary reactions was obtained. The propylene epoxidation was also studied by Carnevale et

al. [32] using Au-doped PDMS membranes coated on the inner side of a tubular alumina support. They used a H_2-O_2 mixture which is catalyzed by the noble metal to the in-situ formation of hydroperoxidic species and where subsequently the vapour phase propylene epoxidation occurs. They tested this reaction in a membrane reactor at 25 ºC or 80 ºC, in order to determine membrane performance in the selective oxidation of propylene. It was found that the hydrophobic PDMS selectivity removes propylene oxide from the reaction medium, but a compromise should be sought between a reasonably high reaction rate (high temperature) and a selective separation of propylene oxide from the reaction medium (low temperature).

The limonene oxidation over cobalt acetylacetonate encapsulated in the cages of zeolite Y and dispersed in a PDMS matrix was studied by Oliveira et al. [33], as limonene oxide is a raw material used in a variety of products such as pharmaceuticals, perfumes and food additives. The oxidation reaction was carried out in a liquid phase batch reactor at 60 ºC using t-butylhydroperoxide as oxygen supplier, with a mixture of acetone and t-butanol as solvent. A comparison between the results obtained for the Y zeolite encaged cobalt acetylacetonate in the presence or not of the PDMS matrix was performed. Results indicated that, when using the non embedded catalyst, a polymer resulting from the epoxide polymerization was the main product of the reaction, while with the catalyst embedded in the PDMS matrix, the main reaction product was limonene oxide and no polymer formation was observed.

A particular type of oxidations are the photocatalytic reactions, where the use of oxidizing agents (hydrogen peroxide, ozone, or molecular oxygen itself) in the presence of ultraviolet radiation (UV), and a catalyst, have led to a particular type of advanced oxidation processes. This new oxidation method has been proposed as a viable alternative for the decontamination of either waste water or drinking water for human use, namely for the degradation of the different toxic

organic compounds, particularly chlorinated ones. For such process, finely divided catalysts can be either dispersed in an irradiated aqueous solution as slurry or anchored to a suitable support or even impregnated in a polymer. In this last case, a UV transparent membrane matrix with a good permeability for the organic compounds is required [34].

For that, Bellobono and co-workers produced photocatalytic membranes by photopolymerization and photocrosslinking of a blend containing acrylic monomers, a photoinitiator and the photocatalyst (mostly 30 wt. % TiO_2), photografted onto both sides of a perforated polyester support [35, 36]. They studied the photomineralization (breakdown to carbon dioxide, water and hydrochloric acid, in the case of halogenated compounds) of organic pollutants in potable waters and waste waters treatment, namely chloroaliphatics [35, 37], phenols [38], chlorophenols [39, 40], n-alkanoic acids [41] and triazines (pesticides and herbicides) [35, 40]. The authors have also studied the photomineralization as a method to induce integral biodegradability in non-biodegradable and toxic wastes [35], namely: non-biodegradable surfactants; phenolic components; organic solvents and paint components from wood and metal finishing; lubricating fluids and refinery effluents. Complete mineralization of chloro-hydrocarbons can be carried out satisfactorily, also in conditions of oxygen deficiency, if suitable promoting photocatalysts (synergistic mixture of trialkyl vanadates) are co-immobilized with TiO_2 into the membrane.

In addition, the photooxidation of organic pollutants in water with oxygen was carried out using novel membranes made of PVDF incorporating phosphotungstic acid $H_3PW_{12}O_{40}$ (W12) [42]. These photocatalytic membranes gave good proof of their possible recycling with no loss of activity. Further research work will be focused on better understanding the membrane based structure-reactivity trend in order to improve the potential of the method.

Ingested pharmaceuticals, used for medical and veterinary purpose, are usually excreted in wastewaters because they are not completely metabolized. Actually, monitoring of residual drugs in the effluents of sewage treatment plants and in surface waters indicated concentrations values up to several mg L^{-1}, as it is often difficult to (bio)degrade or to remove those compounds using conventional treatments. This way, the study of the photooxidation of different pharmaceuticals with oxygen in ultra pure water by using a hybrid photocatalytic membrane reactor was performed recently [43]. Polycrystalline TiO_2 was used as photocatalyst and different types of commercial polymeric nanofiltration membranes were tested. The membrane photoreactor worked in continuous and total recirculation regimes, and with such process both the photocatalyst and the pollutant were retained by the membrane. Different operative conditions such as pH, initial concentration of pollutant, pressure and permeate flow rate were tested, but further investigations are still on progress.

1.1.2.3 Other types of reactions

Polymeric catalytic membrane reactors have also been used for conducting other types of reactions. For instance, the conversion of fuels into hydrogen for fuel cells has widely attracted interest in the chemical and petrochemical industries. However, the carbon monoxide produced (for example through steam-reforming processes) has a detrimental effect over the fuel cell performance, because it poisons the Pt catalyst. This way, the reaction of the produced carbon monoxide and water to generate more hydrogen and also carbon dioxide has a considerable interest and has been undertaken in the so-called Water Gas Shift (WGS) reaction. As the WGS reaction is an equilibrium-limited reaction, high concentrations of unconverted CO in the H_2 product stream are usually obtained. Notwithstanding, this exothermic reaction can be enhanced

significantly if a CO_2-selective and/or H_2-selective membrane removes the reaction products, CO_2 and/or H_2, leading to high conversions even at lower temperatures. A WGS membrane reactor has been developed using a novel CO_2-selective polymeric membrane with high CO_2 permeabilities and high CO_2/H_2 and CO_2/CO selectivities [44]. This CO_2-selective membrane was obtained by incorporating amino groups in the polymeric network of the membrane and this type of polymeric membrane reactor can produce a H_2 rich product stream with less than 10 ppm of CO at 150 °C.

Alternative diesel fuels are usually prepared by transesterification of vegetable oils with methanol in the presence of strong acids. Membranes with acidic character can also be used to catalyse such reactions, and due to environmental reasons such heterogeneous catalysts are a desirable goal. Vital and co-workers compared the performance of the acidic character of a Nafion membrane in the transesterification of soybean oil with a poly(vinyl alcohol) (PVA) membrane containing sulfonic acid groups [45]. They observed a ten fold increase in the catalytic activity of PVA membranes despite the number of acid sites increases only four times, suggesting that membrane hydrophilicity may play an important role in the process.

1.1.3 Modelling

Most of the works found on modelling of membrane reactors refer to modelling and simulation of catalytic membrane reactors with inorganic membranes [46]. Very few reports dealing with modelling polymeric membrane reactors were published, with most of them considering liquid-phase systems. Next are referred some modelling works using polymeric catalytic membranes.

A simple diffusion-reaction model to calculate the reaction rate constant and its activation energy for the dehydrogenation of cyclohexane to benzene was reported by Frisch et al. [27]. The

experiments were carried out in a dense membrane reactor with the membrane supporting zeolite 13X loaded with Ti or Ni. The diffusion coefficients of the reactants in the membranes were determined using the time-lag method by preparing control membranes containing zeolite 13X, but without catalyst. The calculated values indicated a surface-diffusion control of the process if assumed a pseudo first-order reaction relatively to cyclohexane.

Modelling of a membrane reactor used in *n*-hexane oxidation with hydrogen peroxide to form a mixture of hexanols and hexanones was performed by Kaliaguine and co-workers [47]. They used a PDMS membrane occluding microporous titanium silicalite zeolites where a simple diffusion-reaction model was proposed. The model describes the reactants concentration profiles and products formation rate distributions inside the membrane, and a good fitting to the experimental average oxygenates formation rate was observed.

Also, modelling of the liquid phase epoxidation of alkenes to epoxides in an interfacial membrane contactor was performed by Yawalkar et al. [48]. These authors assumed homogeneous concentration in the bulk phases and the membrane was modelled as a homogeneous polymeric phase containing cubic zeolite catalyst particles uniformly dispersed. They focused on the influence of different parameters such as peroxide and alkene concentration in the liquid phase, sorption coefficient of the membrane for peroxide and alkene and catalyst loading. The model predictions indicated how the synergetic effect between an organophilic membrane phase and the zeolite particles lowered the excess of peroxide at the catalyst active sites, thus reducing drastically peroxide decomposition and catalyst deactivation. High peroxide efficiency and significant rate of epoxide formation could be obtained with a proper selection of the different parameters.

A mathematical model has also been developed for the partial oxidation of propane with hydrogen peroxide, carried out in a three-phase polymeric membrane reactor [49]. Two types of microporous flat membranes with the catalyst loaded in the dense polymeric phase were considered: a symmetric and an asymmetric membrane. The model was able to determine the operating conditions and the membrane properties for minimizing the mass transfer resistances and for increasing the recovery of products in the gas phase. The model was validated by comparing the theoretical results with experimental data obtained for a reaction temperature of 80 ºC. It was concluded that a higher recovery of products in the gas phase could be achieved by using the asymmetric catalytic membrane.

Regarding gas phase modelling, very recently, a one-dimensional model was used to simulate the reaction and the transport process using a rectangular flat-sheet membrane with well-defined countercurrent gas flows in a Water Gas Shift membrane reactor. The reactor contained a CO_2-selective polymeric membrane and a commercial $Cu/ZnO/Al_2O_3$ catalyst over it (i.e., in a packed-bed membrane reactor configuration) that were used for hydrogen processing for fuel cells. The reaction rate equation for the $Cu/ZnO/Al_2O_3$ catalyst obtained from literature was incorporated into the model and the modelling results agreed well with the experimental data [44].

A theoretical study considering a dense polymeric membrane reactor, conducting a reversible gas phase generic reaction of the type $A+B \leftrightarrow C+D$, was performed by Sousa [2]. The study of the conversion enhancement was performed under isothermal conditions and perfectly mixed or plug flow pattern. The same author developed a model to study a consecutive/parallel gas phase reaction of the type $A+B \rightarrow C$ and $B+C \rightarrow D$. The proposed model considers non-isothermal, non-adiabatic, one-dimensional, pseudo-homogeneous behaviour. The study was

conducted to evaluate the selectivity, yield and the outlet stream composition of the membrane reactor, and compares its performance with a conventional packed bed reactor.

Finally, another theoretical study developed simple mathematical equations to predict the mass-transfer rates in a catalytic membrane layer reactor with dispersed catalyst particles. Two physical models, namely the heterogeneous model for larger particles and the pseudo-homogeneous model for very fine particles, were developed. It was assumed that the first order irreversible chemical reaction occurred only inside the catalyst particles, and that a one-dimensional diffusion process was occurring through a planar, catalytic membrane layer that contained dispersed, cubic catalyst particles for the heterogeneous model and spherical particles for the pseudo homogeneous model. Using a simple physical model for the distribution of the catalyst particles in the membrane layer and for the mass transport into it, explicit mathematical equations were developed. These explicit equations enable to predict the mass-transfer rate as a function of every physical and chemical parameter that characterizes the catalytic membrane layer, such as: diffusion coefficients, solubility coefficients, reaction rate constant, catalyst particle size, particle hold-up, and membrane thickness in the case of a first-order, irreversible chemical reaction. [50].

1.2 References

[1] S. S. Ozdemir, M. G. Buonomenna, E. Drioli, Catalytic polymeric membranes: preparation and application, Appl. Catal. A: Gen. 307 (2006) 167.

[2] J. Sousa, Modelling and simulation of dense polymeric catalytic membrane reactors, PhD Thesis, University of Porto, Porto, Portugal, 2005.

[3] A. Julbe, D. Farrusseng, C. Guizard, Porous ceramic membranes for catalytic reactors - overview and new ideas, J. Membr. Sci. 181 (2001) 3.

[4] S. Miachon, J. A. Dalmon, Catalysis in membrane reactors: what about the catalyst?, Top. Catal. 29 (2004) 59.

[5] I. F. J. Vankelecom, Polymeric membranes in catalytic reactors, Chem. Rev. 102 (2002) 3779.

[6] I. K. Song, W. Y. Lee, Heteropolyacid (HPA)-polymer composite films as heterogeneous catalysts and catalytic membranes, Appl. Catal. A: Gen. 256 (2003) 77.

[7] I. F. J. Vankelecom, K. A. L. Vercruysse, P. E. Neys, D. W. A. Tas, K. B. M. Janssen, P. P. Knops-Gerrits, P. A. Jacobs, Novel catalytic membranes for selective reactions, Top. Catal. 5 (1998) 125.

[8] K. K. Sirkar, P. V. Shanbhag, A. S. Kovvali, Membrane in a reactor: a functional perspective, Ind. Eng. Chem. Res. 38 (1999) 3715.

[9] J. Woltinger, K. Drauz, A. S. Bommarius, The membrane reactor in the fine chemicals industry, Appl. Catal. A: Gen. 221 (2001) 171.

[10] H. R. Gao, Y. Xu, S. J. Liao, R. Liu, D. R. Yu, Catalytic-hydrogenation and gas permeation properties of metal-containing poly(phenylene oxide) and polysulfone, J. Appl. Polym. Sci. 50 (1993) 1035.

[11] H. R. Gao, Y. Xu, S. J. Liao, R. Liu, J. Liu, D. C. Li, D. R. Yu, Y. K. Zhao, Y. H. Fan, Catalytic polymeric hollow-fiber reactors for the selective hydrogenation of conjugated dienes, J. Membr. Sci. 106 (1995) 213.

[12] C. Q. Liu, Y. Xu, S. J. Liao, D. R. Yu, Y. K. Zhao, Y. H. Fan, Selective hydrogenation of propadiene and propyne in propene with catalytic polymeric hollow-fiber reactor, J. Membr. Sci. 137 (1997) 139.

[13] C. Q. Liu, Y. Xu, S. J. Liao, D. R. Yu, Mono- and bimetallic catalytic hollow-fiber reactors for the selective hydrogenation of butadiene in 1-butene, Appl. Catal. A: Gen. 172 (1998) 23.

[14] C. Q. Liu, Y. Xu, S. J. Liao, D. R. Yu, Selective hydrogenation of cyclopentadiene in mono- and bimetallic catalytic hollow-fiber reactors, J. Mol. Catal. A: Chem. 157 (2000) 253.

[15] J. F. Ciebien, R. E. Cohen, A. Duran, Catalytic properties of palladium nanoclusters synthesized within diblock copolymer films: hydrogenation of ethylene and propylene, Supramol. Sci. 5 (1998) 31.

[16] J. F. Ciebien, R. E. Cohen, A. Duran, Membrane catalysts for partial hydrogenation of 1,3-butadiene: catalytic properties of palladium nanoclusters synthesizes within diblock copolymer films, Mat. Sci. Eng. C-Bio. S. 7 (1999) 45.

[17] J. Theis, D. Fritsch, F. Keil, Catalysis with non-porous membranes loaded with nanoscale metallic clusters, in: Proceedings of the ESF, Network Catalytic Membrane Reactors-Final Workshop: Applications and Future Possibilities of Catalytic Membrane Reactors, Turnhout, Belgium, October 16-17, 1997, 35-41.

[18] S. Ziegler, J. Theis, D. Fritsch, Palladium modified porous polymeric membranes and their performance in selective hydrogenation of propyne, J. Membr. Sci. 187 (2001) 71.

[19] K. Ludtke, K. V. Peinemann, V. Kasche, R. D. Behling, Nitrate removal of drinking water by means of catalytically active membranes, J. Membr. Sci. 151 (1998) 3.

[20] O. M. Ilinich, E. N. Gribov, P. A. Simonov, Water denitrification over catalytic membranes: hydrogen spillover and catalytic activity of macroporous membranes loaded with Pd and Cu, Catal. Today 82 (2003) 49.

[21] D. Fritsch, K. Kuhr, K. Mackenzie, F. D. Kopinke, Hydrodechlorination of chloroorganic compounds in ground water by palladium catalysts - Part 1. Development of polymer-based catalysts and membrane reactor tests, Catal. Today 82 (2003) 105.

[22] I. Petrova, V. Lebedeva, R. van der Vaart, V. Volkov, G. Tereshchenkob, E. L. J. Van Soest-Vercammen, L. Plyasova, D. Kochubey, Low-temperature catalytic membrane reactor for removal of dissolved oxygen from water, Desalination 199 (2006) 424.

[23] M. J. Kim, K. H. Lee, Degassing of dissolved oxygen from water by catalytic membrane contactor, in: Proceedings of the 7th International Conference on Catalysis in Membrane Reactors, CS, Italy, 11-14 September, 2005, 376-378.

[24] T. Takahashi, A. Shono, K. Sato, T. Sato, N. Itoh, Palladium membrane reactor with high hydrogen flux for hydrogen recovery from cyclohexane as a chemical hydride, in: Proceedings of the 6th International Conference on Catalysis in Membrane Reactors, Lahnstein, Germany, July 6-9, 2004, 133.

[25] G. Saracco, H. W. J. P. Neomagus, G. F. Versteeg, W. P. M. van Swaaij, High-temperature membrane reactors: potential and problems, Chem. Eng. Sci. 54 (1999) 1997.

[26] M. E. Rezac, W. J. Koros, S. J. Miller, Membrane-assisted dehydrogenation of *n*-butane influence of membrane-properties on system performance, J. Membr. Sci. 93 (1994) 193.

[27] H. L. Frisch, S. Maaref, H. Deng-Nemer, Low-temperature dehydrogenation reaction-separation membranes using zeolite 13X polyethylacrylate, J. Membr. Sci. 154 (1999) 33.

[28] R. F. Parton, I. F. J. Vankelecom, M. J. A. Casselman, C. P. Bezoukhanova, J. B. Uytterhoeven, P. A. Jacobs, An efficient mimic of cytochrome-P-450 from a zeolite encaged iron complex in a polymer membrane, Nature 370 (1994) 541.

[29] R. F. Parton, I. F. J. Vankelecom, D. Tas, K. B. M. Janssen, P. P. KnopsGerrits, P. A. Jacobs, Membrane occluded catalysts: a higher order mimic with improved performance, J. Mol. Catal. A: Chem. 113 (1996) 283.

[30] G. Langhendries, G. V. Baron, I. F. J. Vankelecom, R. F. Parton, P. A. Jacobs, Selective hydrocarbon oxidation using a liquid-phase catalytic membrane reactor, Catal. Today 56 (2000) 131.

[31] S. Kaliaguine, C. Bouchard, S. Q. Wu, J. Shu, Use of catalytic membranes as interphase contactors for multiphase reactions, Canadian Patent 2,206,626, 1998.

[32] M. Carnevale, G. Golemme, J. C. Jansen, C. Milone, Catalytic membranes for propylene epoxidation, in: Proceedings of the 7th International Conference on Catalysis in Membrane Reactors, CS, Italy, 11-14 September, 2005, 231-234.

[33] P. Oliveira, A. Machado, A. M. Ramos, I. M. Fonseca, A. Botelho do Rego, A. Vital, Limonene oxidation over Y-zeolite encaged Co acetylacetonate embedded in a PDMS membrane, in: Proceedings of the 7th International Conference on Catalysis in Membrane Reactors, CS, Italy, 11-14 September, 2005, 79-81.

[34] R. L. Pozzo, M. A. Baltanas, A. E. Cassano, Supported titanium oxide as photocatalyst in water decontamination: state of the art, Catal. Today 39 (1997) 219.

[35] I. R. Bellobono, B. Barni, F. Gianturco, Preindustrial experience in advanced oxidation and integral photodegradation of organics in potable waters and waste-waters by PHOTOTERM^{TM} membranes immobilizing titanium-dioxide and promoting photocatalysts, J. Membr. Sci. 102 (1995) 139.

[36] I. R. Bellobono, R. Morelli, C. M. Chiodaroli, Photocatalysis and promoted photocatalysis during photocrosslinking of multifunctional acrylates in composite membranes immobilizing titanium dioxide, J. Photoch. Photobio. A 105 (1997) 89.

[37] F. Gianturco, L. Vianelli, L. Tatti, F. Rota, P. Bruzzi, L. Rivas, I. R. Bellobono, M. Bianchi, H. Muntau, Pilot-plant photomineralization of dichloromethane and tetrachloroethene in

aqueous solution, by photocatalytic membranes immobilizing titanium dioxide and photopromoters, Chemosphere 33 (1996) 1531.

[38] F. Rota, M. Cavassi, D. Niego, R. Gorlani, L. Vianelli, L. Tatti, P. Bruzzi, A. Moroni, I. R. Bellobono, M. Bianchi, H. Muntau, Mathematical modelling of photomineralization of phenols in aqueous solution, by photocatalytic membranes immobilizing titanium dioxide, Chemosphere 33 (1996) 2159.

[39] L. Tatti, D. Niego, F. Rota, P. Bruzzi, A. Moroni, I. R. Bellobono, M. Bonardi, M. Bianchi, H. Muntau, Mathematical modelling of pilot-plant photomineralization of chlorophenols in aqueous solution, by photocatalytic membranes immobilizing titanium dioxide, Chemosphere 34 (1997) 41.

[40] R. Morelli, I. R. Bellobono, C. M. Chiodaroli, S. Alborghetti, EPR spin-trapping of hydroxyl radicals onto photocatalytic membranes immobilizing titanium dioxide, and spin adduct competition, as a probe of reactivity with aqueous organic micropollutants, J. Photoch. Photobio. A 112 (1998) 271.

[41] L. Rivas, I. R. Bellobono, F. Ascari, Photosynthetic membranes - Part 67 - Photomineralization of n-alkanoic acids in aqueous solution by photocatalytic membranes. Influence of radiation power, Chemosphere 37 (1998) 1033.

[42] E. Fontananova, L. Donato, E. Drioli, L. Lopez, P. Favia, R. d'Agostino, Heterogenization of polyoxometalates on the surface of plasma-modified polymeric membranes, Chem. Mater. 18 (2006) 1561.

[43] R. Molinari, F. Pirillo, V. Loddo, L. Palmisano, Heterogeneous photocatalytic degradation of pharmaceuticals in water by using polycrystalline TiO_2 and a nanofiltration membrane reactor, Cat. Today 118 (2006) 205.

[44] J. Zou, J. Huang, W. S. W. Ho, CO_2-Selective water gas shift membrane reactor for fuel cell hydrogen processing, Ind. Eng. Chem. Res. 46 (2007) 2272.

[45] L. Guerreiro, J. E. Castanheiro, I. M. Fonseca, R. M. Martin-Aranda, A. M. Ramos, A. Vital, Transesterification of soybean oil over sulfonic acid functionalised polymeric membranes, Cat. Today 118 (2006) 166.

[46] J. S. Marcano, T. T. Tsotsis, Catalytic Membranes and Membrane Reactors, Chapter 5, Wiley-VCH Verlag GmbH, Weinheim, 2002.

[47] S. Q. Wu, J. E. Gallot, M. Bousmina, C. Bouchard, S. Kaliaguine, Zeolite containing catalytic membranes as interphase contactors, Catal. Today 56 (2000) 113.

[48] A. A. Yawalkar, V. G. Pangarkar, G. V. Baron, Alkene epoxidation with peroxide in a catalytic membrane reactor: a theoretical study, J. Membr. Sci. 182 (2001) 129.

[49] A. Criscuoli, C. Espro, A. Parmaliana, E. Drioli, Modelling of a three-phase catalytic membrane reactor for the partial oxidation of light alkanes, in: Proceedings of the 7th International Conference on Catalysis in Membrane Reactors, CS, Italy, 11-14 September, 2005, 58-61.

[50] E. Nagy, Mass transfer through a dense, polymeric, catalytic membrane layer with dispersed catalyst, Ind. Eng. Chem. Res. 46 (2007) 2295.

Part II

2. Kinetics of Propylene Hydrogenation on Nanostructured Palladium Clusters*

Abstract

Surfactant-stabilized palladium nanoclusters with an average diameter of about 7.3 nm (determined by XRD) are used as catalysts in propylene hydrogenation. Experiments performed in an isothermal batch reactor (T = 308 K), with total pressures in the range 0.25 – 9.0 bar and with initial hydrogen molar ratios varying between 0.05 – 0.40, provide a further insight on the reaction kinetics. It is shown that a Langmuir-Hinshelwood rate equation well represents the reaction data, which mechanism involves competitive adsorption of the reagents, with dissociation of hydrogen on the catalyst surface, and where surface reaction is the limiting step. Nonlinear optimization of the initial rate data provided the kinetic parameters of the rate law (k = 5.569 mol g_{Pd}^{-1} s^{-1}; K_{H_2} = 3.799 × 10^{-2} bar^{-1} and $K_{C_3H_6}$ = 0.996 bar^{-1}), which is validated by integration of the mass balance in the batch reactor.

**** L. Brandão, D. Fritsch, L. M. Madeira, A. M. Mendes, Chem. Eng. J. 103 (2004) 89.***

2.1 Introduction

Nanoclusters have a significant potential as new types of more active and selective catalysts. Because of their size, generally less than 10 nm, they often display unique catalytic properties. Possible reasons for that are: *i*) a large percentage of nanoclusters metal atoms lies on the surface, and thus the surface to volume ratio drastically increases; and *ii*) surface atoms do not necessarily order themselves in the same way that those in the bulk do [1].

Nanoclusters are agglomerates of a few to a few thousand atoms. Some clusters of noble metals, e.g. Pd, Ag or Au, were already synthesized by reduction of the metal ions in solution. The metal atoms form a cluster and an organic ligand (e.g. surfactant, polymer) binds to the cluster surface. The ligand shell stabilizes the cluster and prevents its agglomeration, because as soon as these nanoclusters come into contact with each other, they agglomerate to lower their surface energy [2, 3].

Most studies concerning the catalytic activity of polymer-stabilized nanoclusters have been conducted in solution. For instance, nanoclusters impregnated in Al_2O_3 pellets showed to be 3 times more active in cyclooctene hydrogenation than a comparable, commercially available, industrial catalyst (5 wt. % Pd on Al_2O_3) [4]. A comparatively small number of studies has been undertaken to examine the catalytic activity of metals in polymer-based nanocomposite materials in the presence of gaseous reagents, and some exceptions are their use in hydrogenation reactions [5, 6].

Hydrogenation of olefins is an active subject of research and has been one of the most thoroughly studied chemical processes [7, 8]. In what concerns its mechanism, it has been generally accepted that hydrogenation of olefins over transition metal catalysts proceeds via an associative mechanism through σ-alkyl intermediates, known as Horiuti-Polanyi mechanism [9].

However, metals also tend to form allylic species by abstracting hydrogen from the olefin (dissociative mechanism) [10].

In the case of ethylene hydrogenation, several mechanisms have been proposed in the literature [8, 11]. For instance, Ofner and Zaera [8] suggested a simple Langmuir model that considers competitive adsorption between hydrogen and ethylene. Hydrogen adsorbs dissociatively and the rate limiting step is the hydrogenation of the ethyl intermediate with adsorbed surface hydrogen [8]. Propylene hydrogenation has not been studied so extensively as ethylene hydrogenation, and most of the works have been focused on the use of a platinum catalyst [12-15]. For both reactions, the kinetics and mechanisms are far from being settled, particularly over a Pd catalyst, which is widely used in industrial practice in hydrogenation reactions.

As most of the hydrogenations take place at temperatures below 200 ºC, or even at room temperature, a polymeric catalytic membrane reactor (pCMR) can advantageously be used. But to have access to the parameters governing the separation and the chemical reaction kinetics in a continuous pCMR, independent experiments should ideally be performed. Thus, in the present study, the kinetic parameters of propylene hydrogenation are determined using palladium nanoclusters, which show no mass transport resistances. This data will be important for subsequent modelling of the process in a pCMR and, besides, gives more insight concerning kinetics over metal nanoclusters, which is a recent and innovative topic in catalysis.

2.2 Experimental section

2.2.1 Catalysts preparation

The nanostructured palladium clusters were stabilized using the surfactant tetraoctadecylammonium bromide, *n*-$(C_{18}H_{37})_4N^+Br^-$ [2], whose preparation procedure is reported elsewhere [16, 17]. For immobilizing these nanoparticles in a porous support (polyester textile), 17.0-20.0 mg of the powder-catalyst, containing 15.71 wt. % Pd, was dispersed in tetrahydrofuran (THF) (p.a. Merck) at a concentration of 0.20 wt. %. Ultrasound was used for a better dispersion. One drop of the suspension was then released in each square of a previously defined grid (0.6 cm × 0.6 cm) over the porous textile support (5.4 cm × 4.2 cm).

2.2.2 Catalysts characterization

The average diameter of the surfactant-stabilized palladium clusters was measured using X-ray diffraction (XRD) in a Ditral Siemens D5000 apparatus, employing Cu Kα radiation. The powder was pressed into a squared support (1 cm × 1 cm) and the average diameter was calculated using the Bragg Brentano geometry.

The active surface area of the clusters was obtained from the CO adsorption isotherm, which was determined at 308 K using the gravimetric method in the pressure range of 5-100 mbar.

The palladium-containing samples were also analyzed by scanning electron microscopy (SEM) using a Jeol JSM-6301F apparatus, in conjunction with energy dispersive X-ray spectroscopy (EDS) with a Noran-Voyager equipment, both operating at 20 keV. The specimens were firstly processed by means of a Jeol JFC 1100 ion sputtering device for fine gold coating of the surface, to provide stability and conductivity under the electron beams.

2.2.3 Catalytic experiments

The hydrogenation kinetics of propylene to propane was studied in a jacketed batch cylindrical reactor ($V = 0.55 \times 10^{-3}$ m^3; i.d. = 8.2 cm; h = 10.5 cm), to which a pressure sensor (Druck-PMP 4000 Series - 2 or 10 bar, absolute) and a thermocouple were attached. All the gases admitted to the stainless-steel reactor were supplied by Praxair (propylene 99.5 %, hydrogen 99.999 % and argon 99.999 %) and were previously mixed in a jacketed tank, which was connected to the reactor through an on-off valve. Both pressure history and temperature were monitored along the runs, being recorded in a computer at a frequency of 0.1 s^{-1}. The porous support containing the Pd nanoclusters catalyst was attached to a magnetic bar (with a cross shape and stirring at 600 rpm), and this assembly was inserted into the batch reactor.

Palladium oxide formed on the catalyst surface due to air exposition was removed by admitting 1.0 bar of hydrogen into the reactor, leaving for 20 h, and then evacuating with a rotary vacuum pump (maximum vacuum of 10^{-3} mbar). This procedure was repeated twice, as recommended by Sachs et al. [18], and was followed by dilution in argon and a final evacuation. Using the experimental procedure described, reproducible runs were achieved in most of the experimental conditions. However, at high pressures (P > 4 bar) some deactivation of the catalyst was noticed. In that case a new support was prepared with fresh catalyst.

It is known that under catalytic conditions with partial pressures above the deci-Pascal range, and around room temperature, the hydrogenation of small olefins occurs in the presence of carbonaceous deposits (alkylidynes), seen as spectator species that just block the metal surface sites [7, 19, 20]. In the experimental conditions of this study, it is expected that the surface might be saturated with propylidyne deposits, but such surface coverage should not change under

typical experimental conditions. Otherwise activity decay would be noticed in subsequent experiments.

In the catalytic runs, hydrogen molar ratios in the range 0.05 – 0.40 were used, at an initial total pressure of 1.0 bar. A set of experiments where the initial total pressure was varied between 0.25 and 9.0 bar (absolute) was also performed, at equal composition ($y_{H_2 o}$ = 0.10 and $y_{C_3H_6 o}$ = 0.35). Both the fraction of inert (argon) and the temperature were the same in all runs: 0.55 and 308 K, respectively. Experiments were repeated at least three times, randomly, and were reproducible within ± 5 %. Blank runs were also performed, using the support and the magnetic bar, and showed neither catalytic activity nor adsorption of reagents.

The parameters of the rate law were obtained by solving a nonlinear least squares problem using a commercial statistics software (JMP®, 5.1, SAS). For integration of the mass balances, the time dependent equations were solved using LSODA [21].

In order to evaluate if internal resistances to mass transfer were significant within the nanostructured palladium clusters, due to the presence of the surfactant, well-known intraparticle transport criteria were used [22]. First, to assess the effective diffusivity coefficients, some experiments were carried out in which 3.0 g of *n*-$(C_{18}H_{37})_4N^+Br^-$ powder (supplied by Sigma-Aldrich; assay: > 98 %) were used and the uptake curves determined, through the volumetric method. The experiments have shown that, for all gases considered, the amounts adsorbed are negligible and equilibrium is reached almost instantaneously (ca. 1 s). Comparison of these curves with a mass balance for spherical particles gave us an estimate for the effective diffusivity coefficient ($D_e \sim 2.6 \times 10^{-7}$ m^2 s^{-1}), assuming 1 % deviation from a flat concentration gradient. The following parameter was then evaluated for the maximum particle size found (ca. 20 μm, see below): $\Phi_S = r_{obs}\rho_c R_p^2 / \left(D_e C_{i,s}\right)$, which expresses the ratio of chemical reaction rate to diffusive

flux (r_{obs} is the observed reaction rate, $\rho_c \sim 1.8$ g cm^{-3} is the density of the catalyst pellet, obtained by He pycnometry, R_p is the radius of the particle, and $C_{i,s}$ is the concentration of the limiting reactant at surface conditions). Both the Weisz [23] and Hudgins [24] criteria were applied, after fitting different power-law kinetics to the data herein obtained. These criteria were always verified (Φ_S sufficiently small), thus supporting that internal mass transfer resistances are negligible, and so the hydrogenation reaction proceeds in kinetic regime.

The possible existence of external resistances to mass transfer was also evaluated. For that, different rotation speeds were employed during the experiments. Changing the rotation speed from 0 up to 600 rpm did not change the reaction rate, thus evidencing that external mass transfer effects were absent.

2.3 Results

2.3.1 Catalysts characterization

Data from XRD analyses indicated that the average diameter of the surfactant-stabilized palladium clusters is 7.3 ± 2.0 nm, corresponding to a surface area of about 68 $m^2\ g_{Pd}^{-1}$ (assuming spherical Pd nanoparticles). The active surface area of this sample was obtained from CO chemisorption. The amount of carbon monoxide adsorbed on the Pd surface was calculated from the plateau of the isotherm, which evidenced that the monolayer capacity of Pd is 4.53×10^{-5} mol per gram of sample. Assuming that 0.5 CO/Pd_s is the average maximum coverage over the exposed palladium [25], the active surface area in the nanostructured palladium clusters is 27 $m^2\ g_{Pd}^{-1}$ (metallic dispersion of 6.1 %). This active surface area is significantly different from the surface area computed considering the diameter obtained by XRD. This might indicate that not

all sites are active or the chemisorption stoichiometry is not the assumed one. Anyway, these methods should not be directly compared as they use different approaches to obtain the average sizes of the particles populations [26].

Both the size and the active surface of palladium were determined in a sample before dispersion in THF, i.e., in the unsupported catalyst. Because the mass of Pd used in the textile support is very small, those parameters were not evaluated in the supported sample.

SEM/EDS techniques were used to evaluate if the procedure adopted to immobilise the nanostructured palladium clusters in the textile support affects the structure or size of the catalyst aggregates and, eventually, removed the surfactant shell, thus leading to the possible Pd nanoclusters agglomeration. SEM analyses were performed for the powder-catalyst before (Fig. 2.1A) and after immobilisation (Fig. 2.1B). One can see that the size of the aggregated clusters on the support is retained, with the biggest particles being in both cases about 20 μm in diameter.

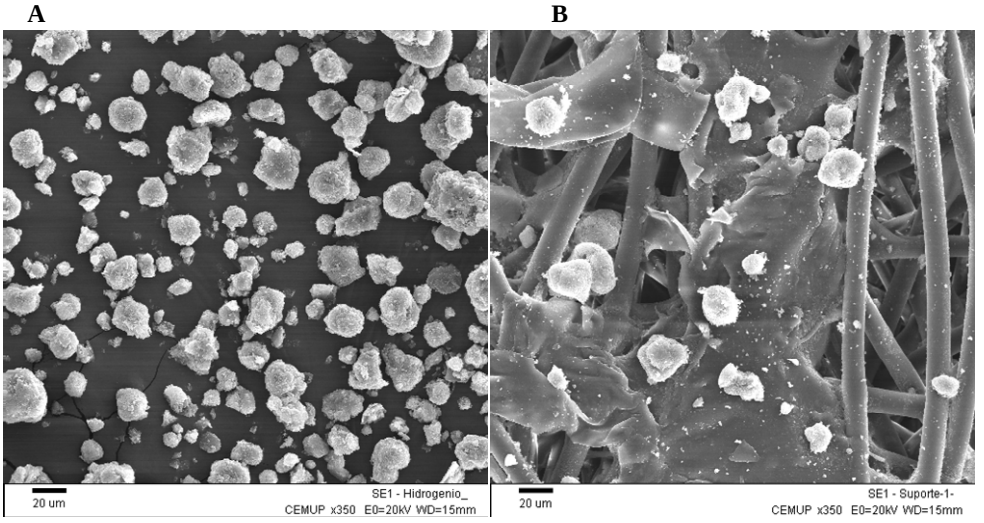

Fig. 2.1 SEM micrographs of the original nanostructured Pd powder-catalyst (A) and after immobilization in the textile support (B), both at a magnification of × 350.

Besides, EDS analysis showed the existence of Br (due to the surfactant used) in the immobilized samples and also proved the existence of Pd inside the particles. Therefore, the technique used to immobilise the catalyst does not liberate the Pd clusters from the shell. Palladium nanoclusters were found to be arranged inside surfactant particles as seeds in a pomegranate.

2.3.2 Catalytic experiments

As above-mentioned, experiments performed in the batch reactor provided total pressure versus time curves, what allowed us to compute the reaction rates. For that, the following concepts were used: *i)* extent or degree of advancement of a reaction, ξ, defined as [27, 28]:

$$\xi = \frac{n_i - n_{i,o}}{\nu_i} \tag{2.1}$$

where n_i and $n_{i,o}$ are the mole number of species i present in the reactor at instant t and at the initial instant, respectively, and ν_i is the stoichiometric coefficient for species i (so that it is positive for products and negative for reagents), and *ii)* normalized advancement:

$$X = \frac{\xi}{n_o} \tag{2.2}$$

where n_o is the total number of reactive moles at the beginning of the run. Using these concepts, and assuming ideal gas behaviour for the gaseous mixture, it can be easily deduced that:

$$X(t) = \frac{1 - P(t)/P_o}{1 - y_{I,o}} \tag{2.3}$$

The total fraction of inert gas, $y_{I,o}$, was kept constant in all runs (0.55). Thus, from experimentally recorded pressure data, advancement results are easily calculated with Eq. (2.3). Reaction rates, per weight of catalyst, were computed using Eq. (2.4), which was deduced from a mass balance to the batch reactor:

$$r = \frac{P_o V\left(1 - y_{I,o}\right)}{wRT}\frac{\mathrm{d}X}{\mathrm{d}t} \tag{2.4}$$

In this equation, w denotes the mass of catalyst used and V the reactor volume.

The methodology adopted to deduce the rate law for propylene hydrogenation over the palladium nanoclusters, under isothermal conditions, was the method of initial rates, firstly proposed by Yang and Hougen [29]. The analysis proposed by Yang and Hougen, i.e. the graphical evaluation of the effect of some initial operating conditions (namely total pressure or reaction mixture composition) over the initial rates, still shows to be a useful tool in kinetic modelling, and can save much time and effort.

First, the initial rates of propylene hydrogenation under different initial compositions of the reaction mixture (propylene to hydrogen ratio) were determined at 1.0 bar. Obviously, initial rates were obtained from the slopes of X versus t curves for initial instant (see Eq. (2.4)). The plot shown in Fig. 2.2 points to a mechanism where surface reaction is the limiting step [29], what is in agreement with previous works [30]. More recently, Zaera and co-workers [8] found, using a molecular beam technique at low temperatures and ultra high vacuum, that a competition exists between ethylene and hydrogen for surface sites. They addressed that an increase of hydrogen adsorbed at the surface of the catalyst increases the initial hydrogenation rate, and that a further increase in the surface coverage by hydrogen leads to a slower amount of adsorbed ethylene [8]. Figure 2.2 also shows that at high hydrogen concentrations the initial rate decreases, possibly due to the mentioned competitive adsorption. Such competition leads to a decrease in the number of sites available for propylene adsorption, and consequently in the reaction rate.

The effect of total the pressure in the initial hydrogenation rate is illustrated in Fig. 2.3. Once again, the graphical methodology proposed by Yang and Hougen [29] indicates, from the shape of the curve, and taking also into account data from Fig. 2.2, that both hydrogen and

propylene adsorb on the catalyst, with surface reaction as the limiting step. However, it is not possible to definitely state if dissociation occurs or not because the expected maximum that appears for dissociative adsorption is not very clear in Fig. 2.3, although it seems to exist. Nevertheless, the dissociative adsorption of hydrogen on the catalyst surface was considered in the proposed mechanism because it provides the best fit to the experimental data, as mentioned below. Besides, this is a well-known phenomenon which occurs on metallic surfaces and widely reported in the literature [31, 32].

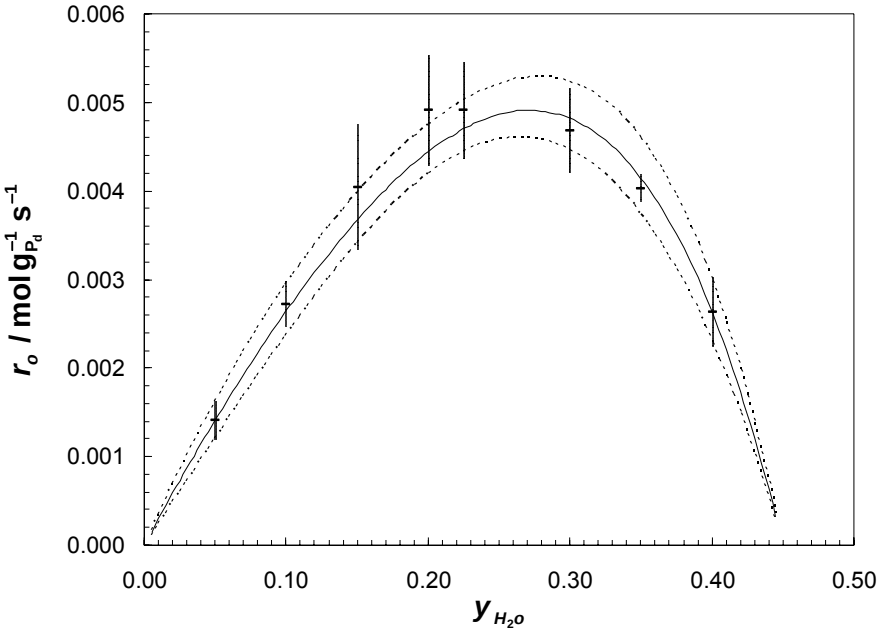

Fig. 2.2 Effect of the initial hydrogen molar fraction in the initial rates of propylene hydrogenation (P_o = 1.0 bar; $y_{I,o}$ = 0.55; T = 308 K) (– : experimental values). The bar errors for the mean values were obtained for a 95 % confidence level (t distribution), using at least three experimental results. The solid line corresponds to the model fitting and dashed lines are the confidence curves (for a 95 % confidence level).

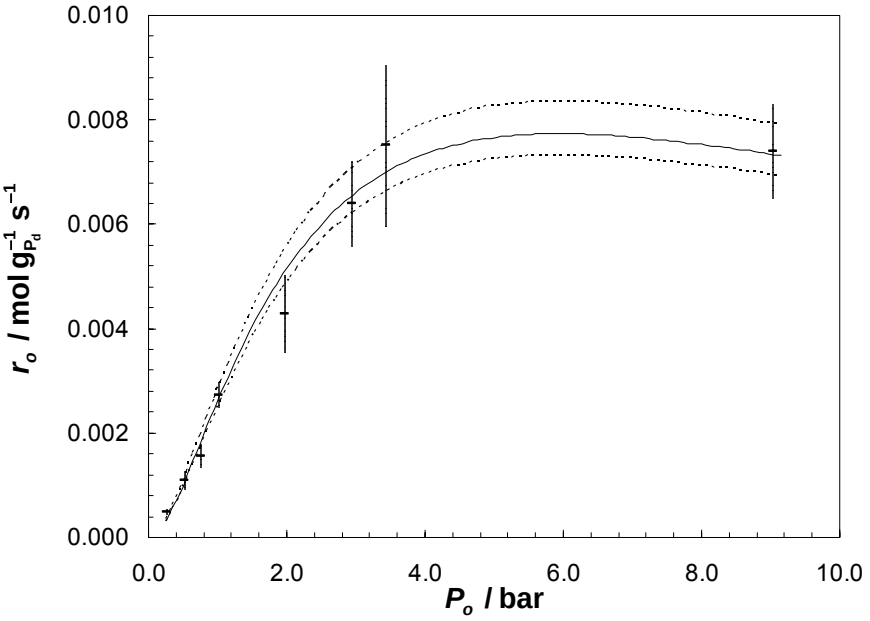

Fig. 2.3 Effect of the initial total pressure in the initial rates of propylene hydrogenation ($y_{H_2o} : y_{C_3H_6o}$ = 0.10:0.35; T = 308 K) (**–** : experimental values). The bar errors for the mean values were obtained for a 95 % confidence level (*t* distribution), using at least three experimental results. The solid line corresponds to the model fitting and dashed lines are the confidence curves (for a 95 % confidence level).

2.4 Discussion

From the experiments described one can determine the kinetic parameters of propylene hydrogenation over palladium nanosized clusters. According to the findings mentioned above, the reaction mechanism can be described by the following steps:

$$H_2(g) + 2M \leftrightarrow 2H - M \tag{2.5}$$

$$C_3H_6(g) + M \leftrightarrow C_3H_6 = M \tag{2.6}$$

$$C_3H_6 = M + 2H - M \xrightarrow{k'} C_3H_8(g) + 3M \tag{2.7}$$

Equation (2.5) takes into account the dissociative adsorption of hydrogen on palladium active sites (*M*), while Eq. (2.6) describes the adsorption/desorption equilibrium for propylene.

Finally, Eq. (2.7) describes the hydrogenation of adsorbed propylene to propane. Assuming that the surface reaction is the limiting step, and using the Langmuir-Hinshelwood (L-H) formulation [28, 29], i.e. assuming that the total concentration of active sites $[M]_T$ is constant with a steady-state approximation for Eqs. (2.5) and (2.6), it can be easily deduced that the overall rate of propane formation is given by:

$$r_{C_3H_8} = \frac{kK_{H_2}K_{C_3H_6}p_{H_2}p_{C_3H_6}}{\left(1+\sqrt{K_{H_2}p_{H_2}}+K_{C_3H_6}p_{C_3H_6}\right)^3} \tag{2.8}$$

where $k = k'[M]_T^3$ (k' is the rate constant for the surface reaction, Eq. (2.7)) and K_i and p_i represent the adsorption equilibrium constant and partial pressure for species *i*, respectively. This rate equation evidences the competitive adsorption of both reagents with dissociation of hydrogen on the catalyst surface, which follows the Horiuti-Polanyi mechanism [9]. However, these authors suggest the involvement of two active sites for adsorption of the olefin.

Ofner and Zaera [8] reported a competitive adsorption for Pt(111) sites between di-σ-bonded ethylene molecules and hydrogen. This di-σ-bonded is a strongly bonded state of adsorption of ethylene that at saturation evolutes to a weakly bonded state (π-bonded ethylene), which is the state that is hydrogenated [8]. More recently, Ofner and Zaera [33] also reported an adsorption mechanism at high coverages of ethylene which involves this π-bonded adsorption. After an initial interaction with the few metal atoms left exposed by an imperfect monolayer, a collective rearrangement of the neighbouring molecules occurs, leading to a new compressed layer (the above-mentioned weakly bonded state). This supports the involvement of one single site, not two, for adsorption of the olefin, similarly to the mechanism herein proposed.

The parameters of Eq. (2.8) were determined by a nonlinear regression analysis, by fitting the rate law to the data shown in Figs. 2.2 and 2.3. The parameters obtained according to the

model proposed are shown in Table 2.1. Limits for a 95 % confidence level are also plotted in Figs. 2.2 and 2.3, showing a good model adhesion to the experimental values. However, parameters *k* and K_{H_2} are linked and the criterion used, minimization of the square residuals, did not allow to obtain high precision values for them.

Table 2.1 Kinetic parameters of propylene hydrogenation over palladium nanoclusters (T = 308 K).

Parameter	Value
k / mol g^{-1}_{Pd} s^{-1}	5.569
K_{H_2} / bar^{-1}	3.799×10^{-2}
$K_{C_3H_6}$ / bar^{-1}	0.996

A great advantage of using nano-sized materials is that the surface to volume ratio increases drastically and the surface atoms include an increasing fraction of the total particulate volume with high defect structures. However, it was not possible to compare the catalytic activity of the palladium nanoclusters with other works, as the majority of propylene hydrogenations are reported over platinum catalysts. In the very few studies found where this hydrogenation was carried out over palladium, the experimental conditions employed were out of the range herein adopted.

Based in the same experimental data, the methodology adopted does not exclude other rate equations or reaction mechanisms. With this in mind, different promising reaction mechanisms were tested. The following model selection criterion (MSC) was adopted [34]:

$$\mathrm{MSC} = \ln\left[\frac{\sum_{i=1}^{m}\left(r_{oobs,i} - \overline{r_{oobs}}\right)^2}{\sum_{i=1}^{m}\left(r_{oobs,i} - r_{ocal,i}\right)^2}\right] - \frac{2f}{m} \tag{2.9}$$

where m is the number of experimental points, f is the number of fitting parameters and $\overline{r_{oobs}}$ is the mean of the experimental results. The criterion adopted gives higher MSC values both for models that fit better and for models with less number of parameters, and therefore allows comparison of different models.

Table 2.2 shows the models considered, ranked by the MSC value. Model 2 was proposed by Rogers and co-workers and takes into account competitive and non-competitive adsorption of the reagents at the catalyst surface [13]. Model 3 is a L-H equation for a mechanism with surface reaction between adsorbed species controlling, but without hydrogen dissociation. Model 4 is based on the Horiuti-Polanyi mechanism [9], with adsorption of the olefin in two sites. Model 5 was adapted for the present reaction and was first proposed by Borodzinski and Cybulki [35] for the selective hydrogenation of acetylene. Model 6 is also a L-H equation that considers the bimolecular shock between the adsorbed propylene and the first hydrogen atom, followed by the addition of the second hydrogen atom. Finally, model 7 is the Rideal-Eley mechanism. However, the best model after using the MSC adopted is model 1, which is proposed in the present study.

For validation of both the proposed rate law and the kinetic parameters determined by the nonlinear regression, the integral method was used [28]. For that, Eq. (2.4) was integrated using the rate law shown in Eq. (2.8) and the kinetic parameters from Table 2.1. Assuming once again ideal gas behaviour, the hydrogen and propylene partial pressures in the rate equation were substituted from their dependence on the advancement of the reaction:

$$p_j = P_o\left[y_{j,o} - \left(1 - y_{I,o}\right)X\right] \tag{2.10}$$

Table 2.2 Initial reaction rate equations employed to fit the propylene hydrogenation data and corresponding model selection criterion (MSC) values.

Model Nr.	$r_{C_3H_8o}$	Ref.	MSC
1	$\frac{kK_{H_2}K_{C_3H_6}p_{H_2o}p_{C_3H_6o}}{\left(1+\sqrt{K_{H_2}p_{H_2o}}+K_{C_3H_6}p_{C_3H_6o}\right)^3}$		7.25
2	$\frac{\alpha K_{H_2}K_{C_3H_6}p_{H_2o}p_{C_3H_6o}}{\left(1+K_{H_2}p_{H_2o}+K_{C_3H_6}p_{C_3H_6o}\right)^2}+\frac{\beta K_{H_2}K_{C_3H_6}p_{H_2o}p_{C_3H_6o}}{\left(1+K_{H_2}p_{H_2o}\right)\left(1+K_{H_2}p_{H_2o}+K_{C_3H_6}p_{C_3H_6o}\right)}$	[13]	7.16
3	$\frac{kK_{H_2}K_{C_3H_6}p_{H_2o}p_{C_3H_6o}}{\left(1+K_{H_2}p_{H_2o}+K_{C_3H_6}p_{C_3H_6o}\right)^2}$		6.48
4	$kK_{H_2}K_{C_3H_6}p_{H_2o}p_{C_3H_6o}\left(\frac{-\left(1+K_{H_2}p_{H_2o}\right)+\sqrt{\left(1+\sqrt{K_{H_2}p_{H_2o}}\right)^2+4K_{C_3H_6}p_{C_3H_6o}[M]_T}}{2K_{C_3H_6}p_{C_3H_6o}}\right)^4$		5.83
5	$\frac{kK_{C_3H_6}p_{H_2o}p_{C_3H_6o}}{\left(1+K_{C_3H_6}p_{C_3H_6o}\right)^2}$	[35]	5.76
6	$\frac{k\sqrt{K_{H_2}p_{H_2o}}K_{C_3H_6}p_{C_3H_6o}}{\left(1+\sqrt{K_{H_2}p_{H_2o}}+K_{C_3H_6}P_{C_3H_6o}\right)^2}$	[8]	5.47
7	$\frac{kK_{H_2}p_{H_2o}p_{C_3H_6o}}{\left(1+\sqrt{K_{H_2}p_{H_2o}}\right)^2}$		2.37

Figs. 2.4 and 2.5 show the plots of some experimental and theoretical curves. In all cases, integration of the mass balance describes quite reasonably the experimental advancement data. Although conversion of the limiting reactant j was always complete, the advancement curves tend to a maximum value which depends on the initial conditions:

$$X_{\max} = \frac{y_{j,o}}{(1 - y_{I,o})} \tag{2.11}$$

For instance, in Fig. 2.4 the curves for y_{H_2o} = 0.05 or 0.40 tend both to $X_{\max}$ = 0.111, while for y_{H_2o} = 0.15 or 0.30 the limit value is 0.333. In Fig. 2.5 all the curves tend to the same $X_{\max}$ value (0.222).

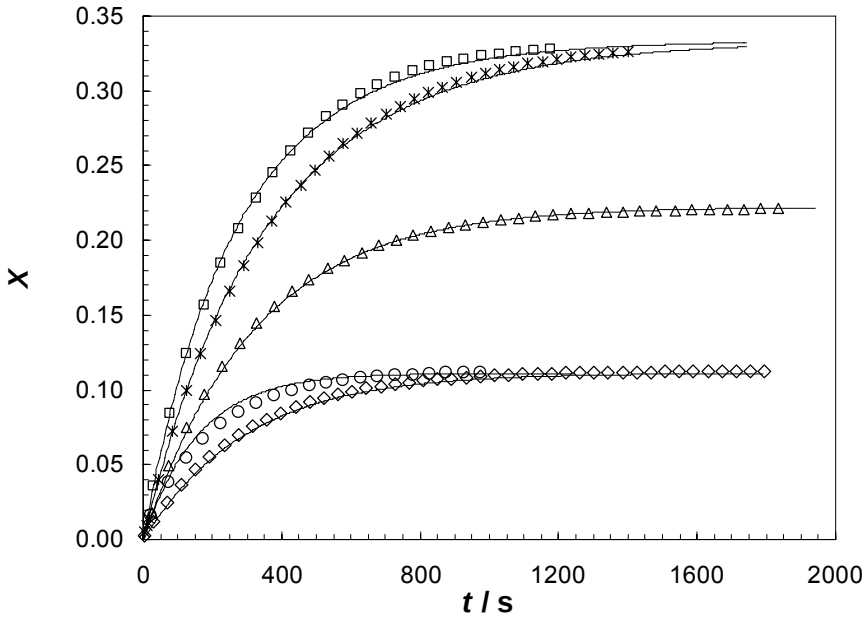

Fig. 2.4 Advancement of the reaction as a function of time for different initial compositions of the reaction mixture: y_{H_2o} = 0.05 (◇), y_{H_2o} = 0.10 (△), y_{H_2o} = 0.15 (∗), y_{H_2o} = 0.30 (□), y_{H_2o} = 0.40 (○), (P_o = 1.0 bar; $y_{I,o}$ = 0.55; T = 308 K; the number of experimental points was reduced for a better visualization). The solid line is the model fit by the integral method.

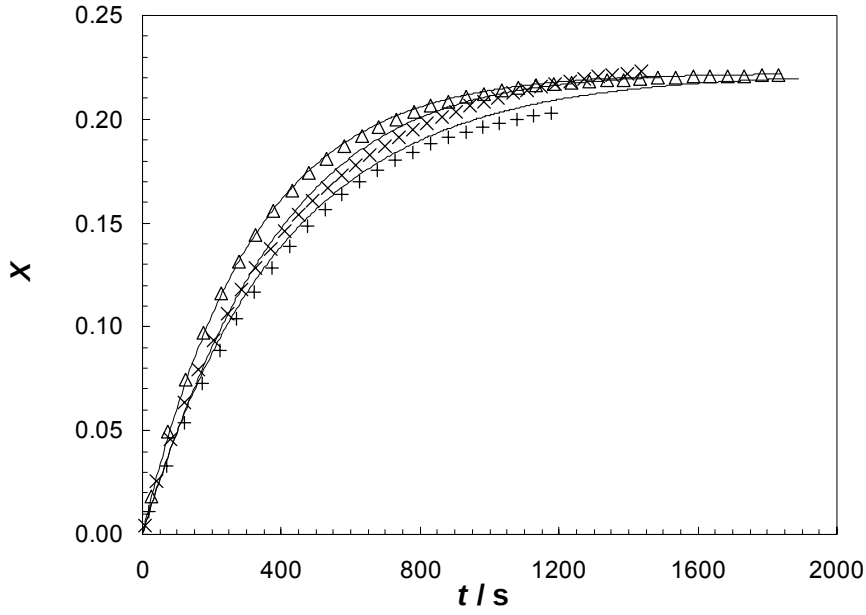

Fig. 2.5 Advancement of the reaction as a function of time for different initial total pressures: P_o = 0.50 bar (+), P_o = 1.0 bar (△), P_o = 3.5 bar (×) ($y_{H_2o} : y_{C_3H_6o}$ = 0.10:0.35; T = 308 K; the number of experimental points was reduced for a better visualization). The solid line is the model fit by the integral method.

2.5 Conclusions

In this chapter, the kinetics of propylene hydrogenation was studied under isothermal conditions using palladium nanosized clusters as catalyst. Because metal nanoclusters are not stable, as they quickly grow and/or fuse together into micrometric aggregates, surfactant-stabilized Pd nanoparticles were used. The technique used to immobilise the catalyst nanoparticles in a textile support, which involves dispersion in a THF solvent, does not affect the structure and dimensions of the catalyst aggregates, for which mass transport resistances are negligible. Besides, SEM/EDS analyses also showed that clusters do not loose their surfactant shell upon such treatment.

Although it was not possible to determine the active surface area of the supported catalyst before and after the hydrogenation reaction, it is reasonable to assume that it possibly remains unchanged, once reaction rates were quite reproducible.

The method of initial rates was adopted to establish the reaction mechanism. Although this approach does not exclude other reaction schemes, it was found that experimental rate data are coherent with a L-H mechanism that involves competitive adsorption between reactants for the catalyst surface, with dissociative adsorption of hydrogen, and where surface reaction is the limiting step. The results agree with a Horiuti-Polanyi mechanism [9], but here it is involved one single site, not two, for olefin adsorption.

The corresponding L-H rate equation represents very reasonably the experimental data of propylene hydrogenation, with the kinetic parameters being determined by nonlinear regression analysis.

For validation of both the proposed rate law and the kinetic parameters obtained, the integral method was used. Upon integration of the mass balance one can conclude that the theoretical and experimental advancement curves agree very well for various sets of experiments.

The rate law of propylene hydrogenation herein determined is crucial for subsequent modelling of a polymeric catalytic membrane reactor (pCMR), which contains the palladium nanoclusters in the polymeric matrix of the membrane.

2.6 Notation

$C_{i,s}$ concentration of the limiting reactant *i* at surface conditions, mol m^{-3}

D_e effective diffusivity coefficient, $m^2\ s^{-1}$

f number of fitting parameters

K_i	adsorption equilibrium constant for species *i*, bar^{-1}
k	rate constant for the overall hydrogenation reaction, mol g^{-1}_{Pd} s
k'	rate constant for the surface reaction, mol g^{2}_{Pd} s^{-1} $sites^{-3}$
m	number of experimental data
M	vacant active site
MSC	model selection criterion
$[M]_T$	total concentration of active sites, sites g^{-1}
P	total absolute pressure, bar
p_i, p_j	partial pressure of species *i*, *j*, bar
n_i	number of moles of species *i*, mol
n	number of reactive moles, mol
R	gas constant, m^3 bar mol^{-1} K^{-1}
R_p	particle radius, m
r_i	reaction rate for species *i*, mol g^{-1}_{Pd} s^{-1}
r_{obs}	observed reaction rate, mol g^{-1}_{Pd} s^{-1}
T	temperature, K
t	time, s
V	reactor volume, m^3
w	mass of catalyst, g
X	advancement of the reaction, -
X_{max}	maximum advancement of the reaction, -
y_i, y_j	molar fraction of species *i*, *j*, -

Greek letters

α	fitting parameter of model 2
β	fitting parameter of model 2
ξ	extent or degree of advancement of the reaction, mol
ν_i	stoichiometric coefficient for species *i*
ρ_c	density of the catalyst pellet, g cm^{-3}
Φ_S	experimental parameter, analogous to Weisz Prater modulus, -

Subscripts

I	inert species (argon)
i	species present in the reactor, i.e. H_2, C_3H_6, C_3H_8 or inert
j	reactant species present in the reactor, i.e. H_2 or C_3H_6
o	initial conditions
obs	observed/experimental conditions

2.7 References

[1] J. D. Aiken, R. G. Finke, A review of modern transition-metal nanoclusters: their synthesis, characterization, and applications in catalysis, J. Mol. Catal. A: Chem. 145 (1999) 1.

[2] M. T. Reetz, W. Helbig, S. A. Quaiser, U. Stimming, N. Breuer, R. Vogel, Visualization of surfactants on nanostructured palladium clusters by a combination of STM and High-Resolution TEM, Science 267 (1995) 367.

[3] A. Zuttel, C. Nutzenadel, G. Schmid, C. Emmenegger, P. Sudan, L. Schlapbach, Thermodynamic aspects of the interaction of hydrogen with Pd clusters, Appl. Surf. Sci. 162 (2000) 571.

[4] M. T. Reetz, S. A. Quaiser, R. Breinbauer, B. Tesche, A new strategy in heterogeneous catalysis: the design of cortex catalysts, Angew. Chem. Int. Edit. 34 (1996) 2728.

[5] H. R. Gao, Y. Xu, S. J. Liao, R. Liu, J. Liu, D. C. Li, D. R. Yu, Y. K. Zhao, Y. H. Fan, Catalytic polymeric hollow-fiber reactors for the selective hydrogenation of conjugated dienes, J. Membrane Sci. 106 (1995) 213.

[6] J. F. Ciebien, R. E. Cohen, A. Duran, Catalytic properties of palladium nanoclusters synthesized within diblock copolymer films: hydrogenation of ethylene and propylene, Supramol. Sci. 5 (1998) 31.

[7] F. Zaera, G. A. Somorjai, Hydrogenation of ethylene over platinum(111) single-crystal surfaces, J. Am. Chem. Soc. 106 (1984) 2288.

[8] H. Ofner, F. Zaera, Isothermal kinetic measurements for the hydrogenation of ethylene on Pt(111) under vacuum: significance of weakly-bound species in the reaction mechanism, J. Phys. Chem. B 101 (1997) 396.

[9] I. Horiuti, M. Polanyi, Exchange reactions of hydrogen on metallic catalysts, Trans. Faraday Soc. 30 (1934) 1164.

[10] S. Naito, M. Tanimoto, Mechanism of deuterium addition and exchange of propene over Pd/SiO_2 at lower temperatures - Direct evidence for intramolecular double-bond migration during hydrogenation, J. Catal. 102 (1986) 377.

[11] A. V. Zeigarnik, R. E. Valdes-Perez, O. N. Temkin, Metal-catalyzed ethylene hydrogenation: the method of interactive search for multiple working hypotheses, Langmuir 14 (1998) 4510.

[12] R. Campostrini, G. Carturan, R. M. Baraka, Propene hydrogenation with Pt-Ag intermetallic phases supported on SiO_2 gels, J. Mol. Catal. 78 (1993) 169.

[13] G. Rogers, M. Lih, O. Hougen, Catalytic hydrogenation of propylene and isobutylene over platinum. Effect of noncompetitive adsorption, AIChE J. 12 (1966) 369.

[14] G. Cocco, R. Campostrini, M. A. Cabras, G. Carturan, Propene hydrogenation on low-temperature reduced Pt/TiO_2 - Effects of TiO_2 phases and H_2 treatment on specific catalytic activity, J. Mol. Catal. 94 (1994) 299.

[15] W. E. Stewart, R. H. Shabaker, Y. T. Lu, Kinetics of propylene hydrogenation on platinum-alumina, Chem. Eng. Sci. 43 (1988) 2257.

[16] M. T. Reetz, W. Helbig, Size-selective synthesis of nanostructured transition-metal clusters, J. Am. Chem. Soc. 116 (1994) 7401.

[17] M. T. Reetz, M. Winter, R. Breinbauer, T. Thurn-Albrecht, W. Vogel, Size-selective electrochemical preparation of surfactant-stabilized Pd-, Ni-, and Pt/Pd colloids, Chem. Eur. J. 7 (2001) 1084.

[18] C. Sachs, A. Pundt, R. Kirchheim, M. Winter, M. T. Reetz, D. Fritsch, Solubility of hydrogen in single-sized palladium clusters, Phys. Rev. B 64 (2001) 5408.

[19] T. P. Beebe, J. T. Yates, An insitu infrared spectroscopic investigation of the role of ethylidyne in the ethylene hydrogenation reaction on Pd/Al_2O_3, J. Am. Chem. Soc. 108 (1986) 663.

[20] R. J. Koestner, M. A. V. Hove, G. A. Somorjai, Molecular structure of hydrocarbon monolayers on metal surfaces, J. Phys. Chem. 87 (1983) 203.

[21] L. R. Petzold, A. C. Hindmarsh, LSODA, Computing and Mathematics Research Division, Lawrence Livermore National Laboratory, 1997.

[22] J. B. Butt, Reaction Kinetics and Reactor Design, 2nd ed., Chapter 7, Marcel Dekker, Inc., New York, 1999.

[23] P. B. Weisz, Z. Physik. Chem., Neue Folge 11 (1957) 1.

[24] R. R. Hudgins, A general criterion for absence of diffusion control in an isothermal catalyst pellet, Chem. Eng. Sci. 23 (1968) 93.

[25] S. D. Jackson, N. J. Casey, Hydrogenation of propyne over palladium catalysts, J. Chem. Soc. Faraday T. 91 (1995) 3269.

[26] F. Delannay, Characterization of Heterogeneous Catalysts, Marcel Dekker, Inc., New York, 1984.

[27] J. Villermaux, Génie de la Réaction Chimique - Conception et Fonctionnement des Réacteurs, 2nd ed., Chapter 1, Tec & Doc - Lavoisier, Paris, 1993.

[28] G. F. Froment, K. B. Bischoff, Chemical Reactor Analysis and Design, 2nd ed., Chapter 1, John Wiley & Sons, New York, 1990.

[29] K. H. Yang, O. A. Hougen, Determination of mechanism of catalyzed gaseous reactions, Chem. Eng. Prog. 46 (1950) 146.

[30] R. J. Rennard, R. J. Kokes, Hydrogenation of ethylene and propylene over palladium hydride, J. Phys. Chem. 70 (1966) 2543.

[31] K. Christmann, The interaction of hydrogen with metal-surfaces of 2-fold symmetry, Mol. Phys. 66 (1989) 1.

[32] E. Wicke, H. Brodowsky, Hydrogen in Palladium and Palladium Alloys. In: G. Alefeld, J. Völkl (eds.), Hydrogen in Metals II. Application-oriented Properties, Topics in Applied Physics, Vol. 29, Chapter 3, Springer-Verlag, Berlin, 1978.

[33] H. Ofner, F. Zaera, Ethylene adsorption on platinum: kinetics, bonding, and relevance to catalysis, J. Am. Chem. Soc. 124 (2002) 10982.

[34] M. Aitake, Math. Sci. 14 (1976) 5.

[35] A. Borodzinski, A. Cybulski, The kinetic model of hydrogenation of acetylene-ethylene mixtures over palladium surface covered by carbonaceous deposits, Appl. Catal. A: Gen. 198 (2000) 51.

3. Propyne Hydrogenation Kinetics over Surfactant-Stabilized Palladium Nanoclusters*

Abstract

The kinetics of propyne hydrogenation over surfactant-stabilized palladium nanoclusters was studied in a batch reactor under isothermal conditions (308 K). The method of initial rates was adopted to elucidate the reaction mechanism and a rate equation was derived. Although the methodology employed does not exclude other reaction schemes, it was found that experimental rate data agree well with a Langmuir-Hinshelwood mechanism that involves non-competitive adsorption between propyne and hydrogen for the catalyst surface, where hydrogen addition in the surface reaction(s) is the limiting step. Nonlinear model fitting to initial rate data provided the kinetic parameters of the rate equation (k = 4.1 mol g_{Pd}^{-1} s^{-1} bar^{-2}; $K_{C_3H_4}$ = 8.7 x 10^2 bar^{-1} and K_{H_2} = 1.0 x 10^{-5} bar^{-1}). Finally, experimental compositions of the reaction mixture over time, as well as the overall advancement history, were compared favourably with the kinetic model through integration of the mass balance in the batch reactor.

**** L. Brandão, D. Fritsch, A. M. Mendes, L. M. Madeira, Ind. Eng. Chem. Res. 46 (2007) 377.***

3.1 Introduction

Partial hydrogenation of multiple-unsaturated hydrocarbons is an important process in the petrochemical industry. Actually, the selective hydrogenation of alkynes is a crucial step in industrial polymerization processes in order to completely eliminate alkynes and dienes from alkene feed stocks. In the particular case of the selective removal of propyne and propadiene from propylene-rich streams, high propylene yields are required without deeper hydrogenation to propane [1].

Palladium appears to be by far the most selective metal to achieve selective hydrogenations [1]. Two kinds of selectivity can be defined: mechanistic selectivity, where the rate of the alkyne hydrogenation is higher than the alkene one, and thermodynamic selectivity, where the alkyne molecule prevents the readsorption of the alkene and hence the consecutive hydrogen addition cannot take place [1]. Over palladium, alkyne and subsequent alkene hydrogenation have approximately the same rate [1], or the first reaction is even slower (*Chapter 2*). The selectivity of palladium is, therefore, attributed to the stronger adsorption of the alkyne molecule compared to that of the alkene (thermodynamic selectivity).

Although alkyne and alkene hydrogenations seem to be simple reactions, the details of the mechanisms of such transition-metal-catalyzed hydrogenation reactions are still not fully understood [2]. The palladium-catalyzed hydrogenations of ethylene and acetylene are classical catalytic reactions that have been extensively studied. Early on, it was established that adsorbed atomic hydrogen adds across the double or triple bond of the adsorbed hydrocarbon, following the so-called Horiuti-Polanyi model [3]. In these hydrogenations, hydrogen reaction orders of unity or greater have been measured, while the order in alkene or alkyne was found to be

negative. The latter effect can be rationalized by assuming that hydrogen adsorption is blocked by the alkene or alkyne, while the reasons for the hydrogen orders found are not clear [2].

Despite the large number of papers on the hydrogenation of alkynes, there are few references in the literature relating to propyne hydrogenation [4], and among those, kinetic studies of alkyne hydrogenations that provide the rate equation are also rather sparse [1]. This is the aim of the present study, where palladium nanoclusters are used as catalyst. The propyne hydrogenation rate equation herein determined is crucial for subsequent modelling of a polymeric catalytic membrane reactor (pCMR) which contains palladium nanoclusters stabilized by the polymeric matrix of the membrane.

3.2 Experimental section

The apparatus used for conducting the experiments has been described in detail in the previous chapter. Briefly, the propyne hydrogenation kinetics was studied in a jacketed batch cylindrical reactor ($V = 0.55 \times 10^{-3}$ m^3; i.d. = 8.2 cm; h = 10.5 cm) at 308 K by monitoring the total pressure history. Also, 20 to 25 mg of powder-catalyst, containing 15.71 wt. % palladium nanoclusters, was used. The metal nanoparticles, with an average diameter of about 7.3 nm (determined by X-ray diffraction (XRD)), were stabilized with the surfactant tetraoctadecylammonium bromide, *n*-$(C_{18}H_{37})_4N^+Br^-$, which prevents the aggregation of catalyst particles and shows negligible mass transport resistance (cf. *Chapter 2*). The preparation method of the surfactant-stabilized clusters is reported elsewhere [5].

The powder-catalyst was immobilized in a porous support (polyester textile) attached to a magnetic bar (with a cross shape and stirred at 600 rpm). This assembly was inserted into the batch reactor (cf. *Chapter 2*).

First, several experiments with different initial propyne/hydrogen molar ratios, at an initial total pressure of 1.0 bar, were carried out and the total pressure history was monitored. The fraction of inert (argon) was 0.70. Three experiments were performed for each gas phase composition, after reaching the steady catalytic activity. These three experiments were reproducible within ± 5 % relative error. It is worth mentioning that the steady catalytic activity was reached after performing two or three consecutive runs with the same initial gas phase composition. During this preconditioning step, a slight increase in activity and selectivity of the catalyst was noticed, when compared with the previous run under the same conditions. This phenomenon was also observed by other authors [6, 7]. For palladium regeneration, the catalyst was exposed to air between runs and then left under 1 bar of hydrogen pressure before the next run.

A second set of runs where the initial total pressure was varied between 0.3 and 9.0 bar was also performed, at a constant initial propyne/hydrogen molar fraction of $y_{H_2o} : y_{C_3H_4o} =$ 0.03:0.15.

Complete characterization of the catalyst has been described at *Chapter 2*. An active surface area of the nanostructured palladium clusters of 27 $m^2\ g_{Pd}^{-1}$ (metallic dispersion of 6.1 %) was obtained by CO chemisorption. Scanning electron microscopy (SEM)/energy dispersive X-ray spectroscopy (EDS) techniques were used to access the structure and size of the catalyst aggregates, because they could be affected by the procedure used to immobilize the Pd clusters in the textile support. It was concluded that the size of the metallic nanoclusters on the support is retained and that the procedure used to immobilize the catalyst does not liberate the Pd clusters from the surfactant shell.

To evaluate if internal mass transport limitations were significant during the hydrogenation reactions, due to the presence of the surfactant, well-known intraparticle transport criterion was used. This criterion makes use of the following parameter, analogous to the Weisz-Prater modulus and defined as $\Phi_S = r_{obs}\rho_c R_p^2 / \left(D_e C_{i,s}\right)$, which expresses the ratio of chemical reaction rate to diffusive flux (r_{obs} is the observed reaction rate, $\rho_c \sim 1.8$ g cm^{-3} is the density of the catalyst particle obtained by He pycnometry, R_p is the radius of the catalyst particle, $C_{i,s}$ is the concentration of the limiting reactant at surface conditions and $D_e \sim 2.6 \times 10^{-7}$ m^2 s^{-1} is the hydrocarbon effective diffusivity coefficient in the surfactant shell). The absence of internal mass transfer resistances (kinetic regime) is observed when Φ_S is sufficiently small ($\Phi_S << 1$), assuring that the chemical reaction rate is much lower when compared with the diffusive flux. This situation was observed in the previous chapter for the propylene hydrogenation over the same surfactant-stabilized palladium catalyst. According to this, it becomes clear that propyne hydrogenation also proceeds under the kinetic regime, as r_{obs} is an order of magnitude lower than the observed reaction rate during propylene hydrogenation. This is valid because all the parameters, including the concentration of the limiting reactant, are approximately equal in both hydrogenations.

The possibility of having external resistances to mass transfer was evaluated by employing different rotation speeds in the porous support/magnetic bar assembly. However, this did not change the apparent reaction rate, thus evidencing that external mass transfer effects are also absent.

Gas chromatography was used to analyze the gas mixture composition during the course of the reaction. The samples from the batch reactor were kept in a Multiposition Valve Actuator (Valco Inc.), with 12 loops and 50 μL each, which was connected to the injector. The samples

were supplied to the gas chromatograph (Dani GC 1000 equipped with a Flame Ionization Detector and a Thermal Conductivity Detector - Valco Inc.) with argon as carrier gas. The different compounds were separated using a 30 m capillary plot-fused silica column (GS-GasPro, J&W). The temperature program used started at 50 ºC and ended at 130 ºC, with a rate of 10 ºC min^{-1}. The analysis method allowed for simultaneous quantification of hydrogen, propyne, propylene and propane.

A gravimetric method was employed to measure pure component isothermal adsorption equilibrium data for propyne and propylene on the palladium nanoclusters. The equilibrium data were determined on a Rubotherm suspension magnetic balance, which has a 0.01 mg weighting resolution and a 0.02 mg reproducibility. The entire system was fully thermostated at 308 K.

The parameters of the rate equation were obtained by fitting the model to the experimental data using a nonlinear least squares approach implemented with a commercially available statistics software (JMP® [8]). For integration of the mass balances, the time dependent equations were solved using LSODA [9].

3.3 Results and discussion

The methodology adopted to obtain the rate equation for propyne hydrogenation over palladium nanoclusters, at 308 K, was the method of initial rates, first established by Yang and Hougen [10]. As mentioned above, several experiments performed in a batch reactor provided total pressure versus time curves, from which the advancement history and initial reaction rates can be computed. For that, one needs to use the concepts of [11]: *i)* extent or degree of advancement of a reaction:

$$\xi = \frac{n_i - n_{i,o}}{\nu_i} \tag{3.1}$$

where n_i and $n_{i,o}$ are the mole number of species *i* present in the reactor at instant *t* and at the initial instant, respectively, and ν_i is the stoichiometric coefficient for species *i*, and *ii)* normalized advancement:

$$X = \frac{\xi}{n_o} \tag{3.2}$$

where n_o is the total number of reactive moles at the beginning of the run. Assuming ideal gas behaviour for the gaseous mixture, advancements along time were computed using the following equation:

$$X(t) = \frac{1 - P(t)/P_o}{1 - y_{I,o}} \tag{3.3}$$

where P_o is the initial total pressure and $y_{I,o}$ is the initial molar fraction of inert. To obtain the initial reaction rates, advancement data for propyne hydrogenation were calculated for short reaction times where propyne hydrogenation was the main reaction and propylene hydrogenation was highly suppressed (otherwise Eq. (3.3) would not apply because the total pressure change would be due to both consecutive reactions). Furthermore, gas chromatography analyses confirmed the reduced propane formation during propyne hydrogenation. For runs with initial propyne/hydrogen molar ratios higher than 1, propane was not present to a considerable extent during the whole run. On the other hand, runs with excess of hydrogen indicated that propane formation was suppressed only during the first part of the advancement history. This will be explained later in the text.

Initial reaction rates, obtained from the slopes of *X* versus *t* curves for the initial instant ($t = 0$), were then computed using Eq. (3.4), which was deduced from a mass balance to the batch reactor [11]:

$$r = \frac{P_o V\left(1 - y_{I,o}\right)}{wRT}\frac{\mathrm{d}X}{\mathrm{d}t} \tag{3.4}$$

where V is the volume of the reactor and w is the mass of palladium catalyst.

The initial reaction rates for propyne hydrogenation under different initial compositions of the reaction mixture were determined at 1.0 bar (Fig. 3.1). The results indicate that the propyne hydrogenation rate decreases almost linearly with the propyne initial fraction (except for very low hydrocarbon concentrations), thus indicating the opposite trend for hydrogen (the inert fraction is kept constant in the runs). Figure 3.2 shows the effect of the total pressure in the initial

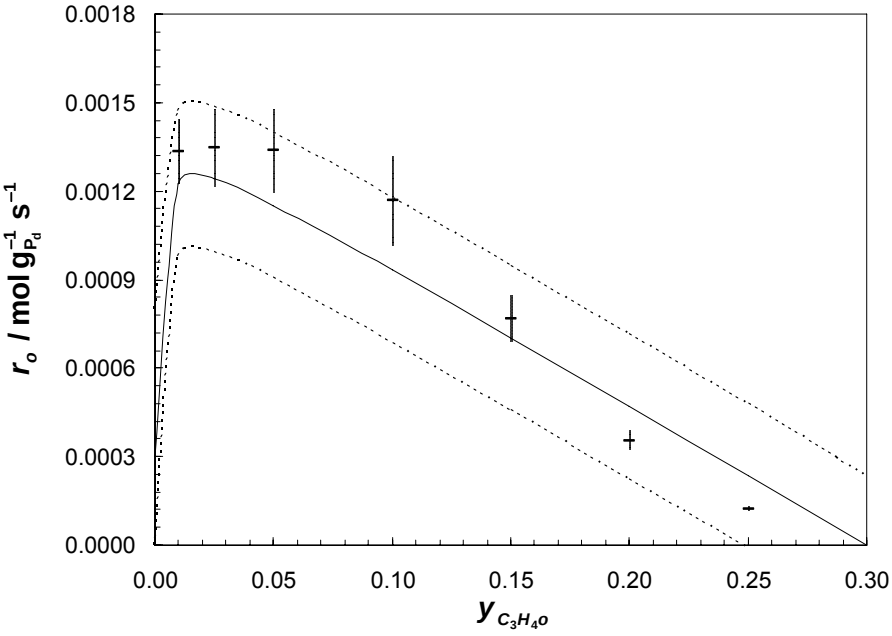

Fig. 3.1 Initial rates of propyne hydrogenation as a function of the initial propyne molar fraction (P_o = 1.0 bar; $y_{I,o}$ = 0.70; T = 308 K). The error bars for the mean values were obtained for a 95 % confidence level (t distribution), using at least three experimental results. The solid line corresponds to the model fitting and dashed lines are the confidence curves (for a 95 % confidence level).

hydrogenation rate, keeping the hydrogen/propyne ratio constant. Here the initial reaction rate increases almost linearly with the initial total pressure.

The graphical methodology proposed by Yang and Hougen [10], which was employed in the present study, indicates from the shape of both curves (Figs.3.1 and 3.2), that the surface reaction is the limiting step. The shape of Fig. 3.2 also suggests that, in the surface reaction, hydrogen adsorption is very limited, an important issue that will be discussed later on. Such a surface-reaction-limited mechanism is in agreement with most of the studies found in the open literature regarding the hydrogenation of alkenes and alkynes, e.g. [2, 7]. It is however worth

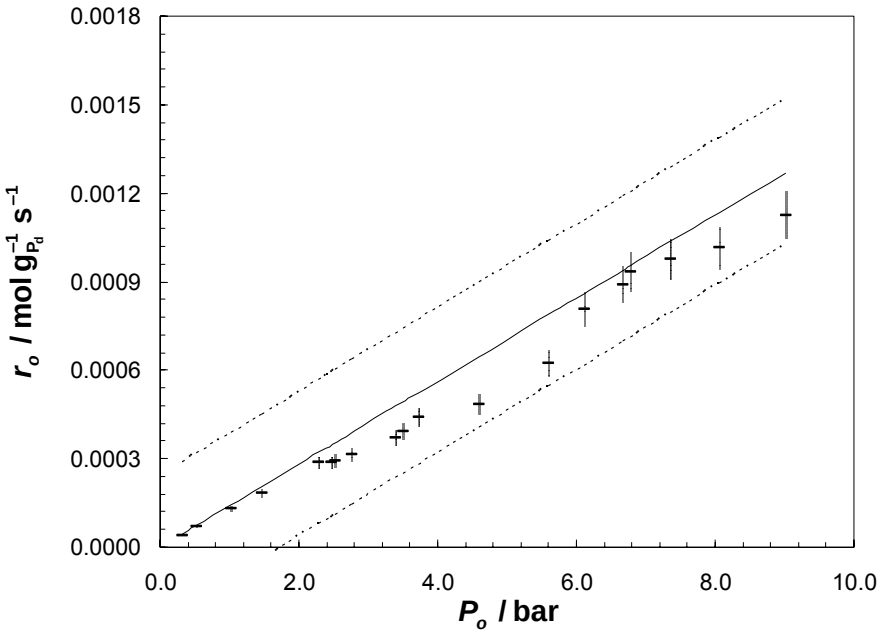

Fig. 3.2 Initial rates of propyne hydrogenation as a function of the initial total pressure ($y_{H_2\,o}$: $y_{C_3H_4\,o}$ = 0.03:0.15; T = 308 K). The error bars were obtained by the error propagation method. The solid line corresponds to the model fitting and dashed lines are the confidence curves (for a 95 % confidence level).

mentioning that the trends shown by the curves point toward the possibility of considering also other reaction mechanisms, for instance, adsorption-limited reactions. However, a reasonable fitting to the corresponding reaction rate equations, when considering the data of both figures (Fig. 3.1 and Fig. 3.2) simultaneously, was not possible to obtain, as shown below.

The reaction mechanism could therefore be described by the following steps:

$$H_2(g) + 2Z \leftrightarrow 2H - Z \tag{3.5}$$

$$C_3H_4(g) + S \leftrightarrow C_3H_4 - S \tag{3.6}$$

$$C_3H_4 - S + H - Z \rightarrow C_3H_5 - S + Z \tag{3.7}$$

$$C_3H_5 - S + H - Z \rightarrow C_3H_6 - S + Z \tag{3.8}$$

$$C_3H_6 - S \leftrightarrow C_3H_6(g) + S \tag{3.9}$$

Equation (3.5) takes into account the dissociative adsorption of hydrogen on Pd surface active sites (Z), while Eq. (3.6) describes the adsorption/desorption equilibrium of propyne at different surface sites (S). Equations (3.7) and (3.8) describe the first and second hydrogen addition to adsorbed propyne. Finally, Eq. (3.9) takes into account the desorption of propylene. Considering all these steps different mechanisms were formulated (i.e. with different rate-limiting steps) and the corresponding kinetic equations were derived. Then, a criterion based upon statistical analysis was used to discriminate between possible kinetic models.

In this way, assuming that the simultaneous atomic hydrogen additions are the limiting steps, that is, Eqs. (3.7) and (3.8) are conjugated such that two adsorbed hydrogen atoms are added at the same time to adsorbed propyne, and using a Langmuir-Hinshelwood (L-H) formulation for noncompetitive adsorption [10], one can easily derive the overall rate of propyne hydrogenation:

$$-r_{C_3H_4} = \frac{k\, p_{C_3H_4}\, p_{H_2}}{\left(1 + K_{C_3H_4}\, p_{C_3H_4} + K_{C_3H_6}\, p_{C_3H_6}\right)\left(1 + \sqrt{K_{H_2}\, p_{H_2}}\right)^2} \quad (3.10)$$

where k is the overall kinetic constant (which involves also both $K_{C_3H_4}$ and K_{H_2}) and K_i and p_i represent the adsorption equilibrium constant and partial pressure of species i, respectively. From the experiments described above one can determine the kinetic parameters of the propyne hydrogenation reaction at 308 K. This way, Eq. (3.10) was fitted to the experimental data at the initial conditions (therefore, $K_{C_3H_6}$ cannot be determined because $p_{C_3H_6o} = 0$). The resolution of a nonlinear least squares problem provided the following parameters of the rate law: k = 4.1 mol g_{Pd}^{-1} s^{-1} bar^{-2}; $K_{C_3H_4}$ = 8.7 x 10^2 bar^{-1} and K_{H_2} = 1.0 x 10^{-5} bar^{-1}. The confidence limit interval for a 95 % confidence level of the nonlinear regression is also plotted in Figs. 3.1 and 3.2. The confidence limit accounts for the uncertainty in both the parameter estimates and in the error for the model. The results indicate a reasonable adhesion of the model to the experimental values. However, the confidence limits for k and $K_{C_3H_4}$ are large.

The rate equation presented (Eq. (3.10)) is typical of L-H kinetics, with non-competitive adsorption between reactants for the catalyst surface. However, it can be seen that there is a preferential adsorption of the alkyne relative to hydrogen (adsorption constants of 8.7 x 10^2 and 1.0 x 10^{-5} bar^{-1}, respectively). The non-competitive adsorption was also observed in an earlier study using temperature programmed desorption of coadsorbed hydrogen and acetylene on Pd(111) [12]. This indicated that acetylene adsorption was still observed even with a saturated hydrogen overlayer on the catalyst surface at 180 K [12]. Moreover, another work, performed on the hydrogenation of acetylene over commercial palladium catalysts, at 300 K, also addressed the presence of uncompetitive hydrogen surface sites at the catalyst surface [6]. On the other hand, even though the reactants do not compete for surface sites, alkynes lower hydrogen adsorption

due to steric hindrance, as is evident from the low K_{H_2} value obtained. This is probably related to the high adsorption capacity of the catalyst surface toward the large alkyne molecules. This hydrocarbon steric hindrance was also evidenced in earlier studies, in which hydrogen adsorption was highly suppressed over an ethylene covered platinum surface, under low pressure and temperature conditions [13, 14].

The simultaneous atomic hydrogen addition to propyne was assumed to limit the surface reaction (actually, it is not possible to distinguish between the second or simultaneous addition), despite Stacchiola et al. [2] having reported that the first hydrogen addition is the rate liming step in alkyne and alkene hydrogenations under low-pressure conditions. In fact, during ethylene hydrogenation over Pd(111), the rate constant for the addition of the first hydrogen to form ethyl species was found to be smaller than that of the second hydrogen addition [15]. But some controversy exists. For instance, Molero et al. [16] emphasized that this does not necessarily imply that the addition of the first hydrogen is the rate-limiting step under catalytic high-pressure reaction conditions. They mentioned that it also depends on the reactant coverages, and the steady-state ethylene coverage is likely to be higher than that of the ethyl intermediate, thus potentially overwhelming any differences in the intrinsic rate constants. Other reports revealed the controversy on hydrocarbon hydrogenation, and some of them concluded that the further hydrogenation of a half hydrogenated alkyl intermediate to the alkene is the rate liming step of the whole process [17, 18].

In any case, the methodology adopted and previously described does not exclude these other reaction mechanisms. With this in mind, some of the possibilities found in the literature were tested. Then, the following model selection criterion (MSC) was adopted [19]:

$$\mathrm{MSC} = \ln\left[\frac{\sum_{i=1}^{m}\left(r_{oobs,i} - \overline{r_{oobs}}\right)^2}{\sum_{i=1}^{m}\left(r_{oobs,i} - r_{ocal,i}\right)^2}\right] - \frac{2f}{m} \tag{3.11}$$

where m is the number of experimental points, f is the number of fitting parameters and $\overline{r_{oobs}}$ is the mean of the experimental results. The model selection criterion adopted gives higher MSC values for models that fit better to experimental data and for models with less fitting parameters and, therefore, allows comparison of different models.

Table 3.1 **s**hows the models considered, ranked by the MSC parameter. Model 1 is proposed in the present study, while model 2 takes into account a dissociative hydrogen adsorption-limited mechanism. Model 3 takes into account the reaction between adsorbed propyne and gas phase hydrogen as the limiting step, in the so-called Rideal-Eley mechanism. On the other hand, models 4-7 consider that the limiting step is the surface reaction with the adsorption of propyne and hydrogen on the same catalyst active sites and dissociation of hydrogen, with the exception of model 5, where hydrogen adsorption is molecular. The main difference between these four models is the hydrogen addition. In model 4, the second hydrogen addition is the limiting step. Model 5 assumes that the molecular hydrogen addition is the limiting step of the reaction. In model 6, the first hydrogen addition is the limiting one, and in model 7, the simultaneous addition is used. Finally, model 8, which is also a reaction-limited mechanism, takes into account different adsorption sites at the catalyst surface for propyne and hydrogen, with dissociative hydrogen adsorption. Here, the first hydrogen addition is the liming step. Using the above-mentioned statistic, it is clear that the reaction mechanism herein described provided the reaction rate equation that yields the best fit to the experimental data herein obtained.

Table 3.1 Initial reaction rate equations employed to fit propyne hydrogenation data and corresponding model selection criterion (MSC) values.

Model Nr.	$-r_{C_3H_4o}$	MSC
1	$\frac{k\,p_{H_2o}\,p_{C_3H_4o}}{\left(1+K_{C_3H_4}\,p_{C_3H_4o}\right)\left(1+\sqrt{K_{H_2}\,p_{H_2o}}\right)^2}$	2.73
2	$\frac{k\,p_{H_2o}}{\left(1+K_{C_3H_4}\,p_{C_3H_4o}\right)^2}$	2.67
3	$\frac{k\,p_{H_2o}\,p_{C_3H_4o}}{1+K_{C_3H_4}\,p_{C_3H_4o}}$	2.02
4	$\frac{k\,p_{H_2o}\,p_{C_3H_4o}}{\left(1+K_{C_3H_4}\,p_{C_3H_4o}+\sqrt{K_{H_2}\,p_{H_2o}}\right)^2}$	2.02
5	$\frac{k\,p_{H_2o}\,p_{C_3H_4o}}{\left(1+K_{C_3H_4}\,p_{C_3H_4o}+K_{H_2}\,p_{H_2o}\right)^2}$	1.97
6	$\frac{k\sqrt{p_{H_2o}}\,p_{C_3H_4o}}{\left(1+K_{C_3H_4}\,p_{C_3H_4o}+\sqrt{K_{H_2}\,p_{H_2o}}\right)^2}$	1.73
7	$\frac{k\,p_{H_2o}\,p_{C_3H_4o}}{\left(1+K_{C_3H_4}\,p_{C_3H_4o}+\sqrt{K_{H_2}\,p_{H_2o}}\right)^3}$	1.25
8	$\frac{k\sqrt{p_{H_2o}}\,p_{C_3H_4o}}{\left(1+K_{C_3H_4}\,p_{C_3H_4o}\right)\left(1+\sqrt{K_{H_2}\,p_{H_2o}}\right)}$	0.75

The use of power-law rate equations can be of interest in several applications, although no phenomenological explanation is behind their formulation. Reaction orders of (*a*) -0.02 and (*b*) 1.09 for propyne and hydrogen partial pressures, respectively, were obtained for a power-law type model ($-r_{C_3H_4}=k\,p_{C_3H_4}^{a}\,p_{H_2}^{b}$) fitted to the initial rate data herein obtained. The MSC value obtained was 2.95 for the power-law kinetics case; despite of the higher MSC value when compared to Model 1, this rate equation does not take into account any reaction mechanism. The

representation of the power-law kinetics computed rates *vs.* the experimental results is shown in Fig. 3.3. Comparing the power-law model with Eq. (3.10) under initial conditions, allows to conclude that both provided similar orders for the reactants partial pressures because $K_{C_3H_4}$ is very high (thus, $K_{C_3H_4}\, p_{C_3H_4} >> 1$ and $1 >> \sqrt{K_{H_2}\, p_{H_2}} \Rightarrow -r_{C_3H_4} \approx k' p_{H_2}$).

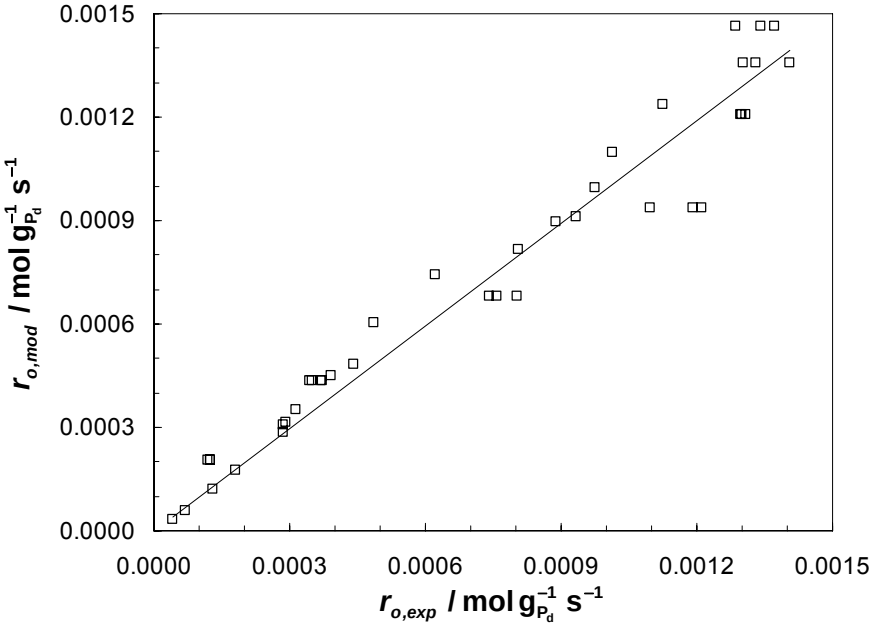

Fig. 3.3 Comparison of initial reaction rates for propyne hydrogenation obtained by fitting a power-law model to the experimental results.

It was addressed by several authors that the negative to zero orders for alkyne partial pressures indicate that the hydrogen adsorption competes unfavourably with that of the alkyne, where alkyne is ascribed as site locking [16, 20, 21]. Specific reports of propyne hydrogenation over palladium [22-24] also showed the same reaction orders for propyne and hydrogen as those here found. So, the positive order toward hydrogen (1.09) indicates that hydrogen is weakly

adsorbed on the catalyst surface and its surface coverage should be correspondingly low, in agreement with the small K_{H_2} value obtained. The almost zero order toward propyne indicates a strongly adsorbed species and that its catalyst surface coverage should be high, in accordance with the high $K_{C_3H_4}$ value obtained.

For validation of both the proposed rate law (Eq. (3.10)) and the kinetic parameters determined by the nonlinear regression, the integral method was used [10]. However, it must now be taken into account that during the course of the reaction (longer reaction times) further hydrogenation to propane can eventually occur. Therefore, the rate equation for propylene hydrogenation is also required. This was determined in the previous chapter, also using surfactant-stabilized palladium nanoclusters at 308 K:

$$r_{C_3H_8} = \frac{k' K'_{H_2} K'_{C_3H_6} p_{H_2} p_{C_3H_6}}{\left(1 + \sqrt{K'_{H_2} p_{H_2}} + K'_{C_3H_6} p_{C_3H_6}\right)^3} \tag{3.12}$$

where the parameters of the rate equation are: k' = 5.57 mol g_{Pd}^{-1} s^{-1}, K'_{H_2} = 3.80 × 10^{-2} $bar^{-1}$and $K'_{C_3H_6}$ = 0.996 bar^{-1}.

Now, the concepts of degree of advancement of a reaction and normalized advancement should be extended for the two reactions, propyne hydrogenation (reaction 1) and propylene hydrogenation (reaction 2). Assuming ideal gas behavior for the gaseous mixture, the mass balances to the batch reactor can be simplified into a system of two ODE's, Eqs. (3.13) and (3.14):

$$\frac{P_o V\left(1 - y_{I,o}\right)}{wRT} \frac{\mathrm{d}X_1}{\mathrm{d}t} = \alpha \frac{k\, p_{C_3H_4} p_{H_2}}{\left(1 + K_{C_3H_4} p_{C_3H_4} + K_{C_3H_6} p_{C_3H_6}\right)\left(1 + K_{H_2} p_{H_2}\right)^2} \tag{3.13}$$

$$\frac{P_o V(1-y_{I,o})}{wRT}\frac{dX_2}{dt} = \beta \frac{k' K'_{H_2} K'_{C_3H_6} p_{H_2} p_{C_3H_6}}{\left(1+\sqrt{K'_{H_2} p_{H_2}} + K'_{C_3H_6} p_{C_3H_6}\right)^3} \quad (3.14)$$

where α and β are model variables associated with the propyne/propylene adsorption selectivity for the palladium catalyst. From the mono-component adsorption isotherms shown in Figures 3.4A and 3.4B one could conclude that the amount of propyne adsorbed on the catalyst is an order of magnitude higher than that of propylene. The amounts adsorbed as a function of the hydrocarbon partial pressure were fitted to monocomponent Langmuir equations, which fittings are included in Fig. 3.4 and the parameters obtained are given in Table 3.2. Then, the IAST [25] (Ideal Adsorption Solution Theory) model was used to determine the bicomponent propylene/propyne adsorption isotherms, which are also shown in Fig. 3.4. The ratio between the hydrocarbon adsorption concentration, given by the IAST isotherm and the Langmuir equation fitting, allowed computation of the α and β values during the course of the reaction (α for propyne and β for propylene). From Fig. 3.4A, it is clear that β ranges between one, for high propylene fractions, and zero, for low propylene fractions. On the other hand, α (Fig. 3.4B) is always around one, independently of the propyne fraction. If these variables had not been introduced, the experimental results could not be described by the proposed model because the formation of propane would be too high (it must be remarked that the rate laws were established under initial conditions, i.e., when the other hydrocarbons are not present in the reaction mixture). This result is not surprising because the propylene hydrogenation rate is higher than the propyne one over the palladium catalyst (cf. *Chapter 2*). The selectivity of palladium is, therefore, attributed to the stronger adsorption of propyne compared to that of propylene (thermodynamic selectivity). Actually, in studies concerning acetylene hydrogenation over

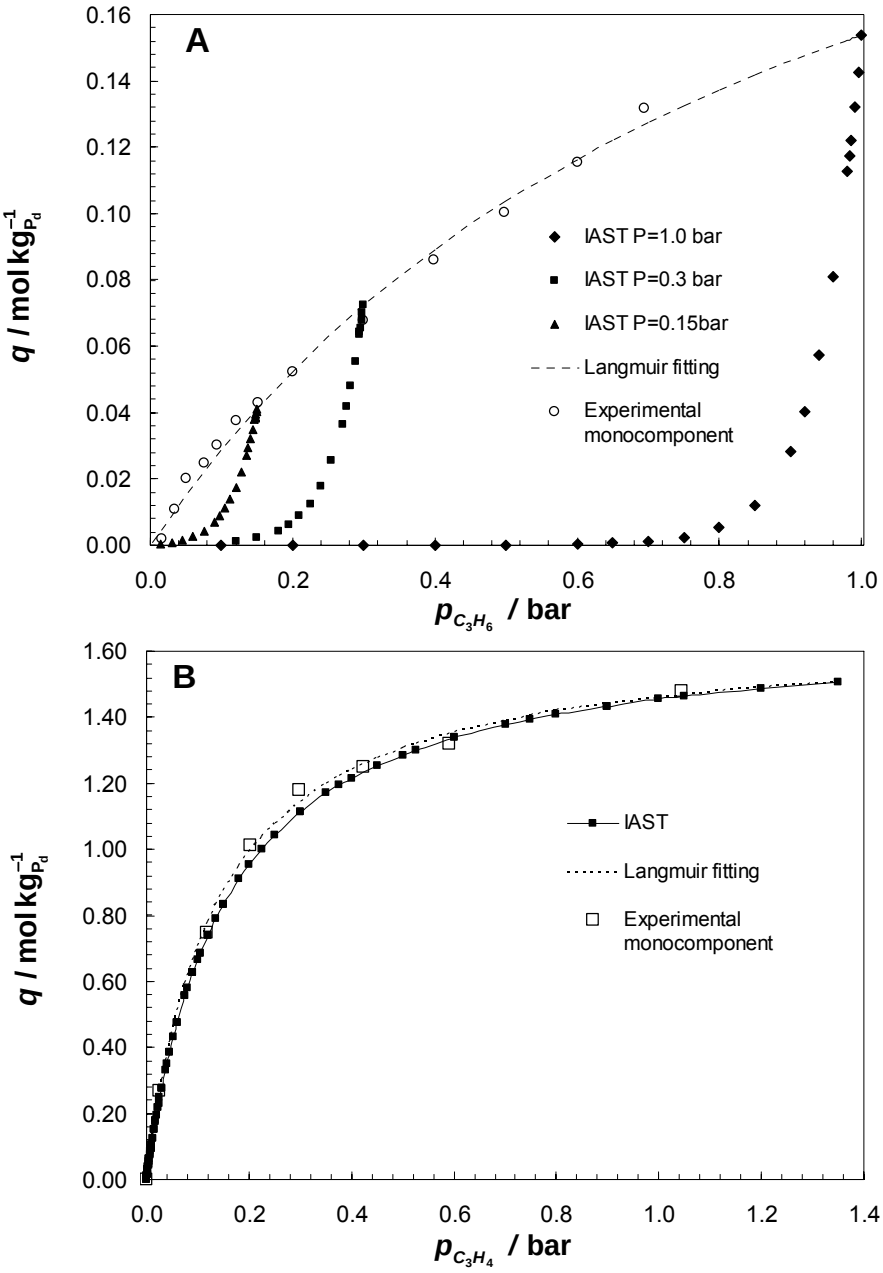

Fig. 3.4 Monocomponent adsorption equilibrium isotherms on surfactant-stabilized palladium nanoclusters at 308 K for propylene (A) and propyne (B) and corresponding bicomponent isotherms determined by the IAST method.

palladium, it has been reported that the rate of ethylene hydrogenation is slow when the feedstock contains acetylene and that ethylene hydrogenation is accelerated with high levels of acetylene conversion [26]. Therefore, the α and β model variables used for the propylene/propyne system probably depend only on the adsorption equilibrium isotherms over the palladium catalyst, as they allow describing reasonably well the experimental advancement history curves and the concentrations of all reagents and products during the course of the reaction, as shown below.

Table 3.2 Parameters obtained for the monocomponent adsorption equilibrium Langmuir fitting, $q = aP/(1+bP)$, to experimental data shown in Fig. 3.4.

Component	a / mol kg_{Pd}^{-1} bar^{-1}	b / bar^{-1}
C_3H_4	1.24×10^{1}	7.49
C_3H_6	3.18×10^{-1}	1.07

Assuming ideal gas behavior, reagents and products partial pressures in the rate equations (3.10) and (3.12) were substituted using the advancement for each reaction:

$$p_j = P_o\left[y_{j,o} + (1 - y_{1,o})\sum_{i=1}^{2} \nu_i X_i \right] \tag{3.15}$$

where i = 1 or 2 refers to propyne or propylene hydrogenation, respectively. Then, Eqs. (3.13) and (3.14) were integrated using the kinetic parameters mentioned above, together with an optimization step for determination of $K_{C_3H_6}$ in reaction 1. The optimization indicated that $K_{C_3H_6}\, p_{C_3H_6}$ is negligible in the term $\left(1 + K_{C_3H_4}\, p_{C_3H_4} + K_{C_3H_6}\, p_{C_3H_6}\right)$ for the reaction conditions of the experiments in this study, due to the high adsorption constant for propyne. A low $K_{C_3H_6}$ value is supported by the propyne/propylene bicomponent adsorption equilibrium isotherm

determined by the IAST method, once propylene adsorption is inhibited in the presence of propyne.

Figures 3.5 and 3.6 show the plots of some experimental and calculated advancement (X_1 + X_2) history curves. The figures were represented using a dimensionless time for better visualization, which was defined as the ratio between the reaction time and the final reaction time observed during the experiment (t_f). In all cases, integration of the mass balance describes quite well the experimental advancement data. Figure 3.5 shows that when propyne is the liming species ($y_{C_3H_4o}$ = 0.01 or 0.05), a sudden change in the advancement curve slope can be observed

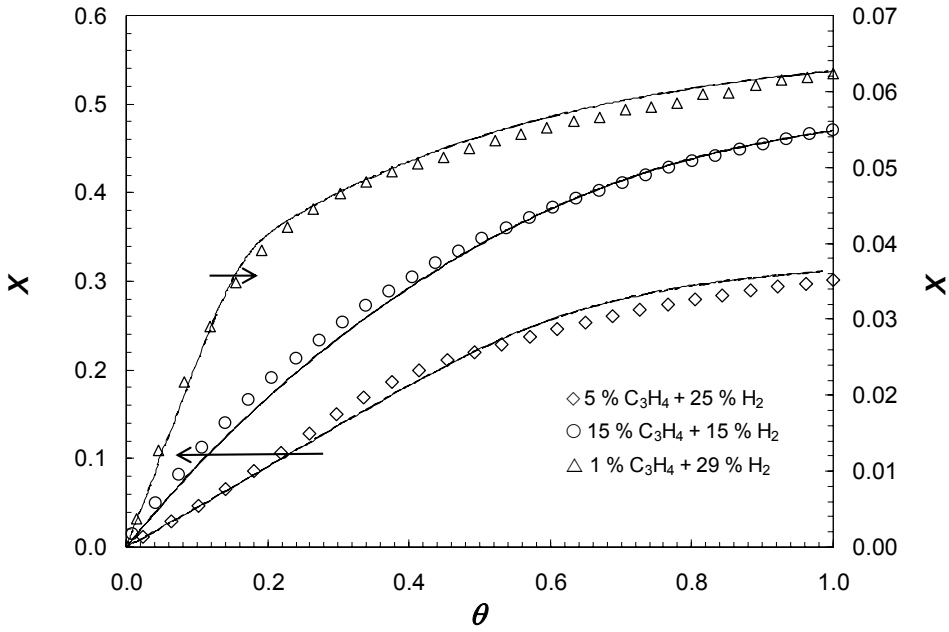

Fig. 3.5 Advancement of propyne and propylene hydrogenation as a function of the dimensionless time ($\theta = t / t_f$) for different initial compositions of the reaction mixture: (△) t_f = 380 s; (◇), t_f = 720 s; (○) t_f = 2 500 s, (P_o = 1.0 bar; $y_{I,o}$ = 0.70; T = 308 K; the number of experimental points was reduced for a better visualization). The solid line is the proposed model (Eqs. (3.13) and (3.14)).

when the propylene hydrogenation becomes significant, i.e., when propyne is almost depleted. When hydrogen is the limiting species, almost only propyne hydrogenation is observed without subsequent conversion into propane. It is still worth noting that the advancement curves tend to a maximum value, indicating that conversion of the limiting reactant j was almost complete. However, such a value depends on the initial compositions, as can be deduced from Eq. (3.15):

$$X_{\max} = \sum_{i=1}^{2} X_{\max,i} = \sum_{i=1}^{2} \frac{y_{j,o_i}}{\left(1 - y_{I,o}\right)} \tag{3.16}$$

In Fig. 3.6, where hydrogen is the limiting reagent and the initial composition is the same in all the runs, the curves tend to the same value (0.167). When propyne is the limiting species,

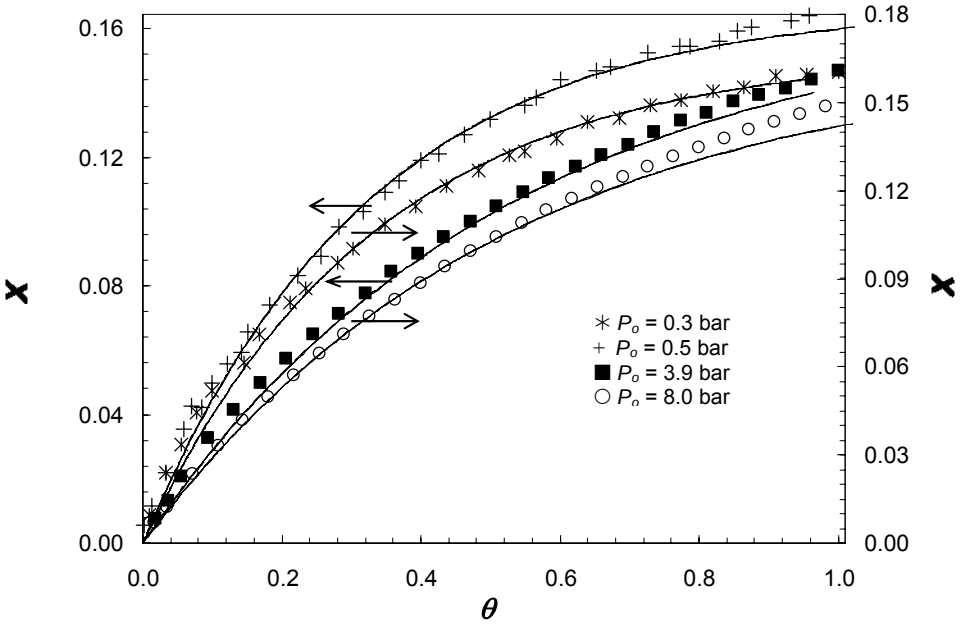

Fig. 3.6 Advancement of propyne and propylene hydrogenation as a function of the dimensionless time ($\theta = t / t_f$) for different initial total pressures: (∗) t_f = 3 700 s; (+) t_f = 3 600 s; (■) t_f = 2 200 s; (○) t_f = 2 300 s; ($y_{H_2o} : y_{C_3H_4o}$ = 0.030:0.15; T = 308 K; the number of experimental points was reduced for a better visualization). The solid line is the proposed model (Eqs. (3.13) and (3.14)).

the maximum advancement should consider the contribution of both consecutive hydrogenations, as shown in Eq. (3.16). Results shown in Fig. 3.5 tend to the values predicted by such an equation.

Finally, the history of the reaction mixture composition and the calculated compositions are illustrated in Fig. 3.7. One can see that the model predicts reasonably well the concentrations of all reagents and products during the course of the reaction for an initial composition of $y_{H_2o} : y_{C_3H_4o}$ = 0.20:0.10 and for an initial total pressure of 1.5 bar. The total pressure in this run was high enough to allow the withdraw of samples from the reactor to the gas chromatograph, while the composition chosen also allowed the formation of all the possible products of the

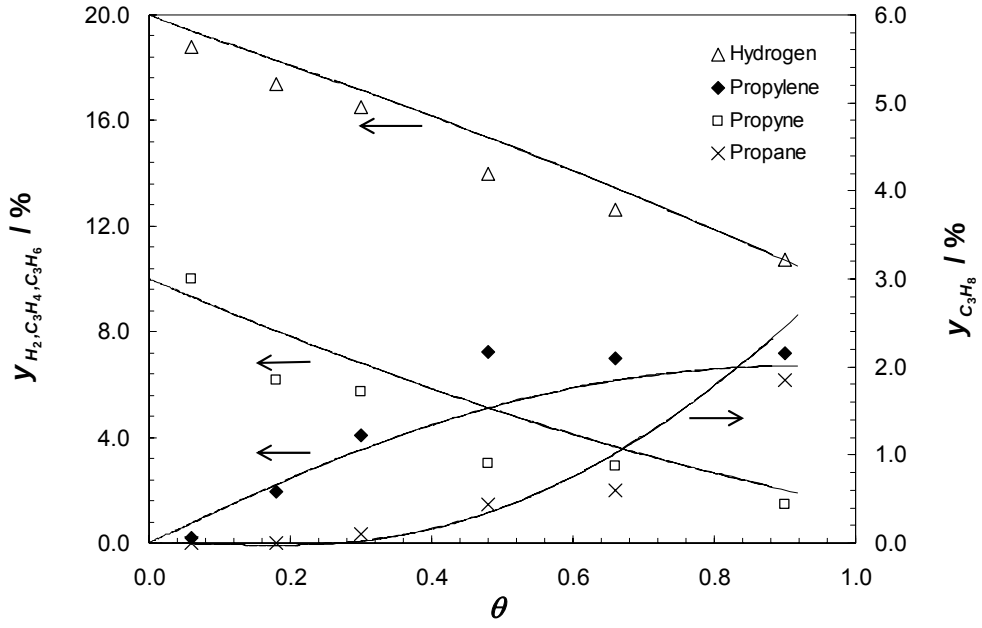

Fig. 3.7 Experimental composition history of the reaction mixture for an initial reaction composition of $y_{H_2o} : y_{C_3H_4o}$ = 0.20:0.10, P_o = 1.5 bar; ($\theta = t / t_f$), t_f = 1 000 s. The solid line is the proposed model (Eqs. (3.13) and (3.14)).

reaction in amounts acceptable for being analyzed. Although the conditions used in this experiment have not been employed in the previous runs, it is noteworthy that the model predicts quite well the hydrogen and propyne consumption, with the simultaneous propylene formation and the deeper hydrogenation to propane.

3.4 Conclusions

In the present chapter, the kinetics of propyne hydrogenation was studied under isothermal conditions (308 K) using surfactant-stabilized palladium nanosized clusters as catalyst and the method of initial rates was adopted to establish the reaction mechanism. Although this approach does not exclude other reaction schemes, a simple Langmuir-Hinshelwood model has been used to fit experimental kinetic data for propyne hydrogenation over the Pd nanoclusters.

The mechanism is described by a noncompetitive adsorption of the reagents, where the limiting step is the surface reaction. The corresponding L-H rate equation represents reasonably well the experimental data of propyne hydrogenation rate, with the kinetic parameters being determined by nonlinear regression analysis.

For validation of both the proposed rate law and the kinetic parameters obtained, the integral method was used. Upon integration of the mass balance it was concluded that the calculated and experimental advancement curves agree fairly well for various sets of experiments.

The simple kinetic rate equation of the propyne hydrogenation over surfactant-stabilized palladium nanosized clusters herein determined will be subsequently used for modelling a continuous polymeric catalytic membrane reactor.

3.5 Notation

a	Langmuir adsorption isotherm parameter, mol kg^{-1}_{Pd} bar^{-1}
b	Langmuir adsorption isotherm parameter, bar^{-1}
$C_{i,s}$	concentration of the limiting reactant i at surface conditions, mol m^{-3}
D_e	effective diffusivity coefficient, m^2 s^{-1}
f	number of fitting parameters
K_i	adsorption equilibrium constant for species i in the propyne hydrogenation, bar^{-1}
$K_i^{'}$	adsorption equilibrium constant for species i in the propylene hydrogenation, bar^{-1}
k	rate constant for the overall propyne hydrogenation, mol g^{-1}_{Pd} s^{-1} bar^{-2}
k'	rate constant for the propylene hydrogenation, mol g^{-1}_{Pd} s^{-1}
m	number of experimental data
MSC	model selection criterion
n_i	number of moles of species i, mol
n_o	total number of reactive moles at the beginning of the run, mol
P	total absolute pressure, bar
p_i, p_j	partial pressure of species i, j, bar
q	adsorbed concentration, mol kg^{-1}
R	gas constant, m^3 bar mol^{-1} K^{-1}
R_p	particle radius, m
r_i	reaction rate for species i, mol g^{-1}_{Pd} s^{-1}
r_{obs}	observed reaction rate, mol g^{-1}_{Pd} s^{-1}
T	temperature, K
t	time, s
V	reactor volume, m^3
w	mass of catalyst, g
X	normalized advancement of the reaction, -
y_i	molar fraction of species i, -

Greek letters

α, β	model variables associated with the catalyst selectivity for propyne/propylene, -

ξ extent or degree of advancement of the reaction, mol

ν_i stoichiometric coefficient for species *i*

θ normalized time, -

ρ_c density of the catalyst pellet, g cm^{-3}

Φ_S experimental parameter, analogous to Weisz Prater modulus, -

Subscripts

cal calculated/computed data

f final conditions

I inert species (argon)

i,j species present in the reactor, i.e. H_2, C_3H_4,C_3H_6, C_3H_8 or inert

o initial conditions

obs observed/experimental conditions

1 reaction 1 – propyne hydrogenation

2 reaction 2 – propylene hydrogenation

3.6 References

[1] A. Molnár, A. Sárkány, M. Varga, Hydrogenation of carbon-carbon multiple bonds: chemo-, region-, and stereo-selectivity, J. Mol. Cat. A: Chem. 173 (2001) 185.

[2] D. Stacchiola, F. Calaza, T. Zheng, W. T. Tysoe, Hydrocarbon conversion on palladium catalysts, J. Mol. Catal. A: Chem. 228 (2005) 35.

[3] I. Horiuti, M. Polanyi, Exchange reactions of hydrogen on metallic catalysts, Trans. Farad. Soc. 30 (1934) 1164.

[4] D. R. Kennedy, G. Webb, S. D. Jackson, D. Lennon, Propyne hydrogenation over alumina-supported palladium and platinum catalysts, Appl. Cat.A: Gen. 259 (2004) 109.

[5] M. T. Reetz, W. Helbig, Size-selective synthesis of nanostructured transition-metal clusters, J. Am. Chem. Soc. 116 (1994) 7401.

[6] D. Duca, F. Arena, A. Parmaliana, G. Deganello, Hydrogenation of acetylene in ethylene rich feedstocks: comparison between palladium catalyst supported on pumice and alumina, Appl. Catal. A: Gen. 172 (1998) 207.

[7] A. Borodzinki, Hydrogenation of acetylene-ethylene mixtures on a commercial palladium catalyst, Catal. Lett. 63 (1999) 35.

[8] JMP® 5.1- The Statistical Discovery Software™, SAS Institute Inc., Copyright© 1989-2003.

[9] L. R. Petzold, A. C. Hindmarsh, LSODA, Computing and Mathematics Research Division, Lawrence Livermore National Laboratory, 1997.

[10] K. H. Yang, O. A. Hougen, Determination of mechanism of catalyzed gaseous reactions, Chem. Eng. Prog. 46 (1950) 147.

[11] G. F. Froment, K. B. Bischoff, Chemical Reactor Analysis and Design, 2nd ed., Chapters 1 and 8, John Wiley & Sons, New York, 1990.

[12] R. M. Ormerod, R. M. Lambert, D. W. Bennett, W. T. Tysoe, Temperature programmed desorption of co-adsorbed hydrogen and acetylene on Pd (111), Surf. Sci. 330 (1995) 1.

[13] H. Ofner, F. Zaera, Isothermal kinetic measurements for the hydrogenation of ethylene on Pt (111) under vacuum: significance of weakly-bound species in the reaction mechanism, J. Phys. Chem. B 101 (1997) 396.

[14] F. Zaera, T. V. W. Janssens, H. Ofner, Reflection absorption spectroscopy and kinetic studies of the reactivity of ethylene on Pt(111) surfaces, Surf. Sci. 368 (1996) 371.

[15] D. Stacchiola, S. Azad, L. Burkholder, W. T. Tysoe, An investigation of the reaction pathway for ethylene hydrogenation on Pd(111), J. Phys. Chem. 105 (2001) 11233.

[16] H. Molero, D. Stacchiola, W. T. Tysoe, The kinetics of ethylene hydrogenation catalyzed by metallic palladium, Catal. Lett. 101 (2005) 145.

[17] G. C. Bond, J. Turkevich, The reaction of propylene with deuterium over a platinum catalyst, Trans. Farad. Soc. 49 (1953) 281.

[18] K. Hirota, Y. Hironaka, Mechanism of catalytic hydrogenation of propene on nickel palladium and platinum (Application of microwave spectroscopy to isotopic analysis), Bull. Chem. Soc. Jpn. 39 (1966) 2638.

[19] M. Aitake, Math. Sci 14 (1976) 5.

[20] R. S. Mann, K. C. Khulbe, Hydrogenation of methylacetylene over platinum and iridium catalysts, J. Phys. Chem. 73 (1969) 2104.

[21] H. Molero, B. F. Barlett, W. T. Tysoe, The hydrogenation of acetylene catalyzed by palladium: hydrogen pressure dependence, J. Catal. 181 (1999).

[22] R. Marshall, G. Webb, S. D. Jackson, D. Lennon, Propyne hydrogenation: characteristics of a carbon supported palladium catalysts that exhibits a kinetic discontinuity effect, J. Mol. Catal. A: Chem. 226 (2005) 227.

[23] S. D. Jackson, N. J. Casey, Hydrogenation of propyne over palladium catalysts, J. Chem. Soc. Farad. Trans. 91 (1995) 3269.

[24] G. C. Bond, J. Sheridan, Studies in heterogeneous catalysts. Part 1. The hydrogenation of methylacetylene, Trans. Farad. Soc. 48 (1952) 651.

[25] D. D. Do, Adsorption Analysis: Equilibria and Kinetics, Series on Chemical Engineering, Vol. 2, Chapter 5, Imperial College Press, London, UK, 1998.

[26] Q. Zhang, J. Li, X. Liu, Q. Zhu, Synergetic effect of Pd and Ag dispersed on Al_2O_3 in the selective hydrogenation of acetylene, Appl. Catal. A: Gen. 197 (2000) 221.

Part III

4. Mass Transport on Composite Dense PDMS Membranes with Palladium Nanoclusters*

Abstract

Mass transport properties (i.e. sorption, diffusion and permeability coefficients) of argon, hydrogen, propane, propylene and propyne were determined for unfilled poly(dimethylsiloxane) (PDMS) membranes at 308 K and for PDMS membrane filled with palladium nanoclusters (5 wt. %). Time-lag and sorption methods were used to obtain the kinetic and equilibrium relevant parameters.

Mass transport in a PDMS composite membrane differs from the corresponding unfilled membrane mainly during the transient regime, when a concentration profile is being settling down across the membrane thickness. The presence of the palladium nanoclusters modifies the mass transport during the transient regime not only because the nanoclusters can act as adsorption wells (mainly in the case of hydrogen), but also because they lead to a tortuosity increase. However, at steady-state the relevant parameters are the permeability coefficients of the polymeric matrix, the filler volume content and the tortuosity factor.

**** Adapted from: L. Brandão, L. M. Madeira, A. M. Mendes, J. Membr. Sci. 288 (2007) 112.***

4.1 Introduction

Catalytic membrane processes using polymeric membranes can advantageously be used for reactions performed at temperatures below 200 ºC [1]. Besides, dense polymeric catalytic membranes can actively interfere in the reaction by regulating the transport of reagents and products [2]. For such applications, membranes with ultra fine clusters (nanosized) and uniformly distributed throughout the membrane can be generated, departing from homogeneously distributed precursors totally solved by the polymer membrane [3].

Testing and modelling polymeric catalytic membrane reactor (pCMR), containing palladium nanoclusters in the polymeric matrix will be performed, which will consider alkyne and alkene hydrogenations, at nearly room temperature and steady-state conditions. However, to have access to the parameters governing the mass transport and the chemical reaction kinetics, independent experiments have to be performed. Kinetic parameters for propylene and propyne hydrogenations were performed for a batch reactor at 308 K (35 ºC) using Pd nanoclusters stabilized with a surfactant (*Chapters 2 and 3*). This chapter discusses the mass transfer across a poly(dimethylsiloxane) (PDMS) membrane filled with palladium nanoclusters, that is critical for subsequent modelling of a pCMR.

PDMS is undoubtedly the most studied polymer system for catalytic reactions, as referred by Vankelecom and Jacobs [2]. First, this highly permeable elastomer is prepared easily and combines a fairly high thermal stability (up to 250 ºC) along with mechanical and chemical resistances, the later being of utmost importance under reactive conditions [2]. On the other hand, a polymer with high diffusivity is strongly favoured on a pCMR because reagents and products must be able to diffuse to and from the catalyst's active sites with an acceptable rate [4].

The mass transport mechanism of a sorbate crossing a dense membrane is normally represented using the so-called sorption-diffusion model [5]. Sorption characterizes the interactions between polymer and sorbate and is described by the thermodynamics. Molecular diffusion characterizes the transport of molecules through the polymer matrix [6].

Usually three methods can be employed to characterize the mass transport in membranes: the so-called sorption, differential and integral methods [7]. All these methods are based on the dynamic response obtained from a sudden change at the membrane boundaries of the partial or total concentration.

In the sorption method, when the polymer contacts a fluid phase, the sorbate present in both phases is exchanged until the chemical potentials become equal [8]. Sorption of a single gaseous species can be determined by exposing a pre-weighed polymeric sample to a controlled pressure and weighing it after equilibrium [9]. Repeating the process under different pressures completes the sorption equilibrium isotherm. By performing sorption experiments, it is possible to obtain both sorption isotherms and the diffusion coefficients by measuring sorption rates during the transient state of the process [8].

In the differential method a constant partial pressure difference (driving force) is applied to both sides of the membrane and the permeate flow rate is measured. This can be done directly, using a flow meter, or indirectly, allowing the permeate flow rate to mix with a carrier gas and analysing the flow rate and composition of the stream leaving the cell. In the differential method both sides of the membrane are at equal total pressure.

In the integral method a quasi-constant pressure difference is applied to both sides of the membrane and the accumulation of gas on the permeate side is measured. This method, usually known as time-lag method, is implemented using an accurate pressure sensor and was first

suggested by Daynes [10]. In the time-lag method the membrane test cell is placed between two tanks, the feed and the permeate tanks. Initially, both chambers are evacuated, meaning that the initial concentration of the sorbed gas in the membrane approaches zero and hence constant in time. At a given instant ($t = 0$), the valve between the feed tank and the membrane cell is opened, originating a positive pressure step perturbation at the membrane feed side. At the same time, the pressure at the permeate tank, which is connected with the permeate chamber of the membrane cell, is recorded. The permeation system must be at constant temperature.

In all three methods, the diffusivity and sorption coefficients, which characterize the mass transfer of a gas in the polymeric matrix, are calculated by fitting the sorption-diffusion model to the experimental data. In this chapter, sorption and time-lag methods are used to characterize the mass transport of different gases through PDMS membranes, loaded or not with palladium nanoclusters.

4.2 Model

The model used to describe the permeation for the synthesized membranes is the sorption-diffusion model [5]. Fick's law is used for describing the diffusion transport through the membrane and it is assumed that the permeating species is in sorption equilibrium at both membrane surfaces. It is also assumed that the sorption equilibrium is described by the Henry's law and that there is no concentration polarization. This appears to be the case in almost all membrane processes, but may fail, for example, in transport processes involving facilitated transport or in diffusion of gases through metals, where interfacial adsorption/desorption can be slow [5].

4.2.1 PDMS membrane

Fick's first law is the starting point for the mathematical description of permeation through polymeric dense membranes:

$$J = -D\frac{\partial C}{\partial x} \tag{4.1}$$

where J is the flux through the membrane, C is concentration of the species inside the membrane, D is the effective diffusion coefficient and x is the membrane spatial coordinate.

Using the Fick's second law under the assumption of a constant diffusion coefficient, the gas transport through the membrane is described by:

$$\frac{\partial C}{\partial t} = D\frac{\partial^2 C}{\partial x^2} \tag{4.2}$$

Assuming that the sorption equilibrium between the gas and polymeric phases obeys to the Henry's law, $C = H \times P$, where H is the Henry's sorption coefficient, Eq. (4.2) can be rewritten as:

$$\frac{\partial P}{\partial t} = D\frac{\partial^2 P}{\partial x^2} \tag{4.3}$$

This equation is subject to the following initial and boundary conditions, when one considers the time-lag method:

$$t = 0, \forall\, x, P = 0 \tag{4.4a}$$

$$t \geq 0, x = 0, P = P^F \tag{4.4b}$$

$$t \geq 0,\ x = \ell\ , -\frac{\partial P}{\partial x} = \frac{1}{L}\frac{V^P}{ART}\frac{\partial P^P}{\partial t} \tag{4.4c}$$

where ℓ is the thickness of the membrane, $L = D \times H$ is the membrane permeability, P^F is the pressure at the feed side, P^P is the pressure at the permeate chamber, A is the membrane effective area, R is the gas constant, T is the absolute temperature and V^P is the permeate volume, which

comprises the volume of the permeate chamber of the membrane module plus the permeate tank. Eq. (4.4c) takes into account the concentration build up inside the permeate volume.

If the time-lag model equations are written in dimensionless form, it can be obtained a response independent of the feed pressure [11]:

$$\frac{\partial \hat{P}}{\partial \theta} = \frac{\partial^2 \hat{P}}{\partial \hat{x}^2} \tag{4.5}$$

$$\theta = 0\,,\ \forall\ \hat{x}\,,\ \hat{P} = 0 \tag{4.6a}$$

$$\theta \geq 0\,,\ \hat{x} = 0,\ \hat{P} = 1 \tag{4.6b}$$

$$\theta \geq 0\,,\ \hat{x} = 1,\ -\frac{\partial \hat{P}}{\partial \hat{x}} = \frac{1}{\eta}\frac{\partial \hat{P}}{\partial \theta} \tag{4.6c}$$

where the superscript (^) refers to the dimensionless variables: $\hat{P} = \left(P - P_o^P\right)/\left(P^F - P_o^P\right)$, with P_o^P being the permeate pressure at the initial instant, considered in the present study to be zero; $\hat{x} = x/\ell$, $\theta = t/\tau_D$ and $\tau_D = \ell^2/D$, which is the diffusion time constant; and η is defined as,

$$\eta = H\frac{A\ell RT}{V^P} \tag{4.7}$$

Both τ_D and η parameters were obtained by fitting the model (solved using a fast Fourier transform algorithm) to the experimental permeation data using the least squares method [11], and where τ_D easily relates with the so-called time-lag,

$$t_L = \frac{\tau_D}{6} = \frac{\ell^2}{6D} \tag{4.8}$$

4.2.2 Pd/PDMS membrane

For modelling the mass transport through the PDMS composite membrane, two situations can be considered: *i)* the nanoclusters act like inert particles for the permeating species and *ii)* sorption

occurs, either at the surface of the palladium nanoclusters or in all the palladium nanoclusters volume, such as when hydrogen is the permeating species [12].

For a non-sorbing gas species, like argon, palladium nanoclusters will augment the diffusion pathway of this molecule through the polymeric phase [13]. The diffusion equation taking into account the change in the diffusion pathway is:

$$J = -(1-\phi)\frac{D}{\tau}\frac{\partial C}{\partial x} \tag{4.9}$$

where τ is a tortuosity factor that takes into account the influence of the solid barrier created by the nanoclusters into the diffusivity and ϕ is the volume fraction of catalyst. The mass balance equation becomes then:

$$\frac{\partial P}{\partial t} = \frac{D}{\tau}\frac{\partial^2 P}{\partial x^2} \tag{4.10}$$

The boundary and initial conditions represented by Eqs. (4.4a) and (4.4b) are still valid, but the boundary condition Eq. (4.4c) becomes:

$$t \geq 0,\ x = \ell\ ,\ -\frac{\partial P}{\partial x} = \frac{\tau}{(1-\phi)}\frac{1}{L}\frac{V^P}{ART}\frac{\partial P^P}{\partial t} \tag{4.11}$$

as the flux into the permeate chamber occurs only through the polymeric phase.

The dimensionless form of Eq. (4.11) originates parameter η', similar to parameter η of Eq. (4.7):

$$\eta' = H\,\frac{A\ell(1-\phi)RT}{V^P} \tag{4.12}$$

and the time-lag equation for this case is:

$$t'_L = \frac{\ell^2\tau}{6D} \tag{4.13}$$

For species sorbing at the solid phase, the mass balance has to take into account the uptake at the palladium nanoclusters. The mass balance to species following a generic sorption equilibrium isotherm is [13]:

$$(1-\phi)\frac{\partial C}{\partial t}+\phi.f'(C)\frac{\partial C}{\partial t}=(1-\phi)\frac{D}{\tau}\frac{\partial^2 C}{\partial x^2} \tag{4.14}$$

where $f'(C)=\frac{\mathrm{d}f(C)}{\mathrm{d}C}$ and $f(C)$ is the sorption equilibrium isotherm at palladium nanoclusters.

If the isotherm of the permeating species at the solid phase is linear (Henry's law), $C_\mu = K \times C$, Eq. (4.14) becomes:

$$\frac{\partial C}{\partial t}\left(1+\frac{\phi}{(1-\phi)}K\right)=\frac{D}{\tau}\frac{\partial^2 C}{\partial x^2} \tag{4.15}$$

where C_μ is the sorbed concentration of the permeating species in the palladium nanoparticles. It is assumed that the permeating species is in equilibrium at the polymer/metal interface. With this assumption, Eq. (4.15) reduces to a similar form of Eq. (4.3):

$$\frac{\partial P}{\partial t}=D_{\mathrm{mod}}\frac{\partial^2 P}{\partial x^2} \tag{4.16}$$

where D_{mod} is a modified diffusivity defined as:

$$D_{\mathrm{mod}}=\frac{D}{\tau\left(1+\frac{\phi}{1-\phi}K\right)} \tag{4.17}$$

Taking this into account, the time-lag for permeating species that adsorb at the solid phase following a linear isotherm becomes:

$$t'_L=\frac{\ell^2}{6D_{\mathrm{mod}}} \tag{4.18}$$

and the boundary condition given by Eq. (4.11) still holds for a gas sorbing in the nanoclusters.

4.3 Experimental section

4.3.1 Chemicals

Palladium (II) acetate (Chempur) was used as catalyst precursor. All solvents were purchased from Merck as analytical grade. The cross-linkable PDMS Dehesive® 942, from Wacker Silicones Corporation, was used to prepare both noble metal containing polymer films and unfilled polymer films.

4.3.2 Membrane preparation

7.5 g of solvent-free PDMS Dehesive® 942 was dissolved in tetrahydrofuran (THF) to form a 10 wt. % solution. The required amount (1 wt. % of polymer) of cross-linker/catalyst was added, followed by mixing with a ca. 10 wt. % solution of palladium (II) acetate in THF to form a final concentration of 10 wt. % palladium (II) acetate in PDMS. Directly after mixing, the solution was poured in a casting ring supported by Teflon®-coated glass plate heated at 50 ºC and left overnight. During this period of time the solvent evaporation occurred along with cross-linking. About 0.025 m^2 of composite membrane was obtained, with ca. 300 μm in thickness. The membrane was reduced by 1 % $NaBH_4$ in ethanol/water (1/1 volume) and then dried in a vacuum oven at 100 ºC overnight. A Pd content of 5 wt. % was calculated, corresponding to a catalyst volume fraction (ϕ) of 0.004, which was obtained from the density of the clusters (ρ_{Pd} = 12 g cm^{-3}), and from the density of the polymer (ρ_{PDMS} = 1 g cm^{-3} [14]). The average size of the palladium clusters was estimated by XRD to be 8.8 nm in diameter and the membrane thickness 280.5 μm, determined by scanning electron microscopy (SEM).

The unfilled membrane was prepared as describe above, but in this case there was no addition of the palladium (II) acetate solution to the polymer one. Membrane thickness of 278.7 μm was determined with a precision digital micrometer.

4.3.3 Gases

Pure sorption and diffusion coefficients of hydrogen, argon, propyne, propylene and propane in the prepared membranes were determined. All gases were supplied by Praxair (propane 99.5 %; propylene 99.5 %; propyne 97 %; hydrogen 99.999 %; argon 99.999 %) and were used as received.

4.3.4 Determination of sorption and diffusivity parameters

The sorption method was implemented using a magnetic suspension balance from Rubotherm (0.01 mg weighing resolution, 0.02 mg reproducibility), which uses a pressure sensor (Druck, ref. 4010, 0.7 bar, absolute, ± 0.04 % FS) and a thermocouple (type K) to control, respectively, the pressure and the temperature in the basket container of the balance. An auxiliary jacketed stainless steel tank was used to supply each gas species to the balance. The temperature was kept at 308 K with the help of a water bath (Hubber, Polystat K6-1, ± 0.1 K).

A turbo-molecular connected to a rotary vacuum pump system was used to evacuate the tanks and to degas the membrane samples. The evacuation system can attain pressures well below 0.1 mbar. The magnetic suspension balance used corrects automatically the buoyancy effect and allows the acquisition of weighing data as a function of time. The complete system is described elsewhere [15, 16].

The lab set-up that implements the time-lag method is shown schematically in Fig. 4.1. It considers two stainless steel tanks of 5 dm^3 (feed) and 28.7 cm^3 (permeate, calibrated volume). These tanks are connected to a permeation cell with 10.2 cm^2 effective area. The permeation cell comprises a sintered disk, used to support the membrane, and a viton O-ring, used to seal the cell. Two pressure sensors are used to determine the pressure; one is placed at the feed tank and is used to read the feed pressure (Lucas Schaevitz, ref. 914, 10 bar, absolute, ± 0.04 % FS, P1). At the permeate tank, a high precision differential pressure sensor was used (Druck, ref. 4110, 20 mbar, ± 0.04 % FS, P3). A reference tank under high vacuum (below 0.1 mbar) is used with the

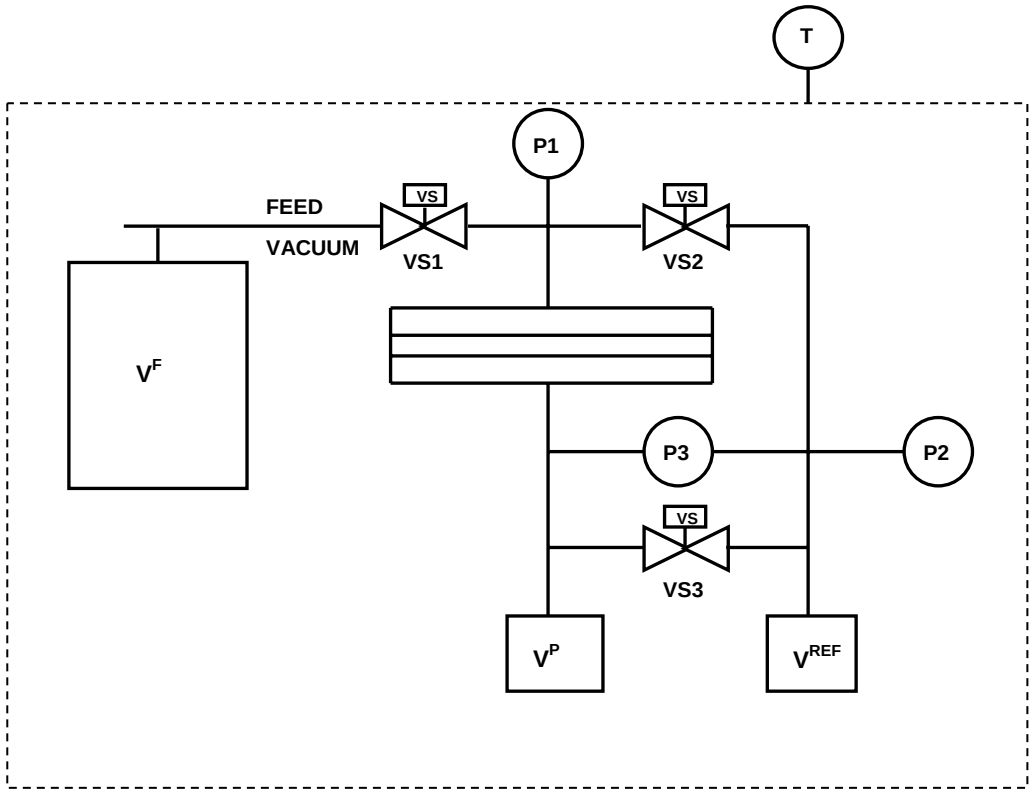

Fig. 4.1 Time-lag experimental set-up. P represents the pressure sensors, VS, the electric valves; V^P, the permeate tank, V^{REF}, the reference tank, V^F the feed tank and T a thermocouple.

differential pressure sensor. In this set-up, the high vacuum system made of a turbo-molecular pump in series with a rotary vacuum pump was also employed.

The time-lag unit is placed inside a thermostatic cabinet at 308 K. This unit is operated with the help of three low power electric valves. These valves are commanded, and the pressures read using an acquisition system based on a personal computer. To control the unit, a software application in LabView 5.0 (National Instruments) was developed.

4.4 Results and discussion

4.4.1 PDMS membrane

Figure 4.2 shows examples of experimental data values of dimensionless permeate pressure as a function of time concerning species permeating through the PDMS membrane. The curves refer to hydrogen, argon, propane, propylene and propyne time-lag experiments at a single feed pressure. The respective model fittings (Eqs. (4.5) and (4.6)) are also presented, from which the permeability, sorption and diffusion coefficients were computed.

The diffusion coefficients determined as a function of the feed pressure are shown in Fig. 4.3, for the different species tested. These values were obtained using Eqs. (4.5), (4.6) and (4.8), at different feed pressures and at 308 K, for a 278.7 μm thick PDMS membrane. Fig. 4.3 shows that the diffusivity of all gases in the PDMS membrane is essentially independent of the feed pressure. This is expectable for permanent gases, which exhibit a linear sorption isotherm in PDMS and for organic vapours at low concentrations, where the linear sorption equilibrium also holds [17].

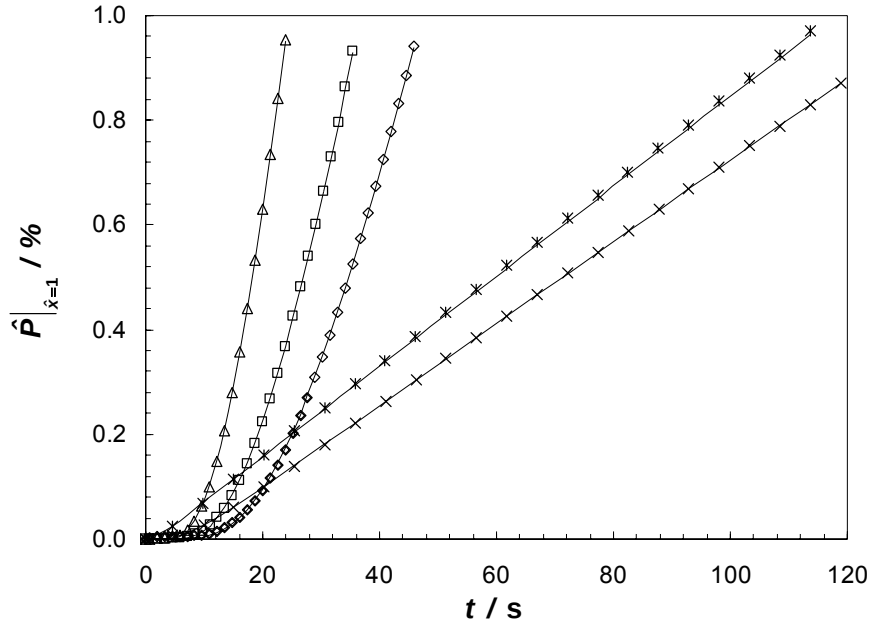

Fig. 4.2 Dimensionless permeate pressure build up in the permeate chamber obtained by the time-lag method for the PDMS membrane with different gases: ◇, propane (P^F = 0.4 bar); □, propylene (P^F = 0.5 bar); △, propyne (P^F = 0. 5 bar); x, argon (P^F = 0.6 bar); ∗, hydrogen (P^F = 1.0 bar).

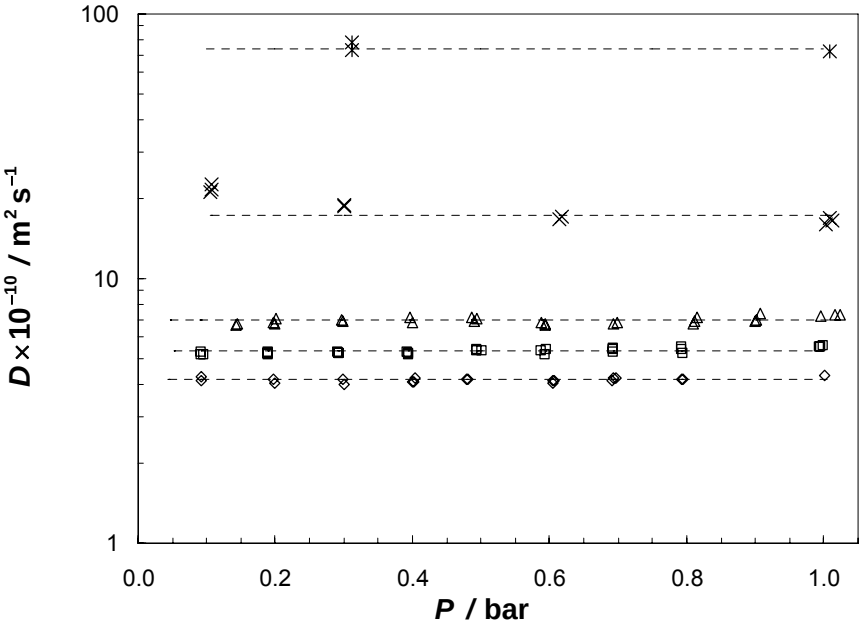

Fig. 4.3 Diffusion coefficients for different gases in PDMS at 308 K at different feed pressures (◇, propane; □, propylene; △, propyne: x, argon; ∗, hydrogen).

Figure 4.4 plots the sorption coefficients obtained by the time-lag method for different feed pressures. Sorption coefficients of argon, propane, propylene and propyne in PDMS at 308 K were obtained according to Eqs. (4.5), (4.6) and (4.7). Figure 4.4 shows that the sorption coefficients are also essentially constant for all gases. Thus, a linear sorption isotherm in PDMS is expected for these sorbates at 308 K and up to the highest pressures studied.

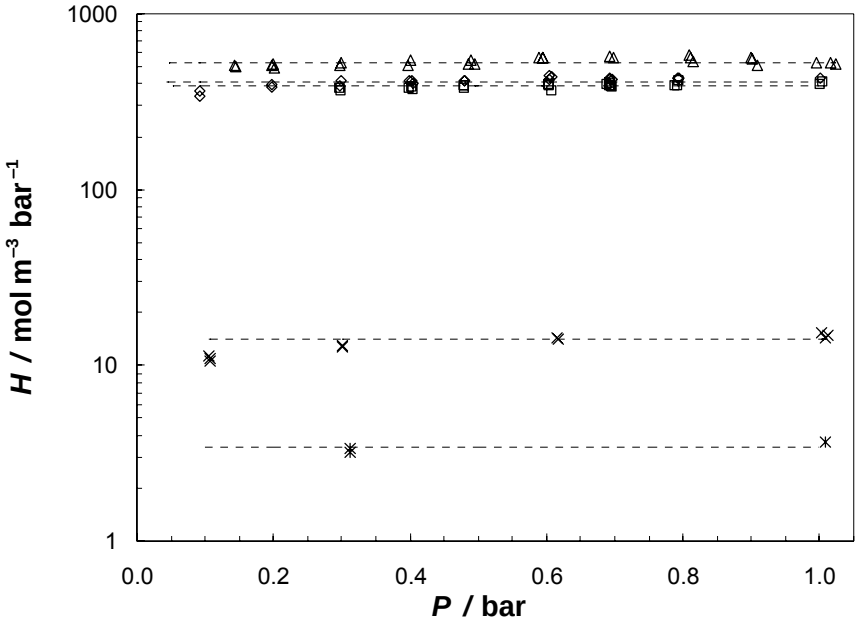

Fig. 4.4 Sorption coefficients for different gases in PDMS at 308 K at different feed pressures (◇, propane; □, propylene; △, propyne; x, argon; ✳, hydrogen).

For confirming the time-lag results, sorption experiments for some of the gases considered above were performed. Figure 4.5 shows the sorption equilibrium data at 308 K for propane, propylene and propyne in PDMS. These sorption equilibrium isotherms are linear in the range of pressures studied. Solid lines were drawn from the average sorption coefficients obtained using the time-lag method. The sorption isotherm of argon was also included in Fig.4.5. This figure

indicates that propane, propylene and propyne adsorb far more in PDMS than argon. Sorption coefficients from both methods agree reasonably for the gases studied.

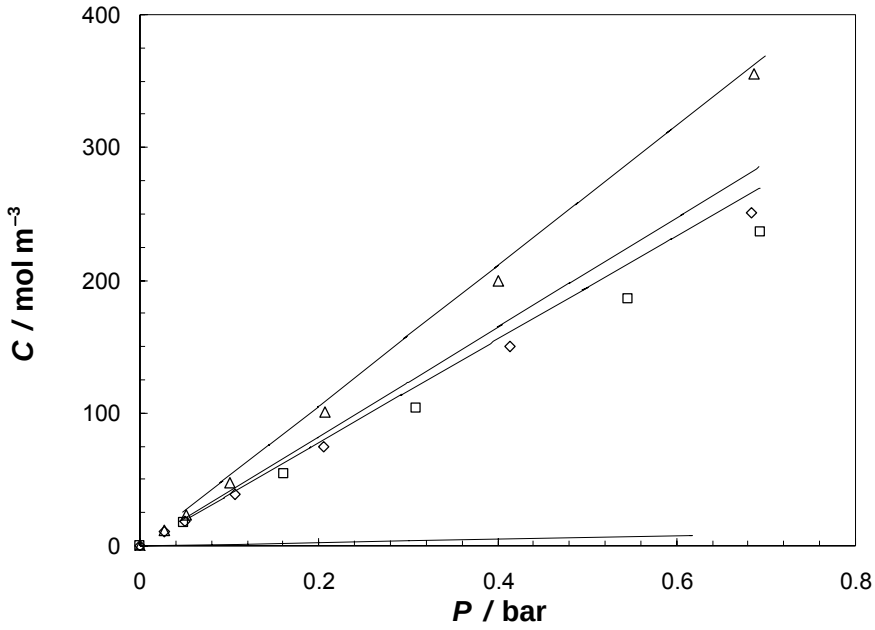

Fig. 4.5 Sorption equilibrium isotherms in PDMS at 308 K for different gases (◊, propane; □, propylene; △, propyne). Solid line is the sorption isotherm obtained by the time-lag method. Argon isotherm obtained by time-lag method (represented by the solid line at the bottom) was also included.

Table 4.1 presents the diffusion, sorption and permeability coefficient values obtained experimentally using the time-lag method for the unfilled PDMS membrane. Regarding the permeability coefficients, it is clear that the most permeable species is propyne and the less permeable are argon and hydrogen. The corresponding values of the mass transport characterization found in literature can also be seen in Table 4.1. Although experimental conditions are, in some cases, slightly different, it is usually seen a reasonable agreement between the results from this study and the ones found in literature.

Table 4.1 Experimental sorption, diffusion and permeability coefficients for different gases in PDMS, obtained through the time-lag method at 308 K, and comparison with literature values.

	Experimental values [a]			Literature values [b]		
Comp.	H / mol m^{-3} bar^{-1}	D x 10^{10} / m^2 s^{-1}	L / barrer	H / mol m^{-3} bar^{-1}	D x 10^{10} / m^2 s^{-1}	L / barrer
H_2	3.41 ± 0.60	74.0 ± 8.0	755 ± 79	2.2-2.9 [17,18]	100 [17]	900-1 000 [17,18,22,23]
C_3H_4	521 ± 15	7.08 ± 0.09	11 014 ± 337			
C_3H_6	384 ± 5	5.36 ± 0.06	6 146 ± 87			6 600 [20][c], 6 440 [24][g], 8 110 [1][e]
C_3H_8	416 ± 8	4.06 ± 0.05	5 043 ± 96	ca. 230-320 [14, 17,18]	4 [17], 5.3 [20][c], 4.5 [21][d]	5 750 [21][d], 5 640 [20][c], 4 600 [19][f]
Ar	14.1 ± 0.9	17.0 ± 1.0	722 ± 6			900 [1][e]

[a] At 308 K, vacuum pressure in the permeate chamber and 1 bar difference across the membrane. The errors were obtained for a 95% confidence level (*t* distribution); [b] Literature references are given between square brackets; [c] Computed from results at 323 K for a pressure difference of 2 bar and vacuum condition in the permeate stream; [d] Value at 293 K; [e] Value at 303 K; [f] Obtained from a model, in this study conditions; [g] Value at 313 K, for a pressure difference of 2 bar across the membrane and atmospheric pressure in the permeate side.

Direct comparison of the sorption and diffusion coefficients for propylene in PDMS with the literature ones was not possible. However, a qualitative comparison can be performed. It should be assumed that the heat of sorption and the diffusion activation energy of propane and propylene in PDMS are similar, which is very reasonable owing to their very similar condensabilities and molecular sizes. Tanaka et al. [20] reported sorption and diffusion selectivities of propylene and propane at 323 K in PDMS. They reported a diffusion selectivity for propylene:propane of 1.3 and a sorption selectivity for propylene:propane of 0.9. Comparing with the experimental results herein obtained, a diffusion selectivity of 1.32 and a sorption selectivity of 0.92 were obtained, that are in agreement with the literature values.

Permeation data for propyne in PDMS were not found in the open literature. Based on condensability parameters, it is expected that the sorption coefficient for propyne is higher than the corresponding one for propane or propylene. Propyne has a smaller molecular diameter than propylene and propane, indicating a higher diffusivity in PDMS. One can thus expect higher values of permeability coefficients due to the higher sorption and diffusion coefficients when compared either with propylene or propane. Indeed, a value of ca. 11 000 barrer was obtained, indicating a permeation selectivity of 2.2 compared with propane and 1.8 compared with propylene (Table 4.1).

4.4.2 Pd/PDMS membrane

Up to now all the mass transport parameters obtained were for unfilled PDMS membranes. These parameters are used as a comparison basis for the study of the mass transport parameters through PDMS membranes filled with palladium nanoclusters.

Time-lag experiments were performed with a PDMS membrane filled with 5 wt. % palladium nanoclusters. Figure 4.6 shows the dimensionless permeate pressure as a function of time for argon, propane and hydrogen at different feed pressures. When argon or propane is the permeating species, these curves are coincident despite the feed pressure. This happens because argon does not adsorb on catalyst surface and propane adsorbs linearly on palladium. In these cases, the model simplifies to equations (4.10) and (4.16) which are independent of the feed pressure.

As argon does not adsorb on the catalyst surface, the palladium nanoclusters will just augment the diffusion pathway of this molecule through the polymeric phase. In the linear region

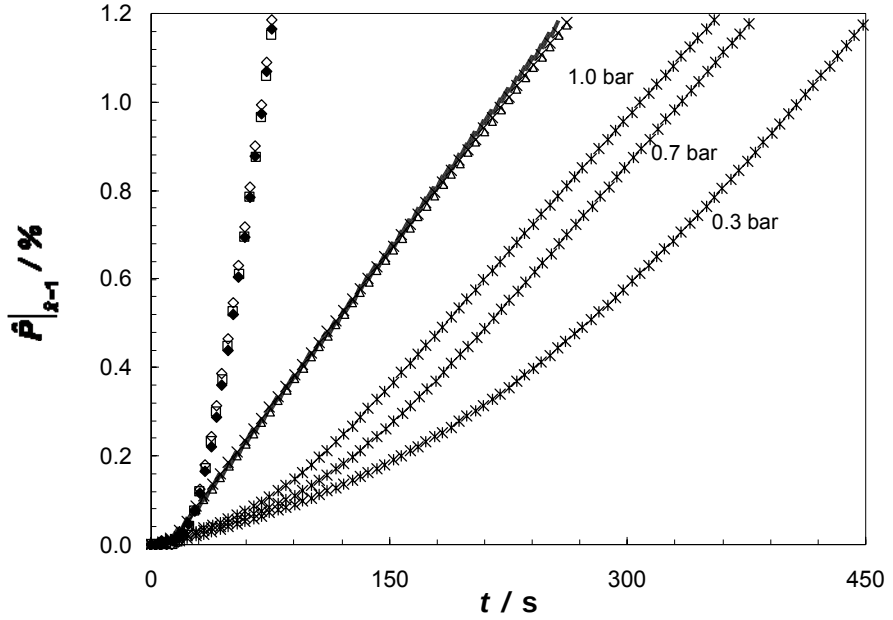

Fig. 4.6 Dimensionless permeate pressure build up in the permeate chamber obtained by the time-lag method for the 5 wt. % Pd/PDMS membrane with different gases and at different feed pressures. Propane: P^F = 0.2 bar (◆), P^F= 0.6 bar (□), P^F= 0.8 bar (◇); argon: P^F = 0.3 bar (▬), P^F = 0.6 bar (△), P^F = 0.9 bar (x); (∗) hydrogen: (P^F = 0.3, 0.7, 1.0 bar).

of the time-lag curves, where a quasi steady-state permeation holds $\left(\frac{\partial P}{\partial x} \approx \frac{\Delta P}{\ell} \approx \text{constant} \right)$, the permeated flux, given by Eq. (4.11), depends only on the membrane transport properties: tortuosity factor, catalyst volume fraction and polymeric matrix permeability. From the slope of the linear region it can be obtained the effective permeability.

Propane adsorbs on palladium nanoclusters following mostly a linear adsorption isotherm within the pressure range studied and at 308 K (data not shown). For the case of linearly adsorbing species in the catalyst, the time-lag values (t'_L) are expected to be greater, not only because tortuosity increases but also because sorption occurs in the palladium clusters. However, at pseudo steady-state conditions $(\partial C/\partial t = 0)$, the permeated flux does not depend on the adsorption equilibrium isotherm (Pd nanoparticles are already in sorption equilibrium concerning the transported species) and at this stage the linear region of the time-lag curves depends, as before, only on the membrane transport properties, on the tortuosity factor and on the catalyst volume fraction. The permeability values were obtained, now for propane, and compared with those of the unfilled membrane (cf. Table 4.2).

When hydrogen is permeating through a Pd/PDMS composite membrane, the transient mass transport of this species is influenced by the large hydrogen uptake in the palladium nanoclusters [25]. After sorbing at palladium's surface, the hydrogen atoms diffuse to the interior of the clusters, which act as a sink for hydrogen. Figure 4.7 shows the adsorption equilibrium isotherm of hydrogen on palladium nanoclusters immobilized inside the PDMS membrane. The sorption equilibrium isotherm is related to different kinds of interactions between hydrogen and palladium and hydrogen-hydrogen [12], and a concentration-dependent diffusion coefficient during the uptake for the different parts of the sorption isotherm has been reported for nanocrystalline palladium [26], what makes the hydrogen sorption pattern in palladium difficult

to model. However, a general and qualitative approach using the sorption equilibrium isotherm of hydrogen on palladium can explain the trend of the time-lag curves for different feed pressures (Fig. 4.6).

For the transient part of the time-lag experiment, the presence of the solid clusters in the membrane works as wells that retain significant amounts of the penetrant hydrogen and increases the pathway for diffusion, making the steady-state to be delayed. Higher hydrogen sorption capacities between feed and permeate conditions ($P^P \approx 0$), which mean higher average slopes, lead to higher retentions times – time-lags. As the feed pressure decreases for values below 1 bar, higher slopes are observed (Fig. 4.7) and consequently higher time-lags should be expected. This is confirmed by the experimental results, see Fig. 4.6.

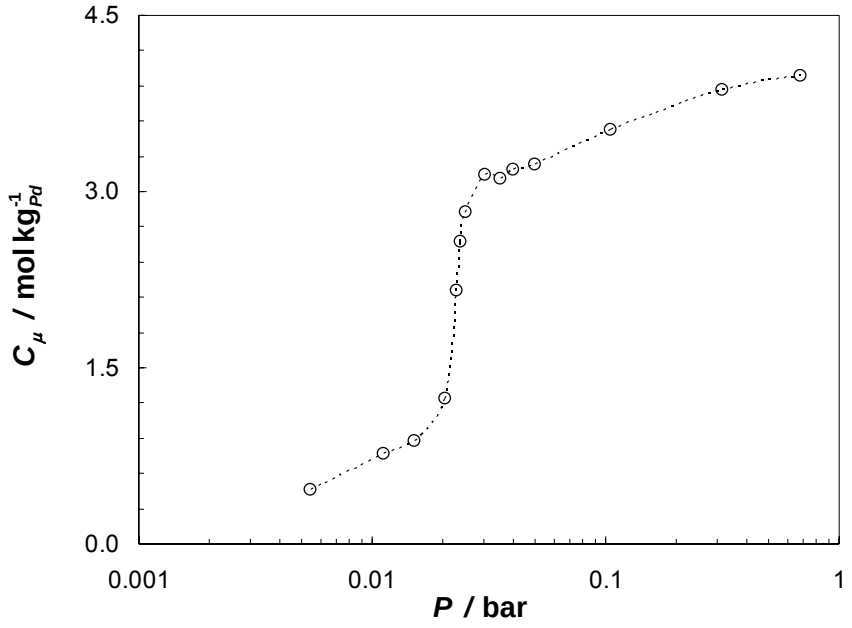

Fig. 4.7 Sorption equilibrium isotherm for hydrogen in palladium nanoclusters at 308 K, using the 5 wt. % Pd/PDMS membrane.

However, at steady-state, the mass transport through the membrane does not depend again on the hydrogen adsorption isotherm in the palladium clusters and the rate of permeation (slope of the linear region in the time-lag curves) is independent of the feed pressure, c.f. Fig. 4.6. For that reason, the relevant parameters that characterize the steady-sate mass transport are the permeability coefficient in the polymeric phase, the catalyst volume fraction and the tortuosity factor. For the case of propylene and propyne, which have Langmuir adsorption isotherms in palladium (*Chapter 3*), it is also observed that the permeability is constant with the feed pressure. Fig. 4.8 illustrates this for both propylene and propyne at three different feed pressures. To better compare the curves' slope, it was performed a translation of the three curves of each species in

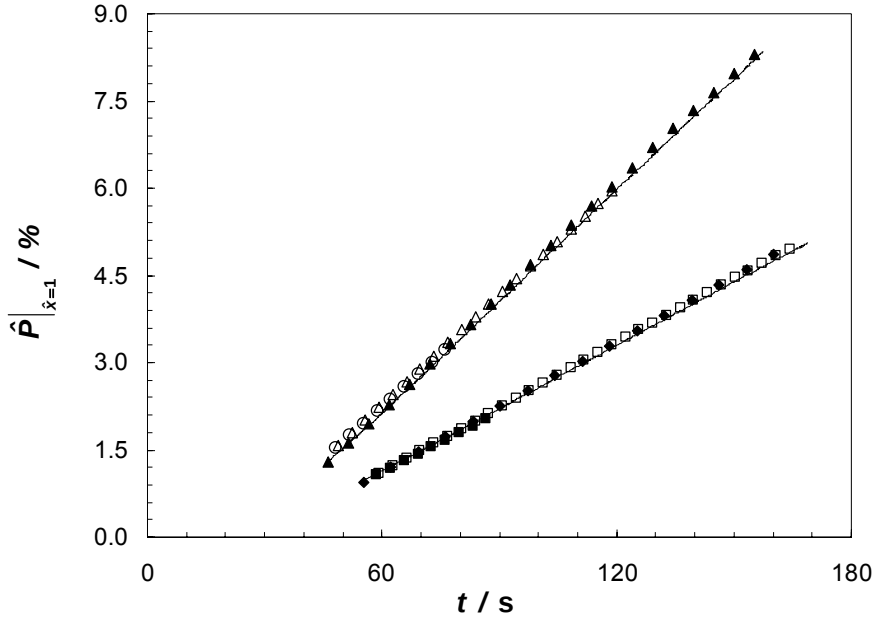

Fig. 4.8 Dimensionless permeate pressure build up in the permeate chamber obtained by the time-lag method for the 5 wt. % Pd/PDMS membrane, at pseudo steady-state, and with different gases. Propylene: P^F = 50 mbar (◆), P^F = 100 mbar (□), P^F = 900 mbar (■); propyne: P^F = 25 mbar (▲), P^F = 200 mbar (△), P^F = 600 mbar (○). The solid line corresponds to the model fitting.

order to have the same time-lag. Cussler and co-workers drawn the same general conclusions, i.e., the added fillers do not affect the steady-sate transport across the film, but they do increase the time before permeability begins [27].

Table 4.2 Permeability ratios between the unfilled PDMS membrane (L) and the 5 wt. % palladium-filled PDMS membrane (L') for the different permeating species tested.

Component	L / barrer	L' / barrer	L/L'
H_2	755 ± 79	446 ± 28	1.69 ± 0.20
C_3H_4	11 014 ± 337	6 395 ± 103	1.72 ± 0.06
C_3H_6	6 146 ± 87	3 613 ± 40	1.70 ± 0.03
C_3H_8	5 043 ± 96	2 917 ± 54	1.73 ± 0.05
Ar	722 ± 6	439 ± 5	1.64 ± 0.02
Average	-	-	1.70 ± 0.22

This way, comparing the effective permeability coefficient obtained for the filled and unfilled membrane one can obtain the tortuosity. Table 4.2 shows the ratio between the permeability of the unfilled and filled membranes, L/L', for the different species studied, where $L' = L/\tau$ once the catalyst volume fraction is negligible (ϕ = 0.004). These ratios are approximately constant (within the experimental error) and averaged to τ = 1.7. This means that the path for diffusion has been increased by a factor of ca. 1.7 relatively to the reference membrane.

Figure 4.8 also shows the model fitting to the time-lag results with propylene and propyne for the pseudo steady-state conditions. The permeability coefficients of the unfilled PDMS membrane and the tortuosity factor obtained represent quite well the experimental data.

4.5 Conclusions

Time-lag method was employed to determine the mass transport parameters of argon, hydrogen, propane, propylene and propyne in PDMS at 308 K. The sorption-diffusion model was used to fit the experimental results, that were successfully modelled and the pertinent parameters determined. The sorption coefficients obtained from independent time-lag and gravimetric experiments agree fairly. The results were compared with reported ones, whenever possible.

It was also concluded that:

- The mass transport of gas species in PDMS membrane filled with palladium nanoclusters differs from that in the unfilled PDMS membrane mainly for the transient part of the time-lag experiment. The presence of solid clusters in the membrane works as wells that may retain significant amounts of the penetrant species and increases the pathway for diffusion, making then the pseudo steady-state of permeation to be delayed;
- The sorption in the palladium nanoclusters leads to the increase of the time-lag, in time-lag experiments;
- At the pseudo steady-state conditions, the relevant parameters for the mass transport are sorption and diffusion (or permeability) coefficients in the polymeric phase, the filler volume content and the tortuosity factor.

4.6 Notation

A membrane area, m^2

C sorbed concentration in the polymer phase, mol m^{-3}_{PDMS}

C_μ concentration in the catalyst phase, mol m_{Pd}^{-3}

D diffusion coefficient, $m^2\ s^{-1}$

D_{mod} modified diffusion coefficient, $m^2\ s^{-1}$

H Henry's sorption constant, mol m^{-3}_{PDMS} bar^{-1}

J membrane flux, mol $s^{-1}\ m^{-2}$

K Henry's adsorption constant in palladium clusters, mol m_{Pd}^{-3} mol^{-1} m^3_{PDMS}

L permeability, barrer (1 barrer = 1×10^{-10} $cm^3_{STP}\ cm^{-1}\ s^{-1}\ cmHg^{-1}$)

ℓ membrane thickness, m

P absolute pressure, bar

R gas constant, m^3 bar $mol^{-1}\ K^{-1}$

T absolute temperature, K

t time, s

t_L time-lag, s

V volume, m^3

x spatial dimension across the membrane thickness, m

Greek letters

η capacitance parameter, -

ϕ volume fraction of catalyst in the membrane, -

τ tortuosity factor, -

τ_D diffusion time constant, s^{-1}

θ dimensionless time, -

Sub/superscripts

P, F permeate or feed

j permeant species

'	refers to the Pd/PDMS membrane
μ	refers to the palladium nanoparticles
^	refers to the dimensionless variable
o	initial conditions

4.7 References

[1] J. Theis, D. Fritsch, F. Keil, Catalysis with non-porous membranes loaded with nanoscale metallic clusters, in: Proceedings of the ESF, Network Catalytic Membrane Reactors-Final Workshop: Applications and Future Possibilities of Catalytic Membrane Reactors, Turnhout, Belgium, October 16-17, 1997, 35-41

[2] I. F. J. Vankelecom, P. A. Jacobs, Dense organic catalytic membranes for fine chemical synthesis, Catal. Today 56 (2000) 147.

[3] D. Fritsch, K. V. Peinemann, Novel highly permselective 6F-poly(amide-imide)s as membrane host for nano-sized catalysts, J. Membr. Sci., 99 (1995) 29.

[4] D. Fritsch, K. Khur, K. Mackenzie, F.-D. Kopinke, Hydrogenation of chloroorganic compounds in ground water by palladium catalysts Part 1. Development of polymer-based catalysts and membrane reactor tests, Catal. Today, 82 (2003) 105.

[5] J. G. Wijmans, R. W. Baker, The solution-diffusion model: a review, J. Membr. Sci. 107 (1995) 1.

[6] R. Gavara, R. J. Hernandez, The effect of water on the transport of oxygen through Nylon-6 films. J. Polym. Sci. Part B, 32 (1994) 2375.

[7] R. M. Felder, Estimation of gas transport coefficients from differential permeation, integral permeation and sorption rate data, J. Membr. Sci. 3 (1978) 15.

[8] P. Hernadez-Munoz, R. Gavara, R. J. Hernadez, Evaluation of solubility and diffusion coefficients in polymer film-vapour systems by sorption experiments, J. Membr. Sci. 154 (1999) 195.

[9] J. M. Toebe, H. Hoojat, R. J. Hernandez, J. R. Giacin, B. R. Harte, Interaction of flavour components from an onion/garlic flavoured sour cream with high impact polystyrene, Packag. Tech. Sci. 3 (1990) 133.

[10] H. A. Daynes, The process of diffusion through a rubber membrane, Proceed. Royal Soc. London 497 (1920) 286.

[11] P. Taveira, A. Mendes, C. Costa, On the determination of diffusivity and sorption coefficients using different time-lag models, J. Membr. Sci. 221 (2003) 123.

[12] E. Wicke, H. Brodowsky, Hydrogen in Palladium and Palladium Alloys. In: G. Alefeld, J. Völkl (eds.), Hydrogen in Metals II. Application-oriented Properties, Topics in Applied Physics, Vol. 29, Chapter 3, Springer-Verlag, Berlin, 1978.

[13] D. D. Do, Adsorption Analysis: Equilibria and Kinetics, Series on Chemical Engineering, Vol. 2, Chapter 12, Imperial College Press, London, UK, 1998.

[14] M. G. De Angelis, T. C. Merkel, V. I. Bondar, B. D. Freeman, F. Doghieri, G. C. Sati, Hydrocarbon and fluorocarbon solubility and dilation in poly(dimethylsiloxane): comparison of experimental data with predictions of the Sachez-Lacombe equation of state, J. Polym. Sci. B 37 (1999) 3011.

[15] P. Cruz, Simulação e optimização de processos cíclicos de adsorção. PhD Thesis, University of Porto, Porto, Portugal, 2003.

[16] J. Santos, Study of new adsorbents and operation cycles for medical PSA units, PhD Thesis, University of Porto, Porto, Portugal, 2005.

[17] T. C. Merkel, V. I. Bondar, B. D. Freeman, I. Pinnau, Gas sorption, diffusion and permeation in poly(dimethylsiloxane). J.Polym. Sci. B 38 (2000) 415.

[18] R. S. Prabhakar, T. C. Merkel, B. D. Freeman, T. Imizu, A. Higuchi, Sorption and transport properties of propane and perfluoropropane in poly(dimethylsiloxane) and poly(1-trimethylsilyl-propyne), Macromol. 38 (2005) 1899.

[19] R. S. Prabhakar, R. Raharjo, L. G. Toy, H. Lin, B. D. Freeman, Self-consistent model of concentration and temperature dependence of permeability in rubbery polymers, Ind. Eng. Chem. Res. 44 (2005) 1547.

[20] K. Tanaka, A. Taguchi, J. Hao, H. Kita, K. Okamoto, Permeation and separation properties of polyimide membranes to olefin and paraffins, J. Membr. Sci. 121 (1996) 197.

[21] G. Mauviel, J. Berthiaud, C. Vallieres, D. Roizard, E. Favre, Dense membrane permeation: from the limitations of the permeability concept back to the solution diffusion model, J. Membr. Sci. 266 (2005) 62.

[22] B. D. Bhide, S. A. Stern, Permeability of silicon polymers to hydrogen, J. Appl. Polym. Sci. 42 (1991) 2397.

[23] I. Pinnau, Z. He, Pure- and mixed-gas permeation properties of poly(dimethylsiloxane) for hydrocarbon/methane and hydrocarbon/hydrogen separation, J. Membr. Sci. 244 (2004) 227.

[24] A. Ito, S.-T. Hwang, Permeation of propane and propylene through cellulosic polymer membranes, J. Appl. Polym. Sci. 38 (1989) 483.

[25] C. Sachs, A. Pundt, R. Kircheim, M. Winter, M. T. Reetz, D. Fritsch, Solubility of hydrogen in single-sized palladium clusters, Phys. Rev. B 64 (2001) 5417.

[26] T. Mutschele, R. Kircheim, Segregation and diffusion in grain boundaries of palladium, Scripta Metallurgica 21 (1987) 135.

[27] C. Yang, E. E. Nuxoll, E. L. Cussler, Reactive barrier films, AIChE J. 47 (2001) 295.

Part IV

5. Propylene Hydrogenation in a Continuous Polymeric Catalytic Membrane Reactor*

Abstract

A continuous polymeric catalytic membrane reactor (pCMR), using a poly(dimethylsiloxane) (PDMS) composite membrane containing palladium nanoclusters, was studied and modelled for the propylene hydrogenation. The PDMS catalytic membrane has an average thickness of 4.4 μm, and was loaded with 5 wt. % of nano-sized Pd clusters about 9 nm in diameter. The reaction was performed at 308 K, and several feed compositions and flow rates were tested.

The pCMR model proposed represents the experimental data, i.e. the flow rates and mixture compositions in the permeate and retentate chambers, and therefore the overall advancement fairly well. In the hydrogenation rate equation, the propylene adsorption parameter and the kinetic constant were obtained by fitting the model to the experimental data. On the other hand, the hydrogen kinetic parameter and the mass transport parameters were obtained from independent experiments.

**** L. Brandão, D. Fritsch, A. M. Mendes, L. M. Madeira, Ind. Eng. Chem. Res. 46 (2007) 5278.***

5.1 Introduction

Catalytic membrane reactors are being used to conduct high temperature reactions (400-1173 K). Therefore, it is not surprising that organic polymers are hardly ever used as materials for catalytic membranes (except for bioreactors that uses enzymes as catalyst), because they lack thermal stability under these harsh conditions. However, under milder conditions, such as those at which hydrogenations occur, organic polymers are applied successfully [1]. On the other hand, some of the main challenges for inorganic, porous membranes in membrane reactors are the control of the thickness, the large-scale preparation, and the crack free synthesis; however, all these factors are much less problematic with polymer-based catalytic membranes.

Among other reactions in which polymeric catalytic membranes might be advantageous, it is worth noting the selective hydrogenation of propadiene and propyne impurities in propylene streams, which is an important reaction in the petrochemical industry. As a monomer for the production of polypropylene, propylene should contain less than 10 and 5 ppm of propadiene and propyne, respectively [2]. In this purification process, the over-hydrogenation of propylene to propane should be avoided. Usually, the hydrogenation process is accomplished in a fixed-bed catalytic reactor [3]. However, the use of polymeric membrane reactors is also possible.

For this and other gas phase hydrogenations, catalytically active membranes based on poly(dimethylsiloxane) (PDMS) have been developed and used. This highly permeable elastomer is prepared easily and combines a fairly high thermal (up to 250 ºC) and mechanical stability with chemical resistance, the latter being of the utmost importance under reactive conditions [4]. Moreover, a polymer with high diffusivity is strongly recommended, because the reactants and products must be able to diffuse to and from the catalyst's active sites at an acceptable rate.

For catalytic membranes that are composed of a dense polymer doped with a catalyst, the membrane acts as a catalyst support and the reaction happens inside the polymer phase. If the catalyst, in the form of nanoclusters, is incorporated into the membrane, higher activity and selectivity can be obtained. The smaller the catalyst particle, the higher the surface area per unit volume (and, therefore, the reactivity). Therefore, membranes with nanosized clusters uniformly distributed throughout the membrane are favoured. In particular, thin-film composite membranes with thicknesses of about 1-10 μm, achieving high fluxes, are in the centre of interest to provide high specific surface areas and short diffusion path lengths in the polymeric catalytic membrane reactor (pCMR) [5].

In this chapter, the propylene hydrogenation at 308 K is studied and modelled in a pCMR, where the membrane is composed of thin PDMS that contains palladium nanoclusters. To have access to the parameters governing the mass transport and the chemical reaction kinetics, independent experiments were performed whenever possible.

5.2 Model development

A schematic picture of the pCMR is shown in Fig. 5.1. The main assumptions of the model are given as follows [6]: 1. steady-state operation; 2. negligible pressure drop in the retentate and permeate chambers; 3. ideal gas behaviour; 4. fickian transport across the membrane; 5. sorption equilibrium between the bulk gas phase and the membrane surface described by the Henry's law; 6. no concentration polarization; 7. constant diffusion coefficients; 8. isothermal operation; 9. perfectly mixed flow pattern in both chambers; and 10. reaction occurs only on the surface of catalyst nanoparticles, which are distributed uniformly across the membrane.

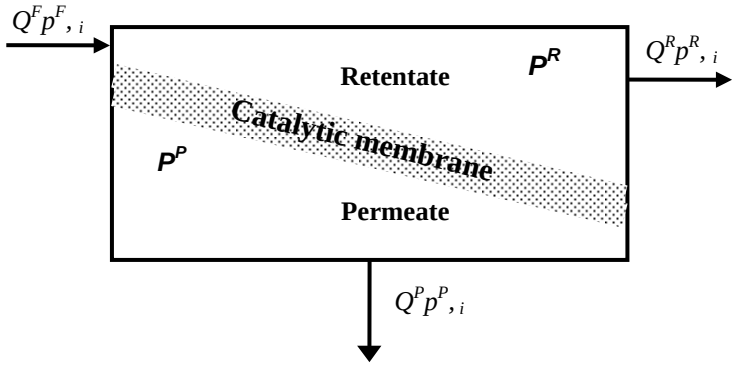

Fig. 5.1 Schematic diagram of the polymeric catalytic membrane reactor (pCMR).

Mass balance in the membrane and boundary conditions:

$$(1-\phi)\frac{D_i}{\tau}\frac{\mathrm{d}^2 C_i}{\mathrm{d}x^2} + \phi\rho\nu_i r = 0 \qquad i = \mathrm{H_2}, \mathrm{C_3H_6}, \mathrm{C_3H_8} \qquad (5.1)$$

$$\mathrm{x}= 0 \qquad \mathrm{C_i} = H_i y_i^R P^R \qquad i = \mathrm{H_2}, \mathrm{C_3H_6}, \mathrm{C_3H_8} \qquad (5.2)$$

$$\mathrm{x} = \delta \qquad \mathrm{C_i} = H_i y_i^P P^P \qquad i = \mathrm{H_2}, \mathrm{C_3H_6}, \mathrm{C_3H_8} \qquad (5.3)$$

Partial and total mass balances in the retentate chamber:

$$F^F y_i^F - F^R y_i^R + (1-\phi)A\frac{D_i}{\tau}\frac{\mathrm{d}C_i}{\mathrm{d}x}\Big|_{x=0} = 0 \qquad i = \mathrm{H_2}, \mathrm{C_3H_6}, \mathrm{C_3H_8} \qquad (5.4)$$

$$F^F - F^R + (1-\phi)A\sum_i \frac{D_i}{\tau}\frac{\mathrm{d}C_i}{\mathrm{d}x}\Big|_{x=0} = 0 \qquad i = \mathrm{H_2}, \mathrm{C_3H_6}, \mathrm{C_3H_8} \qquad (5.5)$$

Partial and total mass balances in the permeate chamber:

$$F^P y_i^P + (1-\phi)A\frac{D_i}{\tau}\frac{\mathrm{d}C_i}{\mathrm{d}x}\Big|_{x=\delta} = 0 \qquad i = \mathrm{H_2}, \mathrm{C_3H_6}, \mathrm{C_3H_8} \qquad (5.6)$$

$$F^P + (1-\phi)A\sum_i \frac{D_i}{\tau}\frac{\mathrm{d}C_i}{\mathrm{d}x}\Big|_{x=\delta} = 0 \qquad i = \mathrm{H_2}, \mathrm{C_3H_6}, \mathrm{C_3H_8} \qquad (5.7)$$

The subscript *i* refers to the *i*th component and the superscripts *F*, *R* and *P* refer to the feed, retentate and permeate conditions, respectively; *x* refers to the spatial coordinate of the membrane, with thickness δ, while ν_i is the stoichiometric coefficient of species *i*. *P* is the total pressure, *D* is the diffusion coefficient, *H* is the Henry's constant, *F* is the total molar flow rate and *y* is the molar fraction. ϕ is the volume fraction of catalyst (0.004), which was obtained from the mass fraction (5 wt. %) and density of the clusters (ρ_{Pd} = 12 g cm^{-3}), and from the density of the polymer (ρ_{PDMS} = 1 g cm^{-3} [7]). The remaining symbols have the usual meaning and are described in the nomenclature section.

To facilitate convergence, and using an approach similar to that described by Sousa et al. [6], the set of equations in dimensionless form was solved by adding a time derivative term to the right-hand side of Eqs. (5.1), (5.4) and (5.6), while Eqs. (5.5) and (5.7) were solved explicitly for the molar flow rate. Eq. (5.1) was further transformed into a set of ordinary differential equations (ODE's) using finite differences and the resulting time-dependent equations were solved using LSODA [8]. The steady-state solution was obtained when a step time increase did not make any further change in the dependent variables, within a pre-defined error.

5.3 Experimental section

5.3.1 Chemicals

Palladium acetate (Chempur) was used as a catalyst precursor. All solvents were analytical grade and purchased from Merck. The cross-linkable PDMS Dehesive® 942, from Wacker, was used to prepare the noble metal-containing polymer films. Porous poly-(acrylonitrile) (PAN) membranes

(GKSS Research Centre) with non-woven backing (200 m^3_N m^{-2} h^{-1} bar^{-1} N_2-flux) were used as thin-film supports.

5.3.2 Membrane preparation

The PDMS solution was obtained by dissolving solvent-free Dehesive® in tetrahydrofuran (THF) to form a 10 wt. % solution. The required amount of cross-linker (1 wt. % of polymer) and catalyst was then added. A ca. 10 wt. % solution of palladium (II) acetate in THF was finally added to the previous solution to form a final concentration of 10 wt. % palladium (II) acetate in PDMS. After mixing, this solution was supplied to a coating machine and the composite membrane prepared on the porous PAN-support via dip-coating. Subsequent cross-linking of the obtained membrane was performed by contacting it with a stream of hot air at 100 ºC. The palladium was then reduced using a solution of 1 % $NaBH_4$ in ethanol/water (1/1 volume), and an isotropical distribution of the catalyst throughout the polymer matrix was obtained [9]. A metal content of 5 wt. % was calculated, corresponding to a volume fraction loading (ϕ) of ca. 0.004. The quality of the films was finally checked by gas-selectivity measurement. A selectivity of α (O_2/N_2) > 2.1 indicates that the membrane is defect-free.

The thickness of the thin catalytic Pd/PDMS membrane was obtained by scanning electron microscopy (SEM). Figure 5.2 shows a micrograph of the supported catalytic PDMS membrane, in which the thickness of the catalytically active layer is not constant; therefore, an averaged thickness of 4.4 ± 0.5 μm was computed from several micrographs. Because it was not possible to obtain a direct read of the Pd clusters via X-ray diffraction (XRD) using the thin membranes, a 300 μm non-supported membrane was prepared using exactly the same procedure and the average size of the corresponding Pd clusters obtained via XRD. The value obtained, 8.8 nm in

diameter, was considered to be equal to the average size of the Pd clusters in the thin catalytic PDMS membrane and is consistent with the literature [9]. This 300-μm thick Pd/PDMS membrane was also used to compute the tortuosity factor (τ = 1.7 ± 0.2) from permeability experiments using different species as probing gases (*Chapter 4*).

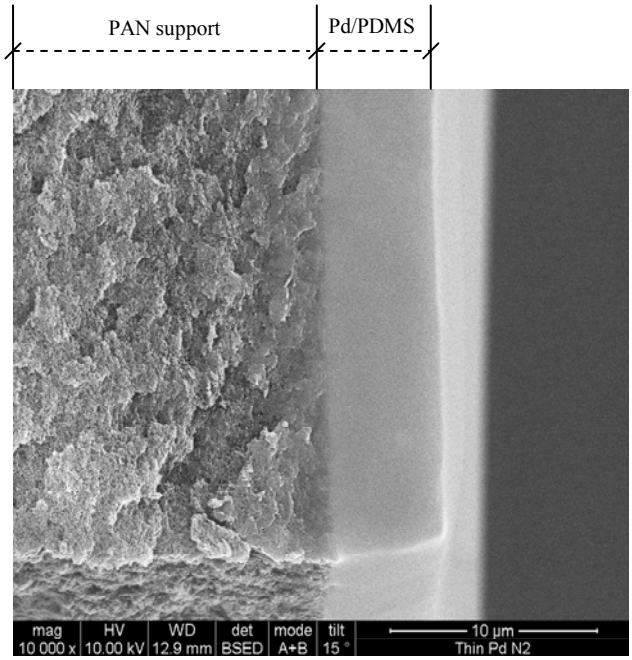

Fig. 5.2 SEM micrograph of the thin 5 wt. % Pd/PDMS supported membrane at a magnification of × 10 000.

5.3.3 Membrane reactor

A scheme of the pCMR experimental set-up is shown in Fig. 5.3A. The feed gas system considers three mass flow controllers (Bronkhorst Hi-Tec; model F201, with flow rates of 0 - 1, 0 - 0.1, and 0 - 0.3 L_N min^{-1}, ± 1 % FS) connected, respectively, to hydrogen, propylene, and propane gas cylinders. The gas mixture is promoted using an expanding-reduction fitting in the

gas line. All gases were supplied by Praxair (hydrogen 99.999 %; propylene 99.5 %; propane 99.5 %).

The membrane reactor has an effective area of 13.9 cm^2 (membrane diameter of 42 mm) and was placed inside a thermostatic oven. Figure 5.3B show a sketch of the membrane cell used. The flow pattern in the retentate chamber is difficult to model, because to the geometry used. However, if high feed flow rates or not too permeable mixtures are used, the input concentration becomes very similar to the outlet concentration and the retentate flow pattern can hence be approximately described by the perfectly mixed model. In this study, high feed flow rates and hydrogen-rich feed compositions (hydrogen is the less permeable component) were used.

A thermocouple (1/16" diameter, type K) was inserted into the membrane reactor to read the temperature directly over the membrane surface, at the retentate side. Different feed gas streams at different flow rates (ranging from 216 ± 7 to 323 ± 14 $mL_N\ min^{-1}$) and different compositions (H_2/C_3H_6 ratios between 2 and 9) were used, at 1.2 bar pressure (Druck, ref. 4010, 7 bar, absolute, ± 0.04 % FS) and 308 K. The permeate pressure was set to 100 mbar (Druck, ref. 4010, 2 bar, absolute, ± 0.04 % FS) with the help of a diaphragm vacuum pump (Thomas®, Ref. 7011-0069). All the experiments were repeated at least twice. Feed, permeate, and retentate streams were fed sequentially, in triplicate, to an on-line gas chromatograph (Dani GC 1000 with FID and TCD (Valco Inc.) in-series detectors), using an automatic injection valve (Valco Inc.). The gas chromatograph (GC) has a 30 m capillary plot fused silica column (GS-GasPro, J&W) operated with argon as the carrier gas, which allowed the simultaneous quantification of hydrogen, propylene, and propane. A temperature program starting at 50 ºC and ending at 110 ºC, with a rate of 10 ºC min^{-1}, was used.

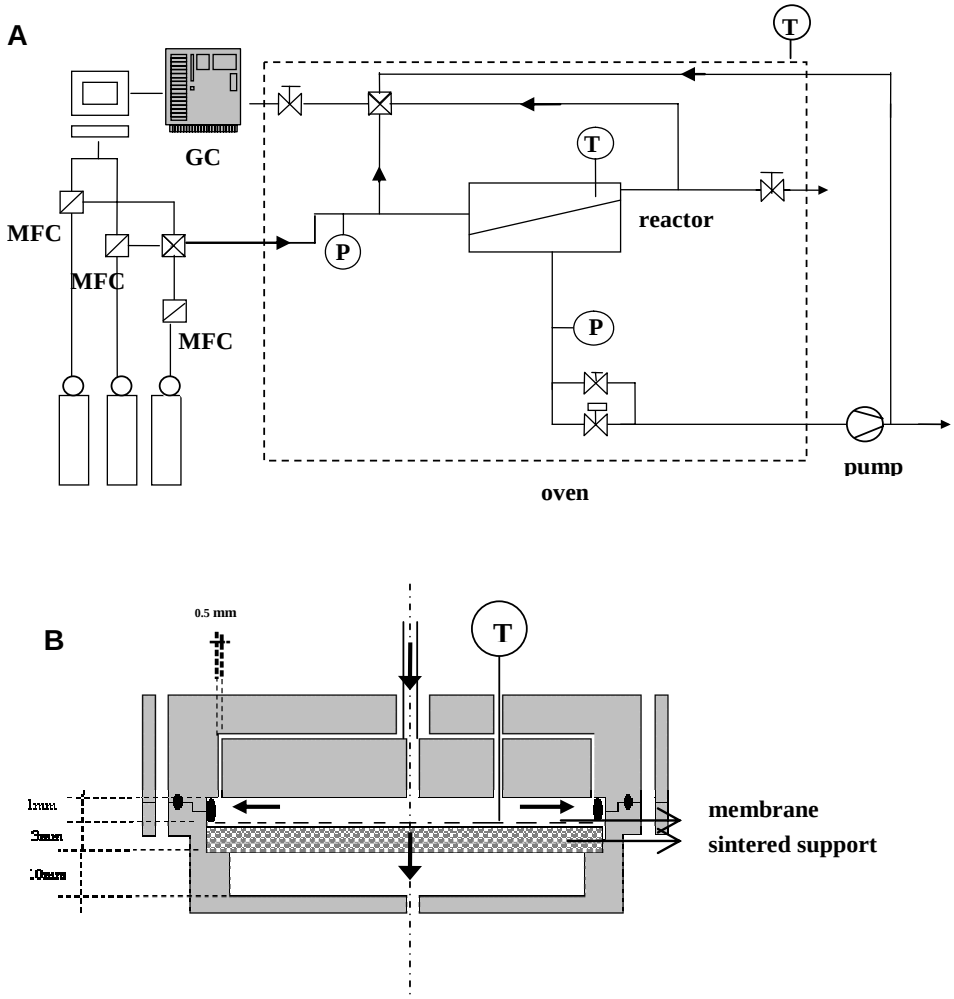

Fig. 5.3 A. pCMR experimental set-up scheme (MFC- mass flow controller, P- pressure sensor, T- thermocouple, GC- gas chromatograph); B. Membrane cell scheme.

5.4 Results and discussion

5.4.1 Mass transport characterization

Mass transfer in dense polymeric membranes is governed by the solution-diffusion model [10]. Thus, sorption and diffusion coefficients of hydrogen, propane and propylene in PDMS at 308 K were determined using the time-lag method (*Chapter 4*). The mass transport of gas species in the

PDMS membrane filled with palladium nanoclusters differs from that in the unfilled PDMS membrane, mainly for the transient regime. Actually, the solid clusters that are present in the membrane function as wells that may retain significant amounts of the penetrant species (particularly hydrogen) and increases the pathway for diffusion, making the steady-state of permeation become delayed. Under steady-state conditions, the relevant parameters to characterize the mass transport are the sorption and diffusion coefficients in the polymeric matrix, the volume fraction of the nanoparticles, and the tortuosity factor (cf. *Chapter 4*).

Table 5.1 gives the sorption, diffusion and permeability coefficients of hydrogen, propane and propylene, determined at 308 K for a non-porous ca. 300 μm thick PDMS membrane.

Table 5.1 Sorption, diffusion and permeability coefficients in a PDMS membrane at 308 K for the different gas species (cf. *Chapter 4*).

Component	H / mol m^{-3} bar^{-1}	D x 10^{10} / m^2 s^{-1}	L x 10^{10} / mol m^{-1} bar^{-1} s^{-1}
H_2	3.41 ± 0.60	74.0 ± 8.0	252 ± 52
C_3H_6	384 ± 5	5.36 ± 0.60	2 057 ± 29
C_3H_8	416 ± 8	4.06 ± 0.05	1 692 ± 32

5.4.2 Determination of the kinetic equation

The kinetics of the propylene hydrogenation was determined previously in a batch reactor using palladium nanoclusters stabilized by a surfactant (n-$(C_{18}H_{37})_4N^+Br^-$) shell that prevents cluster agglomeration and showed no mass transfer resistance (*Chapter 2*):

$$r_{C_3H_8} = \frac{kK^g_{C_3H_6} K^g_{H_2} C^g_{H_2} C^g_{C_3H_6}}{\left(1 + \sqrt{K^g_{H_2} C^g_{H_2}} + K^g_{C_3H_6} C^g_{C_3H_6}\right)^3} \tag{5.8}$$

where k is the kinetic rate constant, C_i^g is the gas phase concentration of species i and K_i^g its adsorption equilibrium constant on the catalyst's surface. Parameters of Eq. (5.8) are given in Table 5.2.

Table 5.2 Kinetic parameters of propylene hydrogenation over palladium nanoclusters stabilized on different matrices (T = 308 K).

	Matrix	
Parameter	Surfactant*	PDMS
k /mol g^{-1}_{Pd} s^{-1}	5.569	18.3
$K^g_{C_3H_6}$ / m^3 mol^{-1}	2.55 x 10^{-2}	1.31 x 10^{-1}
$K^g_{H_2}$ / m^3 mol^{-1}	9.7 x 10^{-4}	9.7 x 10^{-4}
Average Pd-clusters size / nm	7.3	8.8

* *Chapter 2*

Different kinetic parameters may be observed when the catalyst is deposited on different supports [11, 12]. Indeed, the aforementioned kinetic parameters, determined over palladium nanoclusters stabilized with a surfactant, did not accurately describe the propylene hydrogenation experiments in the pCMR, where the palladium nanoclusters are dispersed inside the PDMS membrane. Different factors may account for this discrepancy. First, it has been reported that the active surface area of palladium nanoclusters stabilized with a surfactant and determined by CO

chemisorption is much smaller than the active area of the same catalyst and with identical particle size supported on charcoal [13]. Moreover, it was reported that the alkyl chain length of surfactant-stabilized Pd, Pt and Rh catalysts also affects the active surface area determined by CO chemisorption: the longer the chains (hexyl to decyl), the lower the active surface area [13, 14]. In the present case, the palladium nanoclusters were stabilized using an octadecyl chain surfactant – tetraoctadecylammonium bromide (*Chapter 2*). This surfactant has a large alkyl chain that should interfere strongly with the adsorption of reactant species, especially the larger species such as propylene. It was also reported that, in the case of surfactant-stabilized catalysts, the hydrogenation activity was still relatively high, despite the smaller active metal surface, because hydrogen penetrates through the protecting shell, because of its very small size [14].

XRD measurements and CO chemisorption were then used to obtain the metal surface area of surfactant-stabilized palladium clusters (*Chapter 2*). A surface area of 68 m^2 g^{-1}_{Pd} (assuming spherical Pd nanoparticles) was calculated based on XRD measurements, while a value of 27 m^2 g^{-1}_{Pd} was obtained by CO chemisorption. These results indicate that only ca. 40 % of the metal sites are accessible to the CO molecules because the surfactant is blocking some sites, to stabilize the clusters.

Because of the issues mentioned, the Langmuir-Hinshelwood (L-H) parameters of the propylene hydrogenation kinetics, catalyzed by Pd nanoclusters stabilized with a surfactant, should be different comparatively from those of Pd nanoclusters supported in a PDMS membrane, except for the hydrogen adsorption constant (K_{H_2}). The reaction mechanism is assumed to be the same in both cases. This way, runs using the Pd-doped PDMS membrane were performed in an open reactor and the propylene adsorption constant, $K_{C_3H_6}$, and the kinetic constant, *k*, obtained. These parameters were obtained by fitting the developed pCMR model and

the kinetic rate equation (Eq. (5.8)) to the experimental values by minimizing the sum of the square residues. A surface response analysis was employed to perform the optimization, based on a commercially available software (JMP®, 5.1, SAS).

The hydrogenation of propylene occurs inside the PDMS membrane. Assuming that the reaction mechanism proposed for the reactants in the gas phase (*Chapter 2*) is valid for the reactants in the membrane phase, the following relationship between the adsorption constants can be obtained:

$$K_i = \frac{K_i^g}{H_i RT} \tag{5.9}$$

where H_i is the Henry's constant that relates the gas phase concentration with the sorbed concentration of species *i* in the membrane.

The values of the kinetic parameters are reported in Table 5.2 for surfactant-stabilized palladium and PDMS supported-Pd, the later being obtained by the fitting process already described and using the experimental data shown below. A five times increase on the propylene adsorption constant was obtained for the Pd/PDMS system, suggesting that some surface sites at the surfactant-stabilized palladium are hindered, which is compatible with the observed CO chemisorption data. It is also noticeable an increase in the kinetic constant k by a factor of about 3, indicating that the Pd nanoclusters are more active when incorporated into the PDMS membrane than when stabilized with the surfactant.

5.4.3 Hydrogenation experiments in the pCMR

The performance of the polymeric catalytic membrane reactor was studied for the propylene hydrogenation at 308 K and the results were compared with the proposed model. Fig. 5.4 shows

the experimental values of the permeate flow rate leaving the reactor as a function of the hydrogen/propylene molar ratio fed to the membrane reactor, and for the two feed flow rates tested. The membrane permeability towards propylene is higher than that toward hydrogen

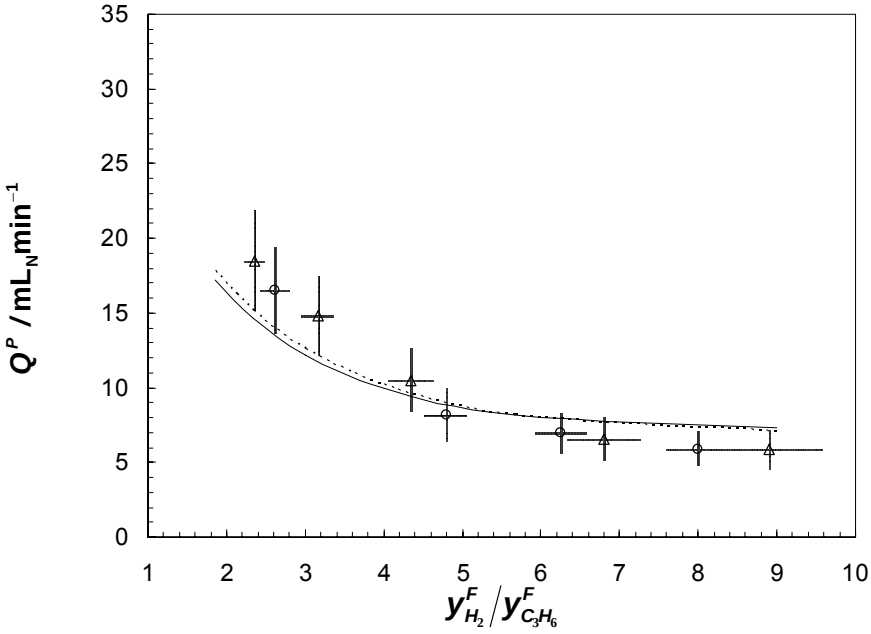

Fig. 5.4 Permeate flow rate as a function of the feed hydrogen/propylene molar ratio, obtained during the steady-state operation of the pCMR. (△) Feed flow rate 323 mL_N min^{-1}, dashed line- model fitting. (○) Feed flow rate 216 mL_N min^{-1}, solid line- model fitting.

(Table 5.1). Consequently, as the feed molar fraction of propylene increases (decrease of $y^F_{H_2}/y^F_{C_3H_6}$), the permeated flow also increases. The model fits reasonably the permeate flow for the different feed hydrogen/propylene ratios and predicts that trend. The non-uniform thickness of the membrane, as well as the uncertainty related with the transport parameters of the different gases in the membrane, should explain some differences between the model and the experimental results, despite the experimental values showing large error bars. These errors are mainly related

with the equipment used to determine the mass flow rates. Indeed, the mass flow meters used to read the permeate flow rate (hot-wire principal) show large uncertainties when the stream is a mixture of gases with very different correction factors [15]. Flow rate relative errors in the range of ± 15 % are then expectable.

Fig. 5.5 shows the hydrogen concentrations (molar fractions, in percentage values) at the retentate and permeate outlet streams for different feed hydrogen/propylene molar ratios and total feed flow rates. Higher hydrogen molar fractions in the retentate and permeate streams are observed for an increasing feed hydrogen/propylene molar ratio, as expected. The model fits quite well the hydrogen compositions in both streams for the different feed flow rates used.

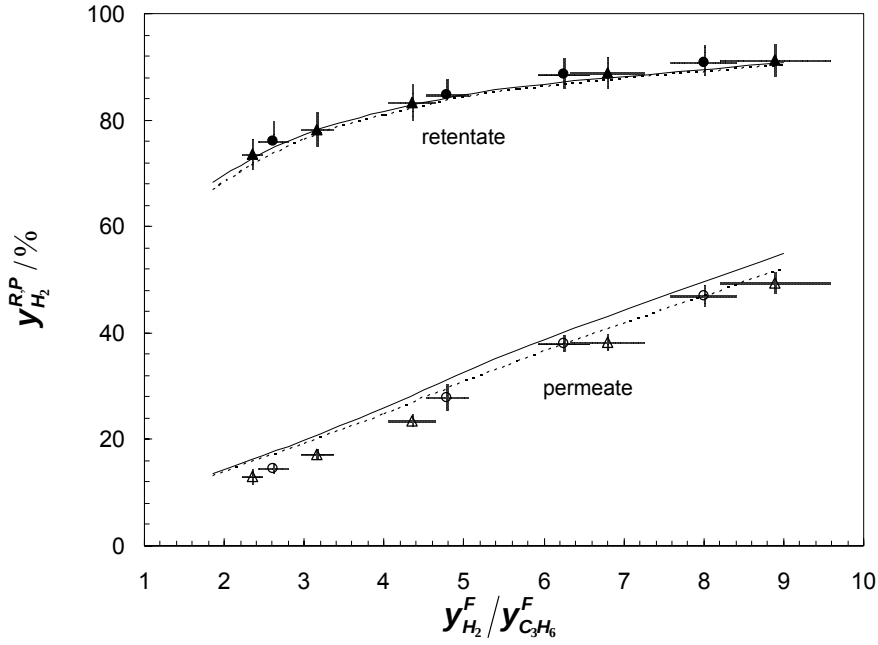

Fig. 5.5 Hydrogen composition in the retentate and permeate chambers as a function of the feed hydrogen/propylene molar ratios, obtained during the steady-state operation of the pCMR. (▲, △) Feed flow rate 323 mL_N min^{-1}; dashed line- model fitting. (●, ○) Feed flow rate 216 mL_N min^{-1}; solid line- model fitting.

Hydrogen compositions at the retentate side for the two total feed flow rates tested are very similar (Fig. 5.5). This happens because of the high feed flow rates and hydrogen concentrations used. This way, the retentate composition is very similar to the feed one. Besides, hydrogen concentrations in the retentate stream are much higher than those in the permeate side, because of the low membrane permeability toward hydrogen.

Fig. 5.6 shows the propylene compositions (molar fractions, in percentage values) at the retentate and permeate chambers, as a function of the feed hydrogen/propylene molar ratios and for both feed flow rates. In this case, higher propylene concentrations are observed in the permeate chamber when compared with the retentate composition, because of the high PDMS

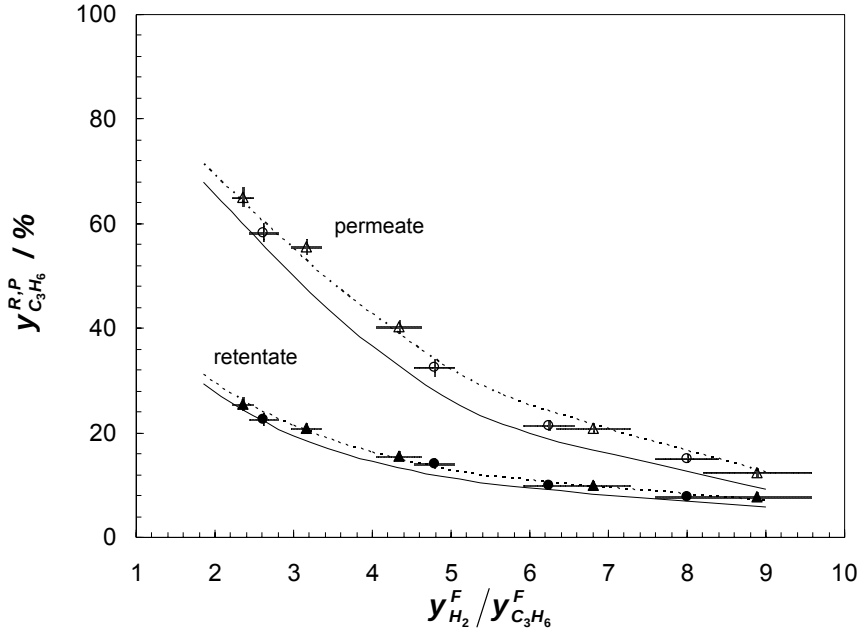

Fig. 5.6 Propylene composition in the retentate and permeate chambers as a function of the feed hydrogen/propylene molar ratios, obtained during the steady-state operation of the pCMR. (▲, △) Feed flow rate 323 mL_N min^{-1} dashed line- model fitting. (●, ○) Feed flow rate 216 mL_N min^{-1}; solid line- model fitting.

permeability toward propylene (Table 5.1). Fig. 5.6 also shows the fitting of the model to the experimental data; a reasonable agreement can be observed again. One can also notice that as the feed flow rate increases, the retentate composition approaches the feed composition. This leads to a slight increase of the permeate flow rate (Fig. 5.4), which is essentially attributed to an increase of the permeated propylene, the most permeable species. Consequently, its concentration increases in both chambers (Fig. 5.6). This way, the assumption of completely mixed flow pattern at the retentate side is only approximately hold. Anyway, the proposed model is able to capture the composition and permeate flow rate trends observed for the tested feed flow rates.

Propane molar fractions in both chambers are presented in Fig. 5.7. Experimental propane molar concentration in the permeate chamber reaches 40 % at feed hydrogen/propylene molar ratios between 5 and 6 and for the lowest feed flow rate. Higher concentrations of propane are expected when gas mixtures that assure a high hydrogen/propylene molar ratio at catalyst's surface are fed to the reactor. However, to define the feed H_2/C_3H_6 molar ratio that originates the highest propane concentration in the permeate chamber is not straightforward. First, the maximum reaction rate is obtained for high hydrogen/propylene molar ratios, ca. 9, as can be deduced from the reaction kinetic equation. On the other hand, H_2 diffusivity in PDMS is much higher than that of C_3H_6 (Table 5.1); therefore, shifting the maximum propane concentration towards smaller H_2/C_3H_6 molar ratios. Theis [16] reported the same trend herein obtained for the propane concentration in the permeate chamber versus feed hydrogen/propylene ratio over PDMS membranes loaded with palladium clusters.

Experimental propane compositions at the retentate chamber differ for the two feed flow rates (Fig. 5.7), what can be mainly ascribed to two reasons. First, an increase of the total feed flow rate leads to a propane concentration decrease at the retentate side, because of a dilution

effect, and then to a higher back-permeation driving force. This pumps propane out of the membrane, which leads also to a concentration decrease of propane at the permeate side (Fig. 5.7). Second, a decrease of the total feed flow rate leads to a higher contact time (I) and then to high propane concentrations in both retentate and permeate chambers.

The model does not fit well the propane concentration at the retentate chamber, possibly because of a non-uniform distribution of the palladium clusters across the polymeric matrix. This could happen during the solvent evaporation in the course of the casting of the membrane. Unfortunately, it was not possible to confirm the non-uniform distribution of the palladium

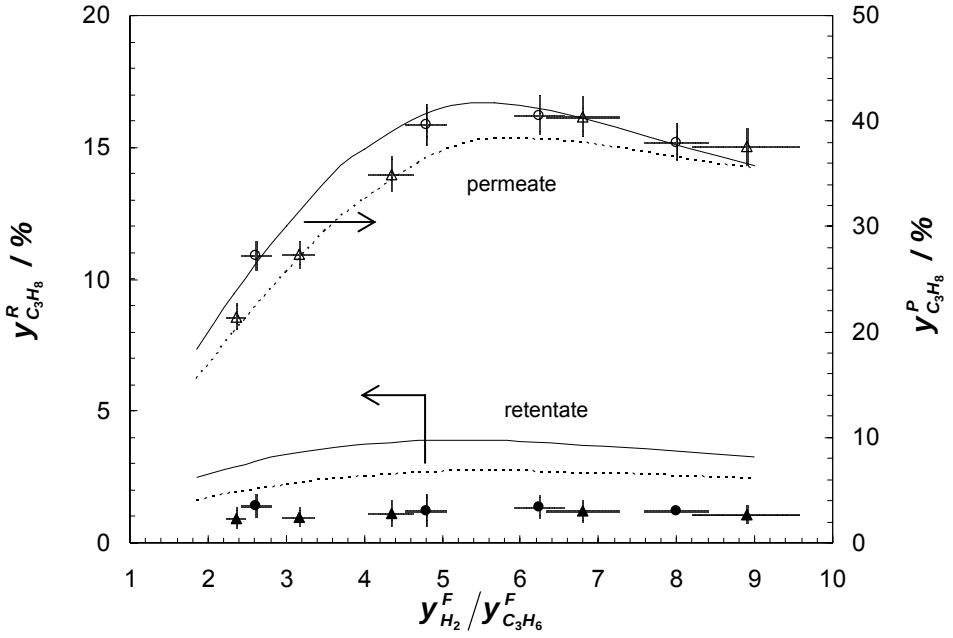

Fig. 5.7 Propane composition in the retentate and permeate chambers as a function of the feed hydrogen/propylene molar ratios, obtained during the steady-state operation of the pCMR. (▲, △) Feed flow rate 323 mL_N min^{-1}; dashed line- model fitting. (●, ○) Feed flow rate 216 mL_N min^{-1}; solid line- model fitting.

clusters inside the membrane. A lower concentration of palladium clusters near the surface, at the retentate chamber, could explain the lower values for propane concentration obtained experimentally in this chamber. This can be shown using the developed model, although the proof will not be done here.

Fig. 5.8 shows the advancement of propylene hydrogenation as a function of the feed hydrogen/propylene molar ratios, calculated according to the following expression:

$$X = \frac{F^R y^R_{C_3H_8} + F^P y^P_{C_3H_8}}{F^F} \tag{5.10}$$

It can be observed that the model describes the tendency of the experimental advancement, which increases with $y^F_{H_2} / y^F_{C_3H_6}$ up to values of 5, decreasing afterwards. The maximum

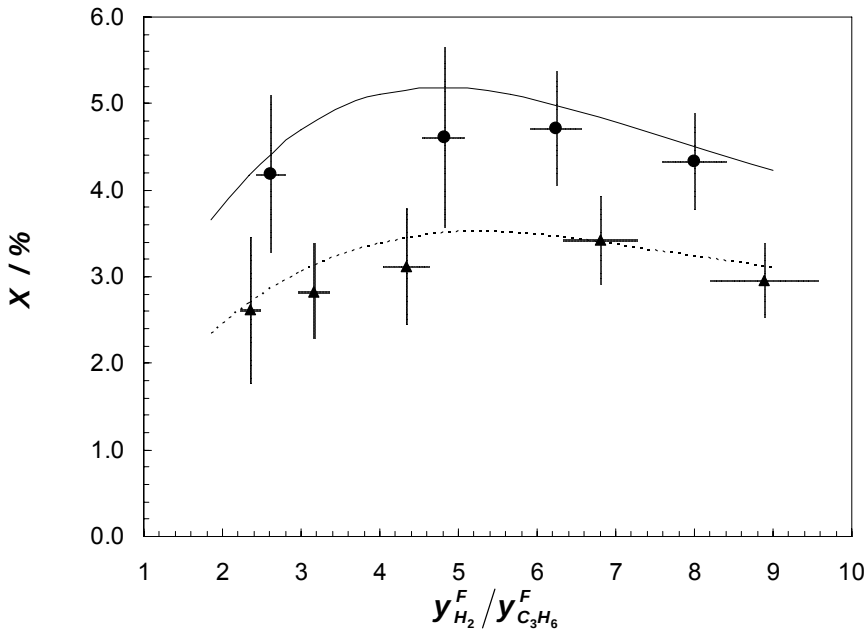

Fig. 5.8 Advancement of propylene hydrogenation as a function of the feed hydrogen/propylene molar ratios, obtained during the steady-state operation of the pCMR. (▲) Feed flow rate 323 $mL_N\ min^{-1}$; dashed line- model fitting. (●) Feed flow rate 216 $mL_N\ min^{-1}$; solid line- model fitting.

advancement is obtained for a hydrogen/propylene molar ratio slightly below that which considers only the permeate stream (see Fig. 5.7), what can be ascribed to the contribution of the retentate stream that shows maximum propane concentrations at slightly smaller H_2/C_3H_6 values (Fig. 5.7). Higher advancement values are observed in Fig. 5.8 for the 216 $mL_N\ min^{-1}$ feed flow rate experiments because of the reasons previously mentioned, regarding propane concentration in both chambers (Fig. 5.7). Experimental errors are significant, whereas the flow rate errors are the most important.

A sensitivity analysis based on the pCMR model, written in the dimensionless form, was performed to give some insight about the influence of some parameters in the advancement of the reaction, permeate flow rate, propane recovery, and permeate composition. The sensitivity analysis was extended to the kinetic and transport parameters, membrane characteristics, and process variables, and a positive change of 10 % in the parameter's values was considered.

Table 5.3 indicates that the parameters affecting more significantly the advancement are the kinetic constant (k) and the contact time (Γ), defined below, where a change of 10 % causes an increase in the advancement of around 7 % and 10 %, respectively. The contact time, defined as the ratio between the intramembrane flux for the reference component (C_3H_8) and the total feed flow rate, is expressed as:

$$\Gamma = \frac{AL_{C_3H_8}(1-\phi)P^{REF}}{\tau\delta F^{REF}} \tag{5.11}$$

where the reference pressure (P^{REF}) is 1 bar and the reference flow rate (F^{REF}) is the feed flow rate. The contact time also affects the permeate flow rate by 10 %. The reactants permeabilities (L_i), affect mainly the corresponding permeate composition and flow rate. The propane molar fraction at the permeate side ($y^{P}_{C_3H_8}$) is mainly affected by the kinetic constant (7 %), as expected; however it is also affected by the hydrogen adsorption constant at catalyst surface

(K_{H_2}) (6 %). From this analysis, it can be concluded that the permeabilities do not affect the advancement as much as they affect the permeate flow rate or composition. On the other hand, the retentate flow rate and its composition are essentially insensitive to these parameters (data not shown).

Table 5.3 Relative change of the advancement and permeate's flow rate and composition, obtained by changing 10 % each parameter. Reference conditions: feed flow rate = 323 mL_N min^{-1}, $y^F_{H_2} \big/ y^F_{C_3H_6} = 5.67$, retentate pressure = 1.2 bar and permeate pressure = 0.1 bar.

Parameter	ΔX / %	ΔQ^P / mL_N min^{-1}	$\Delta y^P_{H_2}$ / %	$\Delta y^P_{C_3H_8}$ / %	$\Delta y^P_{C_3H_6}$ / %
k / mol g_{Pd}^{-1} s^{-1}	7	-2	-4	7	-5
K_{H_2} / m^3 mol^{-1}	6	-2	-3	6	-5
$K_{C_3H_6}$ / m^3 mol^{-1}	1	-1	-1	2	-1
L_{H_2} / mol m^{-1} bar^{-1} s^{-1}	2	8	10	-3	-8
$L_{C_3H_6}$ / mol m^{-1} bar^{-1} s^{-1}	1	5	-5	-2	9
Γ	10	10	1	2	-4

Simulations for different permeate and retentate pressures, while keeping constant the kinetic and transport parameters, the feed flow rate and the feed reagents ratio, were performed to gain insight to those operating variables. Fig. 5.9 shows the influence of the permeate and retentate pressure, in terms of advancement (Fig. 5.9A) and molar fraction of propane produced and present in the permeate stream – product recovery at the permeate side – (see Fig. 5.9B). The recovery is defined as follows:

$$\varphi_{C_3H_8}^{P} = \frac{F_{C_3H_8}^{P} y_{C_3H_8}^{P}}{F_{C_3H_8}^{P} y_{C_3H_8}^{P} + F_{C_3H_8}^{R} y_{C_3H_8}^{R}} \tag{5.12}$$

Fig. 5.9A shows that, when increasing the retentate pressure, the advancement increases, which is mainly attributed to the reaction rate increase, although the driving force for permeation is also of concern. The advancement also increases with the permeate pressure. Similarly, Theis et al. [1] reported experimentally an increase in the catalytic performance with permeate pressure for propylene hydrogenation over PDMS membranes that contain palladium clusters at 303 K. Finally, Fig. 5.9B shows that $\varphi_{C_3H_8}^{P}$ increases with the retentate pressure but decreases significantly with the permeate pressure. This happens because as the permeate pressure increases, the higher propane partial pressure on the permeate side promotes an increase in the propane molar flux to the retentate side of the membrane, negatively affecting its recovery.

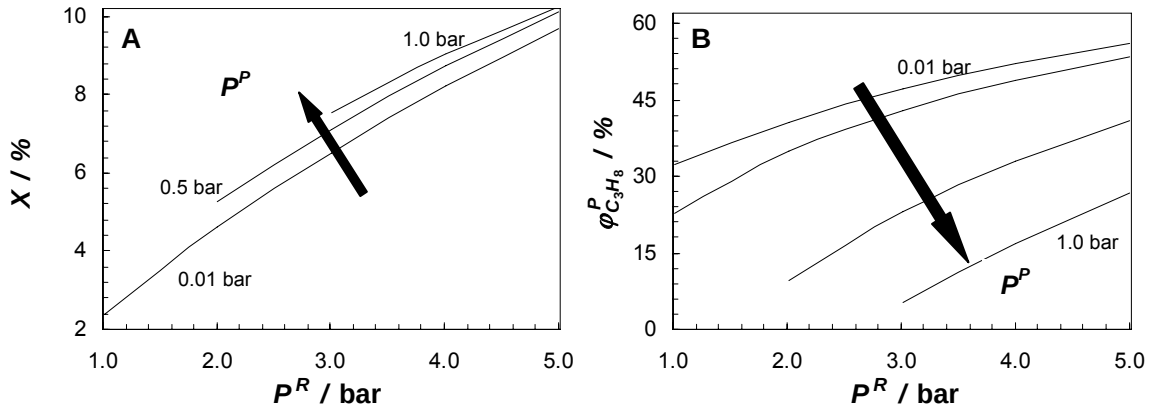

Fig. 5.9 Advancement of reaction (A) and product recovery (B) as a function of the retentate pressure for different permeate pressures. Feed flow rate 323 $mL_N\ min^{-1}$, $y_{H_2}^{F} / y_{C_3H_6}^{F} = 5.67$

5.5 Conclusions

The performance of a continuous polymeric catalytic membrane reactor (pCMR), which contains

palladium nanoclusters in the polymeric matrix of a PDMS composite membrane, was studied for propylene hydrogenation at 308 K, both experimentally and theoretically.

The model developed for the pCMR includes the mass balances to the retentate and permeate chambers as well as the mass balance to the catalytic membrane, which comprises the transport and the propylene hydrogenation kinetics. The mass transport parameters were obtained from an independent study, by the time-lag method. The model predicts the experimental data (i.e. the flow rates and mixture compositions at both chambers) fairly well, with some kinetic parameters (propylene adsorption constant and kinetic constant) being obtained by fitting the model to experimental data, while the hydrogen kinetic parameter was obtained from independent experiments.

The pCMR performance was mainly studied as a function of the feed hydrogen/propylene ratio. It was observed that high concentrations of propane were obtained in the permeate chamber when the feed hydrogen/propylene molar ratio was between 5 and 6. The proposed model allowed to understand this behaviour, which is mainly related to the reaction kinetics and to the diffusion selectivity. The model also predicts the reaction advancement for the various operating conditions considered quite well, showing that it is able to capture the main phenomena present in the studied pCMR.

5.6 Notation

A membrane area, m^2

C_i concentration of component i inside the membrane, mol m^{-3}

C_i^g concentration of component i in the gas phase, mol m^{-3}

D_i diffusion coefficient of component i, m^2 s^{-1}

F	molar flow rate, mol s^{-1}
H_i	Henry's sorption coefficient of component *i*,mol m^{-3} bar^{-1}
k	kinetic constant, mol g_{Pd}^{-1} s^{-1}
K_i	adsorption equilibrium constant of component *i* in the catalyst surface based on membrane concentration, m^3 mol^{-1}
K_i^g	adsorption equilibrium constant of component *i* in the catalyst surface based on gas phase concentration, m^3 mol^{-1}
L_i	permeability coefficient of component *i*, mol m^{-1} bar^{-1} s^{-1}
p_i	partial pressure of component *i*, bar
P	total pressure, bar
Q	volumetric flow rate, mL_N min^{-1}
r	local reaction rate, mol g_{Pd}^{-1} s^{-1}
R	gas constant, bar m^3 mol^{-1} K^{-1}
T	temperature, K
x	spatial coordinate of the membrane, m
X	advancement of reaction, -
y	molar fraction, -

Greek letters

α	selectivity, -
δ	membrane thickness, m
ϕ	catalyst volume fraction, -
ν_i	stoichiometric coefficient of component *i*, -
ρ	catalyst or polymer density, g m^{-3}
$\varphi_{C_3H_8}^P$	recovery, -
τ	tortuosity factor, -
Γ	contact time, -

Sub/superscripts

i	component *i*
F	feed

g gas phase

P permeate

R retentate

5.7 References

[1] J. Theis, D. Fritsch, F. Keil, Catalysis with non-porous membranes loaded with nanoscale metallic clusters. In: ESF, Network Catalytic Membrane Reactors- Final Workshop: Applications and Future Possibilities of Catalytic Membrane Reactors, Turnhout, Belgium October 16-17, 1997, 35-41.

[2] C. Q. Liu, Y. Xu, S. J. Liao, D. R. Yu, Y. K. Zhao, Y. H. Fan, Selective hydrogenation of propadiene and propyne in propene with catalytic polymeric hollow-fiber reactor, J. Membr. Sci. 137 (1997) 139.

[3] B. Gerhand, B. Claus, D. Peiner, Process and catalysis for selective hydrogenation of propyne and propadiene from propylene-containing C_3 hydrocarbon mixtures. Germany (East) Patent 0,261,146, 1988.

[4] G. Langhendries, G. V. Baron, I. F. J. Vankelecom, R. F. Parton, P. A. Jacobs, Selective hydrocarbon oxidation using a liquid-phase catalytic membrane reactor, Catal. Today 56 (2000) 131.

[5] D. Fritsch, K. Kuhr, K. Mackenzie, F. D. Kopinke, Hydrodechlorination of chloroorganic compounds in ground water by palladium catalysts - Part 1. Development of polymer-based catalysts and membrane reactor tests, Catal. Today 82 (2003) 105.

[6] J. Sousa, P. Cruz, A. Mendes, Modeling a catalytic polymeric non-porous membrane reactor, J. Membr. Sci. 181 (2001) 241.

[7] M. G. De Angelis, T. C. Merkel, V. I. Bondar, B. D. Freeman, F. Doghieri, G. C. Sati, Hydrocarbon and fluorocarbon solubility and dilation in poly(dimethylsiloxane): comparison of experimental data with predictions of the Sachez-Lacombe equation of state, J. Polym. Sci.: B 37 (1999) 3011.

[8] L. R. Petzold, A. C. Hindmarsh, LSODA, Computing and Mathematics Research Division, Lawrence Livermore National Laboratory, 1997.

[9] L. Troger, H. Hunnefeld, S. Nunes, M. Oehring, D. Fritsch, Structural characterization of catalytically active metal nanoclusters in poly(amide imide) films with high metal loading, J. Phys. Chem. B 101 (1997) 1279.

[10] J. G. Wijmans, R. W. Baker, The solution-diffusion model: a review, J. Membr. Sci. 107 (1995) 1.

[11] S. Scire, S. Minico, C. Crisafulli, Selective hydrogenation of phenol to cyclohexanone over supported Pd and Pd-Ca catalysts: an investigation on the influence of different supports and Pd precursors, Appl. Catal. A: Gen. 235 (2002) 21.

[12] F. Pinna, F. Menegazzo, M. Signoretto, P. Canton, G. Fagherazzi, N. Pernicone, Consecutive hydrogenation of benzaldehyde over Pd catalysts - Influence of supports and sulfur poisoning, Appl. Catal. A: Gen. 219 (2001) 195.

[13] H. Bonnemann, W. Brijoux, K. Siepen, J. Hormes, R. Franke, J. Pollmann, J. Rothe, Surfactant stabilized palladium colloids as precursors for cis-selective alkyne-hydrogenation catalysts, Appl. Organomet. Chem. 11 (1997) 783.

[14] H. Bonnemann, G. Braun, W. Brijoux, R. Brinkmann, A. S. Tilling, K. Seevogel, K. Siepen, Nanoscale colloidal metals and alloys stabilized by solvents and surfactants - Preparation and use as catalyst precursors, J. Organomet. Chem. 520 (1996) 143.

[15] Bronkhorst® High-Tech-B.V., Fluidat® on the Net, Gas Conversion Factor Calculations, http://www.fluidat.com/ (Accessed: July 2006).

[16] J. Theis, Entwicklung und Anwendung von katalytischen Polymermembranen, PhD Thesis, Technical University of Hamburg, Hamburg, Germany, 2000.

6. Propyne Hydrogenation in a Continuous Polymeric Catalytic Membrane Reactor*

Abstract

Propyne hydrogenation was studied in a continuous polymeric catalytic membrane reactor (pCMR), both experimentally and theoretically. It was used a poly(dimethylsiloxane) (PDMS) composite membrane with an average thickness of 4.4 μm, loaded with 5 wt. % of 9 nm diameter Pd clusters. The reaction was conducted at 308 K and several feed compositions at a fixed flow rate were tested.

The mathematical model proposed includes the mass balances to the retentate and permeate chambers and the mass balance and transport kinetics through the catalytic membrane. The pCMR model also considers a reaction rate equation composed by two terms: the propyne to propylene and the propylene to propane hydrogenations. The selectivity between these two reactions is described by the bicomponent adsorption of propyne and propylene obtained by the IAST model (thermodynamic selectivity). The proposed model represents quite well the experimental data regarding the flow rates and mixture compositions of the permeate and retentate streams.

* *L. Brandão, L. M. Madeira, A. M. Mendes, Chem. Eng. Sci. in press,* **doi:10.1016/j.ces.2007.07.054** *(2007).*

6.1 Introduction

The subject of membrane-based reactive separation otherwise also known as membrane reactors has attracted much interest over the last decade or so. However, the concept has yet to find larger scale industrial applications. One of the major obstacles for further commercial development of membrane reactors are the membrane themselves, which still need to be optimized [1].

The main goals while using catalytic membrane reactors are [2, 3]: *i*) yield-enhancement - the role of the membrane is mainly to remove a reaction product from the reactor, in order to increase the yield compared to conventional reactors. This is obtained either by improving the conversion in equilibrium-restricted reactions or, in consecutive reactions, by improving the selectivity towards a primary product via its selective extraction through the membrane; *ii*) selectivity enhancement - the role of the membrane is to dose a reactant that may react in successive reactions. In this way the concentration of the reagents are kept low by controlled addition through the membrane. This limits side reactions or subsequent reactions of the product; and *iii*) improve the reactants' contact with catalyst – the role of the membrane is to help reactants present in different phases to contact with the catalyst.

Most studies combining membranes and catalysts concern gas phase reactions at relatively high temperatures and in most of these applications inorganic ceramic or metal membranes are applied [1]. The major challenges found in the development of inorganic catalytic membrane reactors for large-scale application are related to material science (synthesis of defect-free membranes, reducing membrane thickness), catalyst science and chemical engineering [4].

Polymeric membranes (porous or dense) can be employed when the reaction takes place in soft reaction conditions. These membranes show some advantages over the more expensive inorganic ones, either ceramic or metallic, namely lower production costs, and the possibility of

synthesizing crack-free thin membranes and the large scale production. Moreover, they show versatile diffusivities and sorption capacities. Furthermore, most of the polymers can be easily manufactured in different shapes as they are elastic and resistant to fatigue, and polymeric membranes can be produced with incorporated catalysts such as nano-sized dispersed metallic clusters [5], zeolites or activated carbons [6]; in some way, polymers can be tailored as needed.

Polymeric membranes can be based on rubbery or glassy polymers. Rubbery polymers usually have high permeabilities towards gases, but relatively lower selectivities, while glassy polymers have high selectivities but lower permeabilities. However, one of the most important membrane characteristics is its permeability because permeability is related with the size of the polymeric catalytic membrane reactor (pCMR). For that reason, research on the synthesis of more selective, permeable membrane materials for gas phase reactions is still going on.

Poly(dimethylsiloxane) (PDMS) has received considerable attention as a membrane material for gas separation due to its high intrinsic permeability to gases and vapours (the highest among rubbery polymers) and also because it combines mechanical, chemical and thermal stability [4]. Among the PDMS membranes applications, there are some works on pCMR [7, 8].

The selective hydrogenation of propadiene and propyne, present as impurities in propylene streams, is an important reaction in the petrochemical industry. One of the most important applications of propylene is to produce polypropylene. For this, propylene should contain less than 10 and 5 ppm of propadiene and propyne, respectively [9]. In this purification process, however, the over-hydrogenation of propylene to propane should be avoided.

In this chapter, it is studied the propyne hydrogenation in a pCMR at 308 K. A PDMS dense membrane 4.4 μm thick and containing palladium nanoclusters 8.8 nm in diameter is used.

A model is proposed, which is compared with the experimental results, being the model parameters obtained from independent experiments whenever possible.

6.2 Model development

The experiments were conducted in an open reactor where the flow pattern in both retentate and permeate chambers can be considered perfectly mixed. A sketch of the pCMR is shown in Fig. 6.1.

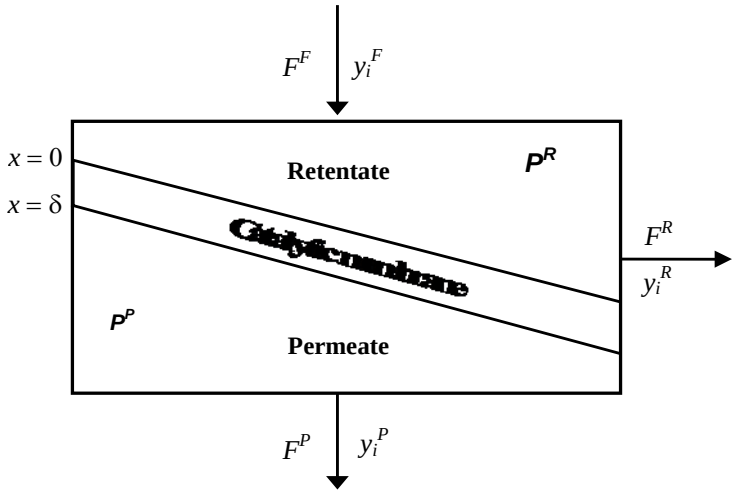

Fig. 6.1 Schematic diagram of the polymeric catalytic membrane reactor.

The model developed is given in *Chapter 5*. Briefly, the main assumptions are: steady-state operation; negligible pressure drop at the retentate and permeate chambers; ideal gas behaviour; fickian transport across the membrane; sorption equilibrium between the bulk gas phase and the membrane surface described by Henry's law; no concentration polarization; constant diffusion coefficients; isothermal operation; and the reaction occurs only on the surface of catalyst nanoparticles, which are distributed uniformly across the membrane.

Mass balance in the membrane and boundary conditions:

$$(1-\phi)\frac{D_i}{\tau}\frac{\mathrm{d}^2 C_i}{\mathrm{d}x^2} + \phi\rho\nu_i r = 0 \qquad i = H_2, C_3H_4, C_3H_6, C_3H_8, Ar \qquad (6.1)$$

$$x = 0 \qquad C_i = H_i y_i^R P^R \qquad i = H_2, C_3H_4, C_3H_6, C_3H_8, Ar \qquad (6.2)$$

$$x = \delta \qquad C_i = H_i y_i^P P^P \qquad i = H_2, C_3H_4, C_3H_6, C_3H_8, Ar \qquad (6.3)$$

Partial and total mass balances in the retentate chamber:

$$F^F y_i^F - F^R y_i^R + (1-\phi)A\frac{D_i}{\tau}\frac{\mathrm{d}C_i}{\mathrm{d}x}\Big|_{x=0} = 0 \qquad i = H_2, C_3H_4, C_3H_6, C_3H_8, Ar \qquad (6.4)$$

$$F^F - F^R + (1-\phi)A\sum_i \frac{D_i}{\tau}\frac{\mathrm{d}C_i}{\mathrm{d}x}\Big|_{x=0} = 0 \qquad i = H_2, C_3H_4, C_3H_6, C_3H_8, Ar \qquad (6.5)$$

Partial and total mass balances in the permeate chamber:

$$F^P y_i^P + (1-\phi)A\frac{D_i}{\tau}\frac{\mathrm{d}C_i}{\mathrm{d}x}\Big|_{x=\delta} = 0 \qquad i = H_2, C_3H_4, C_3H_6, C_3H_8, Ar \qquad (6.6)$$

$$F^P + (1-\phi)A\sum_i \frac{D_i}{\tau}\frac{\mathrm{d}C_i}{\mathrm{d}x}\Big|_{x=\delta} = 0 \qquad i = H_2, C_3H_4, C_3H_6, C_3H_8, Ar \qquad (6.7)$$

The subscript *i* refers to the *i*th component and the superscripts *F*, *R* and *P* refer to the feed, retentate and permeate conditions, respectively (cf. Fig. 6.1). *P* is the total pressure, *D* is the diffusion coefficient, *H* is the Henry's constant, *F* is the total molar flow rate, *y* is the molar fraction of a given component and ϕ is the volume fraction of catalyst. The remaining symbols have the usual meaning and are described in the nomenclature.

The numerical procedure used to solve this set of equations is described in *Chapter 5*. However, the numerical method diverges for very low propyne concentrations owing to the negative reaction order with respect to its partial pressure (cf. Eq. (6.8) below). To overcome this

difficulty an exponential function raised to a very large negative value was multiplied to the reaction rate, which approaches zero as propyne partial pressure becomes very low.

6.3 Experimental section

The pCMR experimental unit as well as the preparation and characterization of the catalytic membrane used are described in *Chapter 5*. A Pd/PDMS composite membrane with 5 wt. % Pd content (volume fraction of catalyst, ϕ, of 0.004), thickness of 4.4 μm and an effective area of 13.9 cm^2 was used. Different hydrogen/propyne molar ratios (gases from Praxair; hydrogen 99.999 %, propyne 97 %) were fed to the membrane reactor at ca. 200 $mL_N\ min^{-1}$ and at 1.2 bar pressure (Druck, ref. 4010, 7 bar, absolute, ± 0.04 % FS). High feed flow rates were employed in order to assure the flow pattern at the retentate side is properly described by the perfectly mixed model. Argon (Praxair, 99.999 %) was employed to dilute the feed, which was composed of hydrogen and propyne in one set of experiments and of hydrogen, propyne and propylene (Praxair, 99.5 %) in the other – Table 6.1. The permeate pressure was set to 100 mbar (Druck, ref. 4010, 2 bar, absolute, ± 0.04 % FS) and the experiments were repeated at least twice at 308 K. Feed, permeate and retentate gas mixture were supplied in triplicate to an on-line gas chromatograph for composition analysis (Dani GC 1000 - FID and TCD (Valco Inc.) detectors).

Table 6.1 Feed composition ranges and volumetric feed flow rate for the two sets of experiments.

Set #	Q^F / $mL_N\ min^{-1}$	$y^F_{H_2}$ / %	$y^F_{C_3H_4}$ / %	$y^F_{C_3H_6}$ / %	y^F_{Ar} / %
1	200 ± 2	20 - 27	1.2 - 8.1	0.0	72
2	209 ± 1	24 - 25	1.2 - 2.6	26	48

6.4 Results and discussion

6.4.1 Mass transport characterization

The mass transport parameters of argon, hydrogen, propane, propylene and propyne in PDMS at 308 K were determined in *Chapter 4*, using the time-lag method. Sorption, diffusion and permeability coefficients of the above-mentioned compounds in a dense PDMS membrane, 300 μm thick, are shown in Table 6.2. A 300-μm thick non-supported Pd/PDMS membrane was also prepared to compute the tortuosity factor (τ = 1.7 ± 0.2) from permeability experiments using different species as probing gases (*Chapter 4*).

Table 6.2 Sorption, diffusion and permeability coefficients of different gases in a PDMS-membrane at 308K (*Chapter 4*).

Component	H / mol m^{-3} bar^{-1}	D x 10^{10} / m^2 s^{-1}	L x 10^{10} / mol m^{-1} bar^{-1} s^{-1}
H_2	3.41 ± 0.60	74.0 ± 8.0	252 ± 52
C_3H_4	521 ± 15	7.08 ± 0.09	3 690 ± 113
C_3H_6	384 ± 5	5.36 ± 0.06	2 057 ± 29
C_3H_8	416 ± 8	4.06 ± 0.05	1 692 ± 32
Ar	14.1 ± 0.9	17.0 ± 1.0	240 ± 21

6.4.2 Determination of the kinetic equation

The kinetics of propyne hydrogenation was determined previously in a batch reactor using palladium nanoclusters (average size 7.3 nm) stabilized by a surfactant shell that prevents cluster

agglomeration and which showed no mass transfer resistance (*Chapter 3*). A power-law model was fitted to the obtained results:

$$-r_{C_3H_4} = k_1^g \, p_{C_3H_4}^a \, p_{H_2}^b \tag{6.8}$$

where k_1^g is the overall kinetic rate constant and p_i is the partial pressure of species *i*. The fitting originated a reaction order of (*a*) -0.02 for propyne and a reaction order of (*b*) 1.09 for hydrogen.

It is important to remark that different kinetics may be observed when the catalyst is supported in different supports [10]. Indeed, the previously determined reaction kinetics for propyne hydrogenation over palladium nanoclusters stabilized with the surfactant *n*-$(C_{18}H_{37})_4N^+Br^-$ did not describe accurately the same hydrogenation experiments in the pCMR, where the nanoclusters of palladium are dispersed inside the PDMS membrane. This same phenomenon was observed with the propylene hydrogenation (*Chapter 5*). The tetraoctadecylammonium bromide surfactant used to stabilize the catalyst nanoclusters interferes especially with the adsorption of larger reactant species such as propyne showing, however, a negligible effect towards the hydrogen adsorption owing to its very small molecular size [11].

Although alkyne hydrogenation seems to be a simple reaction, the details of the mechanism of transition-metal-catalyzed hydrogenations are still not fully understood. During the reaction various carbonaceous species are deposited on the metal catalyst surface and they have been identified as an important part of the reaction mechanism, indicating that the dynamics on the surface of the catalyst is quite complex [12-14]. Moreover, there may be more than one type of active site for each reaction, more than one pathway for obtaining a single product, and finally more than one product. Indeed, kinetic models trying to reflect the true mechanism have been proposed with kinetic rate equations not based on less than four or five different parameters [13,

14]. Therefore, kinetic equations based upon simplified mechanisms or regression functions of arbitrary form have been used for fitting experimental kinetic data [15, 16].

The above-mentioned power-law kinetic equation was obtained using the surfactant-stabilized Pd nanoclusters that, for the reasons mentioned before, should not be valid when the Pd is occluded in the PDMS membrane. Several runs using the Pd-doped PDMS membrane were then performed in an open reactor and the parameters of the power-law rate equation obtained minimizing the sum of the square residues. Due to the complexity of the optimization, a Surface Response Analysis was employed based on a commercially available software - JMP® 5.1, SAS. As the hydrogenation of propyne occurs inside the PDMS membrane, the sorbed concentrations were related with the gas phase partial pressures of the corresponding species using Henry´s law.

The selectivity of the propyne to propylene hydrogenation, defined as the ratio between propylene produced per mole of propyne reacted [17], is attributed to the stronger adsorption of propyne at palladium surface compared to that of propylene (thermodynamic selectivity) (*Chapter 3*). This way, depending on the operating conditions of the pCMR, the propyne hydrogenation can originate mainly propylene or propane can also be formed in a considerable extent. Therefore, the model given by equations ((6.1)-(6.7)) should include an overall rate equation comprising the propylene formation as well as the deeper hydrogenation towards propane. The overall rate equation should combine the partial rate equations regarding propyne to propylene and propylene to propane hydrogenations, using the IAST (Ideal Adsorption Solution Theory) model for obtaining the bicomponent propylene/propyne adsorption at the catalyst surface (*Chapter 3*).

The propylene hydrogenation reaction rate equation in a PDMS membrane loaded with palladium is (*Chapter 5*):

$$r_{C_3H_8} = \frac{k_2 K^g_{H_2} K^g_{C_3H_6} C^g_{H_2} C^g_{C_3H_6}}{\left(1 + \sqrt{K^g_{H_2} C^g_{H_2}} + K^g_{C_3H_6} C^g_{C_3H_6}\right)^3} \quad (6.9)$$

where the parameters of the rate equation are: k_2 = 18.3 mol g_{Pd}^{-1} s^{-1}, $K^g_{H_2}$ = 9.70 x 10^{-4} m^3 mol^{-1} and $K^g_{C_3H_6}$ = 1.31 x 10^{-1} m^3 mol^{-1}, where K^g_i is the Langmuir - Hinshelwood (L-H) adsorption constant of reactant *i* between gas and catalyst phases. The relationship between the L-H adsorption constants when the hydrogenation occurs with the catalyst contacting the membrane phase compared when it occurs contacting the gas phase is (*Chapter 5*):

$$K_i = \frac{K^g_i}{H_i RT} \quad (6.10)$$

Then, the overall kinetic rate equation becomes:

$$r_i = \alpha \nu_{i,1} k_1 C^a_{C_3H_4} C^b_{H_2} + \beta \nu_{i,2} \frac{k_2 K_{H_2} K_{C_3H_6} C_{H_2} C_{C_3H_6}}{\left(1 + \sqrt{K_{H_2} C_{H_2}} + K_{C_3H_6} C_{C_3H_6}\right)^3} \quad (6.11)$$

where $\nu_{i,j}$ is the stoichiometric coefficient of component *i* in the reaction *j*, propyne hydrogenation (reaction *j* = 1) and propylene hydrogenation (reaction *j* = 2). α and β are model variables associated with the propyne/propylene adsorption selectivity for the palladium catalyst given by the IAST model. These variables are defined as the ratio between the hydrocarbon adsorption concentration given by the IAST bicomponent (propyne and proylene) model [18], and the mono-component isotherm, where α is for propyne and β is for propylene (*Chapter 3*). β ranges between one, for high propylene molar fractions (where propyne is mostly absent from the catalyst surface), and much smaller values (for low propylene and high propyne molar fractions). α is one or very close to one when propyne species are present. α and β variables should explain the propylene selectivity of the propyne hydrogenation in the PCMR. However, and as mentioned before, during propyne hydrogenation carbonaceous deposits are formed on the

catalyst surface. These carbonaceous deposits can change the catalyst surface in such a way that different active sites are built. These sites selectively adsorb propyne and propylene based on their steric hindrance. Type I sites are available only to propyne species while type II sites are available for both propyne and propylene species [12, 13]. However, due to the thermodynamic selectivity, when propyne is present in the reaction mixture both types of sites are occupied by this hydrocarbon. When propyne is not present at the catalyst surface, propylene species can adsorb but only on type II sites. In this case, the active sites concentration for propylene hydrogenation is much smaller than the active sites concentration when propylene hydrogenation is occurring in a catalyst with no carbonaceous deposits. Actually, a four times decrease in the propylene hydrogenation rate was observed in a Pd/PDMS sample previously used for propyne hydrogenation compared with a fresh sample (data not shown). Consequently, the propylene hydrogenation kinetic constant used in the combined model reaction rate equation should be four times smaller than the kinetic constant obtained during propylene hydrogenation in the PCMR, i.e. k_2 = 4.6 mol g_{Pd}^{-1} s^{-1}. The dynamics on the surface of the catalyst during propyne hydrogenation is quite complex and the palladium selectivity is not only described by the α and β variables but it is also affected by the presence of the carbonaceous deposits [12, 13, 19].

The power-law equation parameters obtained by model fitting to the experimental data shown below are given in Table 6.3. The fitting parameters indicate a nearly first order dependence on hydrogen partial pressure and a negative order on propyne partial pressure, during propyne hydrogenation over the PDMS-supported palladium clusters at 308 K.

A nearly first order dependence in hydrogen partial pressure (b = 1.09) was also obtained during the same hydrogenation but over the surfactant-stabilized Pd clusters (*Chapter 3*). This was expectable because the hydrogen adsorption on the catalyst surface is low and is

approximately the same either the catalyst is surfactant- or PDMS-stabilized. Actually, the Langmuir-Hinshelwood adsorption constant of hydrogen at the catalyst surface for propylene and propyne hydrogenations on the palladium clusters stabilized with surfactant are much smaller than the corresponding adsorption constants of propylene or propyne, indicating low hydrogen coverage during these reactions (*Chapters 2 and 3*). Other authors also report first order reaction rates with respect to the hydrogen partial pressure during propyne and acetylene hydrogenations on palladium [14-16, 20, 21].

The negative order with respect to propyne indicates strong adsorption and high surface coverage of this reactant at catalyst surface. This same trend was already observed by other authors for the acetylene hydrogenation on palladium, reporting values of -0.66 and -0.6 at temperatures around 300 K [16, 21]. Zero orders in propylene and acetylene at temperatures ranging from 340 to 380 K were obtained during propylene and acetylene hydrogenations over palladium [14, 20], while Vincent and Gonzalez [14] reported first order dependence in acetylene partial pressure for the corresponding hydrogenation over palladium at 420 K. The evolution of the alkyne reaction order, from negative at around 300 K, zero order at around 350 K, to first order at around 420 K, should be related to the high heat of adsorption and then to the strong dependence of the adsorption load with the temperature [14]. The kinetic order value (a = -0.44) obtained for propyne partial pressure is in agreement with the reported values for hydrogenation of small alkynes over palladium, at nearly room temperature [16, 21].

Nearly zero order dependence with respect to propyne partial pressure (a = -0.02) was obtained during hydrogenation of this species at 308 K over palladium clusters stabilized with a surfactant (*Chapter 3*). In the case of palladium clusters supported in the PDMS-membrane and at the same temperature, the propyne reaction order that fits the experimental results is smaller.

This should be related with the lower adsorption constant of propyne at the catalyst surface when the surfactant is supporting the catalyst. Actually, the surfactant interferes strongly especially with the L-H adsorption constant of propylene and propyne, where a higher adsorption constant was found in the case of PDMS stabilized catalyst for propylene hydrogenation (*Chapter 5*).

Table 6.3 Kinetic parameters of the power-law rate equation, $-r_{C_3H_4} = k_1^g \, p_{C_3H_4}^a \, p_{H_2}^b$, describing propyne hydrogenation over the palladium nanoclusters supported in a PDMS-membrane (T = 308 K).

Parameter	Value
k_1^g / mol g_{Pd}^{-1} s^{-1} $(bar^{-1})^{-0.58}$	4.7×10^{-3}
a	-0.44
b	1.02

6.4.3 Hydrogenation experiments in the pCMR

One of the assumptions of the proposed pCMR model is the perfectly mixed flow pattern in both retentate and permeate chambers. In agreement with this assumption high feed flow rates and gas mixtures poorer in the fastest components (hydrocarbons) were employed in order to guaranty that the feed and retentate compositions were close. The nominal feed flow rate of the pCMR experiments was around 200 mL_N min^{-1} while the permeate flow rate range was 5-15 mL_N min^{-1}.

Figure 6.2 shows the experimental values of the permeate flow rate leaving the reactor as a function of the hydrogen/propyne molar ratio fed to the membrane reactor for the experiments with and without propylene present in the feed stream. As the membrane permeability towards propyne is higher than towards hydrogen or argon (Table 6.2), increasing the feed concentration

on propyne (smaller $y_{H_2}/y_{C_3H_4}$ values) increases the global permeate flow rate. A similar effect is observed when argon is partially replaced by propylene (upper *vs.* lower curves). It can be verified that the model fits reasonably the permeate flow rate. The non-uniform thickness of the membrane, confirmed by SEM analyses (*Chapter 5*), as well as the uncertainty related with the transport parameters of the different gases in the membrane, should explain some differences between the model and the experimental results, despite the experimental values show large error bars. These errors are mainly related with the equipment used to determine the mass flow rates. Indeed, the mass flow meters used to read the permeate flow rate (hot-wire principal) show large uncertainties when the stream is a mixture of gases with very different correction factors [22]. The flow rate relative error was estimated to be ± 15 %.

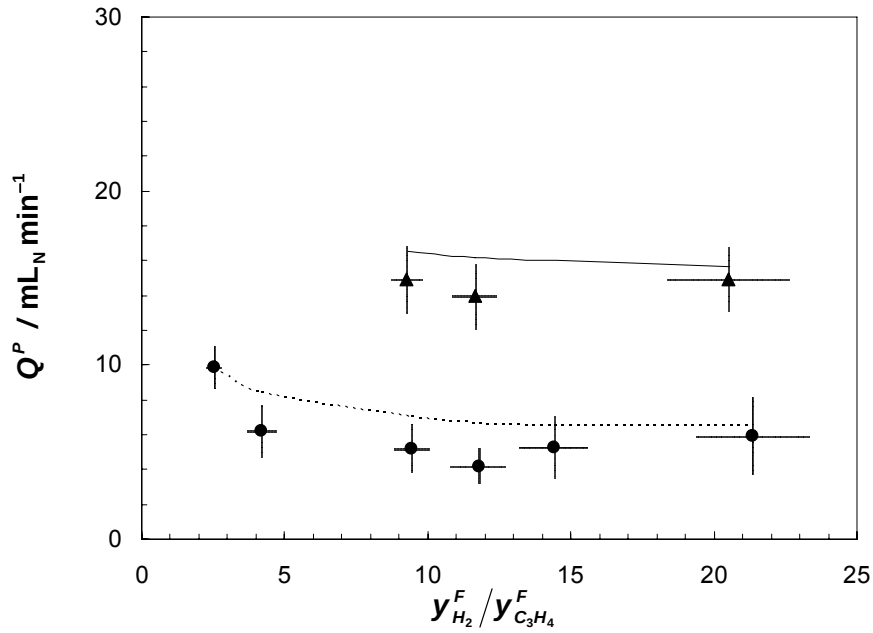

Fig. 6.2 Permeate flow rate as a function of the molar ratio of hydrogen/propyne in the feed obtained during operation of the pCMR. Experiments without propylene (●; dashed line - model fitting) and with propylene (▲; solid line - model fitting) in the feed (cf. Table 6.1).

Figure 6.3 shows the experimental hydrogen compositions at the retentate and permeate outlet streams for different hydrogen/propyne molar ratios at the feed, with and without propylene present in the feed stream. Higher hydrogen concentrations in the retentate than in the permeate chamber are observed for all hydrogen/propyne molar ratios supplied to the pCMR, owing to the lower membrane permeability towards hydrogen compared to the hydrocarbons. As the hydrogen/propyne molar ratio increases one might expect that the hydrogen concentration also increases in both retentate and permeate chambers. However, this is not the case because the hydrogen concentration in either chamber also depends on the hydrogenation rate, which varies with the reactants concentration, as discussed below. The model fits quite well the hydrogen composition in both chambers.

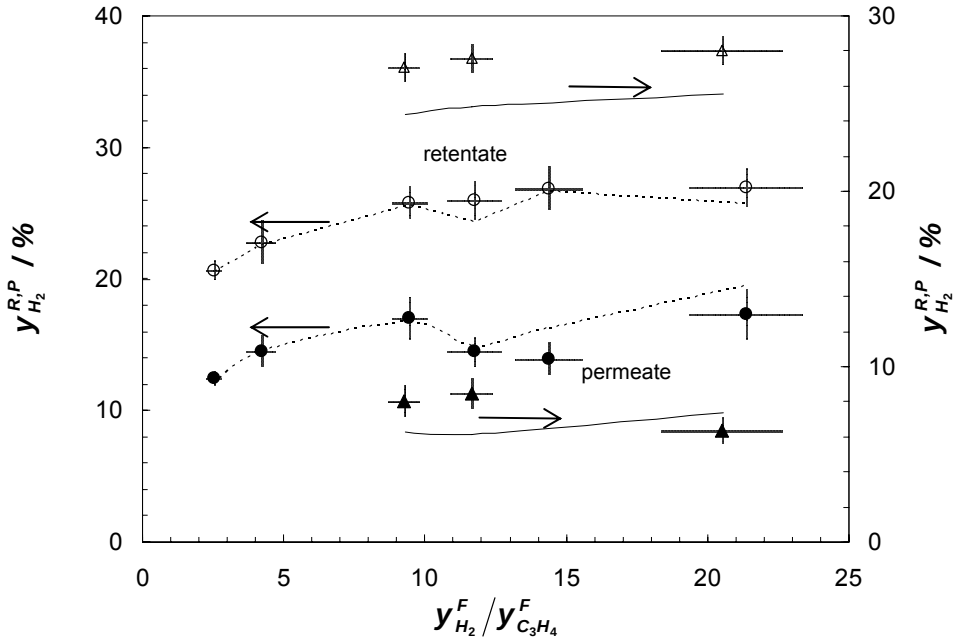

Fig. 6.3 Hydrogen concentration in the retentate and permeate chambers as a function of the molar ratio of hydrogen/propyne in the feed obtained during operation of the pCMR. Experiments without propylene (●, ○; dashed line - model fitting) and with propylene (▲, △; solid line - model fitting) in the feed (cf. Table 6.1).

Figure 6.4 plots the propyne compositions at the retentate and permeate outlet streams as a function of the molar ratio of hydrogen/propyne in the feed, with and without propylene in the feed stream. In this case, much higher propyne concentrations are observed in the permeate chamber when compared to the retentate composition due to the higher PDMS permeability towards propyne (Table 6.2). As the propyne molar fraction increases in the feed stream the propyne composition in the retentate and permeate chambers also increases. Moreover, the PDMS membrane used is more permselective towards propyne when compared to propylene, which leads to the permeance of significant amounts of propyne to the permeate chamber without reacting. Figure 6.4 shows that the model fits fairly well the experimental results.

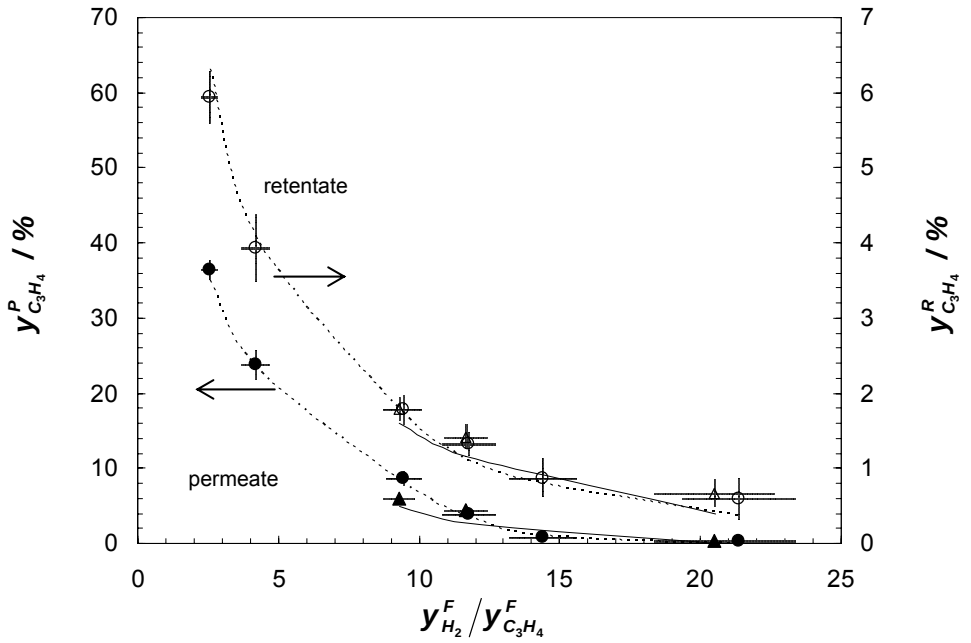

Fig. 6.4 Propyne concentration in the retentate and permeate chambers as a function of the molar ratio of hydrogen/propyne in the feed obtained during operation of the pCMR. Experiments without propylene (●, ○; dashed line - model fitting) and with propylene (▲, △; solid line - model fitting) in the feed (cf. Table 6.1).

Figure 6.5 shows the argon composition in the retentate and permeate chambers as a function of the molar ratio of hydrogen/propyne and when propylene is and is not present in the feed stream. Argon concentration in the permeate chamber increases with the hydrogen/propyne molar ratio when the feed does not contain propylene. This is related to the fact that as the hydrogen/propyne molar ratio increases, decreases the amount of propyne that is the fastest permeable species. The contribution of argon to the permeate composition becomes then more significant. In the experiments with propylene present at the feed, a lower argon molar fraction in the permeate chamber is observed owing to the presence of propylene, which is a very permeable species (cf. Table 6.2). Argon concentration in the retentate stream is very similar to the feed one. This happens because of the high feed flow rate used.

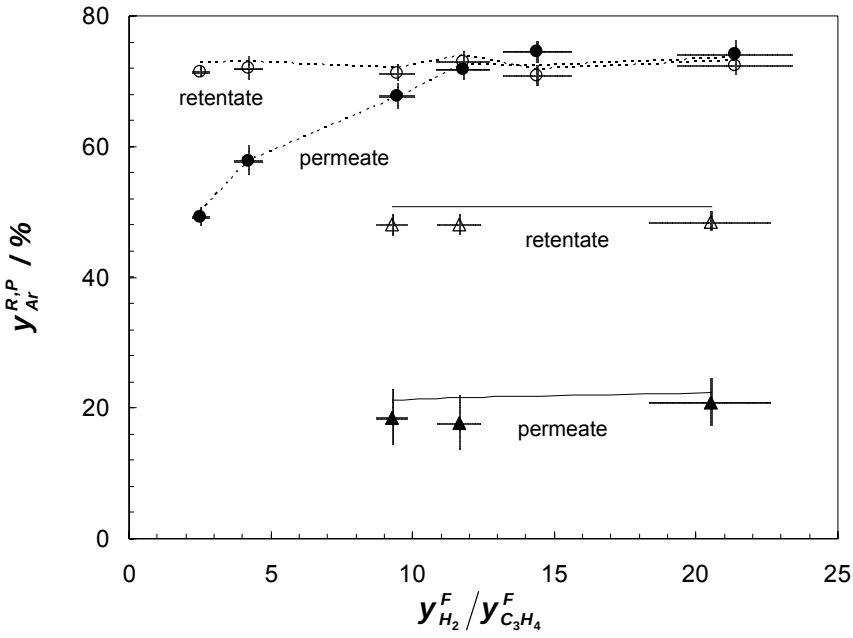

Fig. 6.5 Argon concentration in the retentate and permeate chambers as a function of the molar ratio of hydrogen/propyne in the feed obtained during operation of the pCMR. Experiments without propylene (●, ○; dashed line - model fitting) and with propylene (▲, Δ; solid line - model fitting) in the feed (cf. Table 6.1).

Propylene molar fractions in both chambers are shown in Fig. 6.6 as a function of the molar ratio of hydrogen/propyne in the feed and when propylene is and is not present in the feed stream. Experimental propylene concentrations in the permeate chamber reaches up to ca. 9 %, when there is no propylene in the feed. It is worth to mention that higher propylene molar fractions are observed for high feed hydrogen/propyne molar ratios. As the propyne molar fraction decreases the reaction hindering effect of this species decreases and propylene production rate increases. After a threshold value, at high hydrogen/propyne molar ratios (≈ 15), the propyne molar fraction becomes so low that propylene production starts to decrease. At that point, the deeper hydrogenation of propyne to propane starts increasing, and then propylene

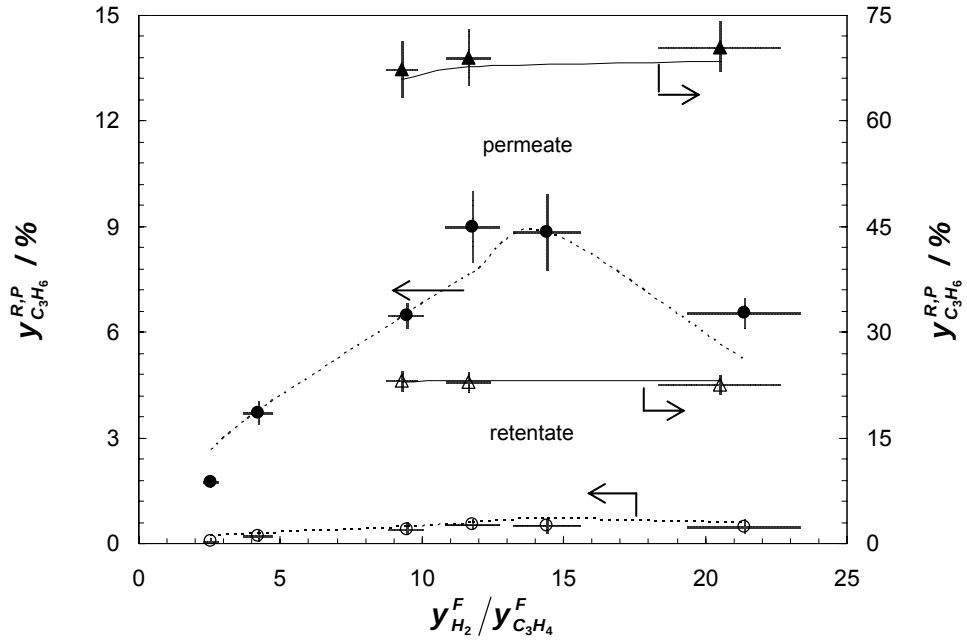

Fig. 6.6 Propylene concentration in the retentate and permeate chambers as a function of the molar ratio of hydrogen/propyne in the feed obtained during operation of the pCMR. Experiments without propylene (●, ○; dashed line - model fitting) and with propylene (▲, △; solid line - model fitting) in the feed (cf. Table 6.1).

molar fraction in the permeate chamber also decreases. It is noticeable the ability of the model to accurately predict this complex competitive reaction. For the experiments with propylene present in the feed, the concentration of this species is around 70 % in the permeate stream mainly due to the high PDMS permeability towards this compound.

Figure 6.7 shows propane concentration in the retentate and permeate chambers as a function of the molar ratio of hydrogen/propyne in the feed, without (Fig. 6.7A) and with (Fig. 6.7B) propylene present in the feed stream. Propane concentration in the retentate and permeate chamber increases with the hydrogen/propyne molar ratio due to the increase of propylene hydrogenation rate (Fig. 6.7A and Fig. 6.7B). Model predicts reasonably the propane concentration for high molar ratios of hydrogen/propyne in the feed. It is, however, noticeable that the model has difficulties to fully represent the propylene hydrogenation repression by the presence of propyne. This could be related with the accurate representation of the multicomponent adsorption of propyne and propylene on the catalyst surface, which is based on the IAST model and monocomponent isotherms obtained using a surfactant-stabilized palladium

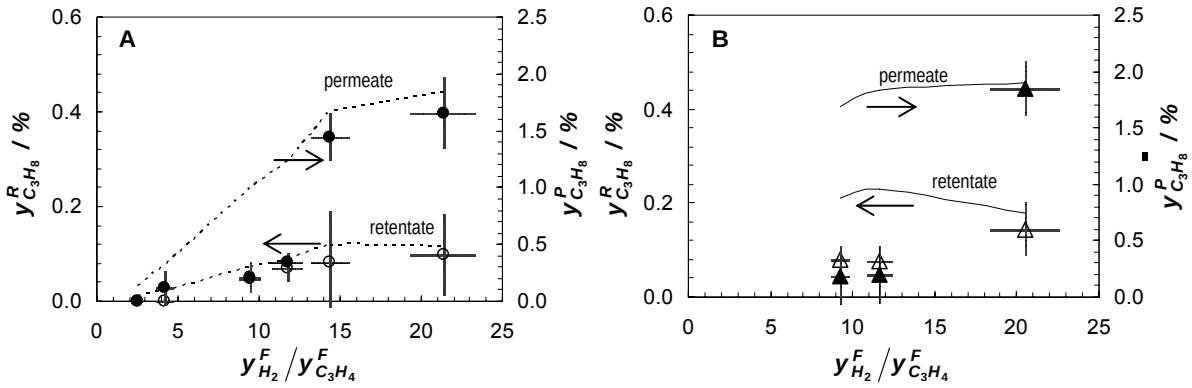

Fig. 6.7 Propane concentration in the retentate and permeate chambers as a function of the molar ratio of hydrogen/propyne in the feed obtained during operation of the pCMR. Experiments without propylene (A) and with propylene (B) in the feed (cf. Table 6.1).

sample. Moreover, and as explained before, the thermodynamic selectivity could not be the only explanation for the high selectivity of palladium for the hydrogenation of alkynes. Besides carbonaceous deposits, the relative adsorption affinities of alkenes and alkynes on palladium (multicomponent adsorption) and their relative subsequent reactivities with hydrogen may also interfere [16]. These results indicate that a further understanding of the propyne hydrogenation kinetics over palladium is still needed.

In Fig. 6.8 it can be seen the propylene selectivity and the overall advancement as a function of the hydrogen/propyne molar ratio and when propylene is and is not present in the feed stream. Selectivity was calculated according to the following expression:

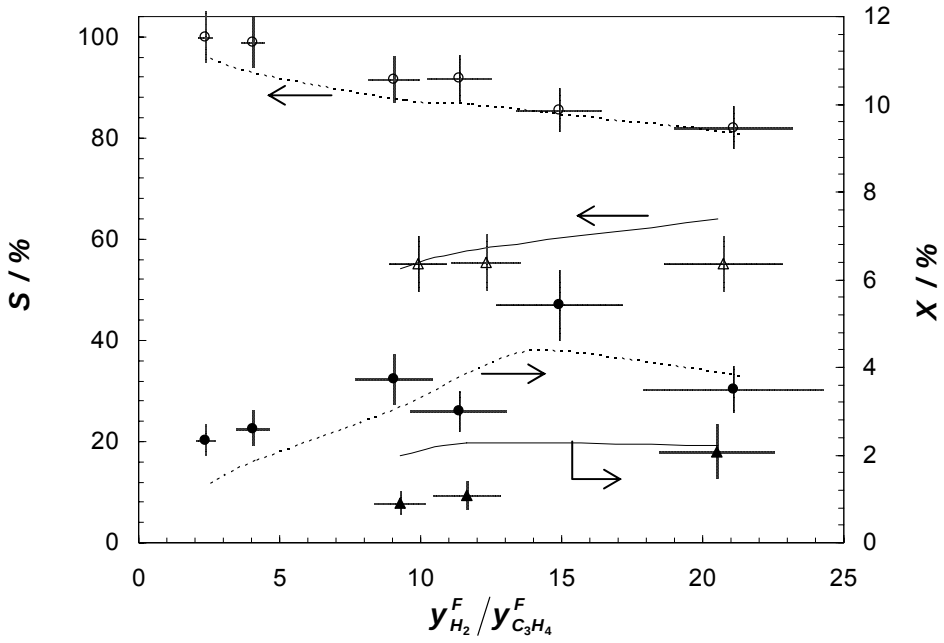

Fig. 6.8 Selectivity for propylene and advancement as a function of the molar ratio of hydrogen/propyne in the feed obtained during operation of the pCMR. Experiments without propylene (●, ○; dashed line - model fitting) and with propylene (▲, △; solid line - model fitting) in the feed (cf. Table 6.1).

$$S = \frac{F^R y^R_{C_3H_6} + F^P y^P_{C_3H_6} - F^F y^F_{C_3H_6}}{F^F y^F_{C_3H_4} - (F^P y^P_{C_3H_4} + F^R y^R_{C_3H_4})} \tag{6.12}$$

An increase in the hydrogen/propyne molar ratio causes a decrease in propylene selectivity for the experiments without propylene in the feed, mainly due to the increase of the propane formation rate. For the experiments with propylene present in the feed stream, the selectivity is lower owing to the high amount of propylene present (26 % in the feed) that is hydrogenated at same time as propyne (propyne feed concentration between ca. 1.2 and 2.6 %).

Figure 6.8 also shows the overall advancement as a function of the feed hydrogen/propyne molar ratio. Advancements for the experiments with propylene present in the feed stream are lower than for the experiments without propylene in the feed mainly because the concentration of reactive species is higher (smaller concentration of inert gas). For the experiments without propylene in the feed, the advancement (related mainly with the rates of the hydrogenation reactions) increases up to a hydrogen/propyne molar ratio of around 15. Up to this stage, the main hydrogenation reaction is the one that converts propyne into propylene. Beyond this stage, the propylene hydrogenation to propane becomes important and eventually the main reaction. The model proposed predicts fairly the experimental results.

6.5 Conclusions

The performance of a continuous polymeric catalytic membrane reactor (pCMR), containing palladium nanoclusters in the polymeric matrix of the membrane, was studied for propyne hydrogenation at 308 K, both experimentally and theoretically.

The performance of the pCMR was studied experimentally as a function of the molar ratio of hydrogen/propyne in the feed. The experimental results indicate that high propylene

concentrations at the permeate chamber can be attained increasing the hydrogen/propyne molar ratio. But, as the propylene production rate increases, propane formation is favoured owing to the high hydrogen molar fractions present.

The PDMS membrane used is more permeable to propyne than to propylene, leading to the permeation of significant amounts of unreacted propyne to the permeate chamber. This makes the PDMS unsuitable for being used in a pCMR flow through contactor arrangement, as the present one, if high purity propylene is to be obtained.

Regarding the theoretical study, the pCMR model includes the mass balances to the retentate and permeate chambers and the mass balance and transport kinetics through the catalytic membrane. The reaction rate equation considered is composed by two terms: the propyne to propylene and the propylene to propane hydrogenations. The selectivity between these two reactions is described by the catalyst bicomponent adsorption of propyne and propylene obtained by the IAST model (thermodynamic selectivity). The transport parameters of the reaction species in the membrane (diffusivity and sorption coefficients) were obtained from independent experiments as well as the thermodynamic selectivity variables (α and β). The kinetic parameters for propyne hydrogenation were obtained by fitting the model to experimental data while the propylene hydrogenation kinetic parameters were obtained from a previous study.

The pCMR model predicts reasonably well the experimental data regarding the flow rates and mixture compositions in permeate and retentate chambers, as well as the general performance of the membrane reactor. Though, the model showed some difficulties to predict the propylene hydrogenation at low/intermediate molar ratios of hydrogen/propyne in the feed.

6.6 Notation

a propyne kinetic order for propyne hydrogenation, -

A membrane area, m^2

b hydrogen kinetic order for propyne hydrogenation, -

C_i concentration of component i inside the membrane, mol m^{-3}

C_i^g gas phase concentration of component i, mol m^{-3}

D_i diffusion coefficient of component i, m^2 s^{-1}

F molar flow rate, mol s^{-1}

H_i Henry's sorption coefficient of component i, mol m^{-3} bar^{-1}

k_1 overall kinetic constant for propyne hydrogenation based on a power-law rate equation and concentrations in the membrane phase, mol g_{Pd}^{-1} s^{-1} $(m^3\ mol^{-1})^{a+b}$

k_1^g overall kinetic constant for propyne hydrogenation based on a power-law rate equation and concentrations in gas phase, mol g_{Pd}^{-1} s^{-1} $bar^{-(a+b)}$

k_2 kinetic constant for propylene hydrogenation, mol g_{Pd}^{-1} s^{-1}

K_i L-H adsorption equilibrium constant of reactant i between the membrane and the catalyst phases, m^3 mol^{-1}

K_i^g L-H adsorption equilibrium constant of reactant i between the gas and the catalyst phases, m^3 mol^{-1}

L permeability, mol m^{-1} bar^{-1} s^{-1}

p_i partial pressure of the component i, bar

P total pressure, bar

Q volumetric flow rate, mL_N min^{-1}

r local reaction rate, mol g_{Pd}^{-1} s^{-1}

R gas constant, bar m^3 mol^{-1} K^{-1}

S selectivity of the reaction, -

T temperature, K

x spatial coordinate of the membrane, m

X advancement of the reaction, -

y molar fraction, -

Greek letters

α, β variables associated with the catalyst propyne/propylene selectivity, -

δ membrane thickness, m

ϕ catalyst volume fraction, -

$\nu_{i,j}$ stoichiometric coefficient of component *i* in the reaction *j*, -

ρ catalyst density, g m^{-3}

τ tortuosity factor, -

Sub/superscripts

i component *i*

F feed

g gas phase

P permeate

R retentate

6.7 References

[1] S. S. Ozdemir, M. G. Buonomenna, E. Drioli, Catalytic polymeric membranes: preparation and application, Appl. Catal. A: Gen. 307 (2006) 167.

[2] A. Julbe, D. Farrusseng, C. Guizard, Porous ceramic membranes for catalytic reactors - overview and new ideas, J. Membr. Sci. 181 (2001) 3.

[3] S. Miachon, J. A. Dalmon, Catalysis in membrane reactors: what about the catalyst?, Top. Catal. 29 (2004) 59.

[4] I. F. J. Vankelecom, P. A. Jacobs, Dense organic catalytic membranes for fine chemical synthesis, Catal. Today 56 (2000) 147.

[5] L. Troger, H. Hunnefeld, S. Nunes, M. Oehring, D. Fritsch, Structural characterization of catalytically active metal nanoclusters in poly(amide imide) films with high metal loading, J. Phys. Chem. B 101 (1997) 1279.

[6] J. Castanheiro, I. Fonseca, A. Ramos, R. Oliveira, J. Vital, Hydration of α-pinene over molybdophosphoric acid immobilized in hydrophobically modified PVA membranes, Catal. Today 104 (2005) 296.

[7] D. Fritsch, K. Kuhr, K. Mackenzie, F. D. Kopinke, Hydrodechlorination of chloroorganic compounds in ground water by palladium catalysts - Part 1. Development of polymer-based catalysts and membrane reactor tests, Catal. Today 82 (2003) 105.

[8] R. F. Parton, I. F. J. Vankelecom, M. J. A. Casselman, C. P. Bezoukhanova, J. B. Uytterhoeven, P. A. Jacobs, An efficient mimic of cytochrome-P-450 from a zeolite encaged iron complex in a polymer membrane, Nature 370 (1994) 541.

[9] C. Q. Liu, Y. Xu, S. J. Liao, D. R. Yu, Y. K. Zhao, Y. H. Fan, Selective hydrogenation of propadiene and propyne in propene with catalytic polymeric hollow-fiber reactor, J. Membr. Sci. 137 (1997) 139.

[10] S. D. Jackson, N. J. Casey, Hydrogenation of propyne over palladium catalysts, J. Chem. Soc. Faraday T. 91 (1995) 3269.

[11] H. Bonnemann, G. Braun, W. Brijoux, R. Brinkmann, A. S. Tilling, K. Seevogel, K. Siepen, Nanoscale colloidal metals and alloys stabilized by solvents and surfactants - Preparation and use as catalyst precursors, J. Organomet. Chem. 520 (1996) 143.

[12] D. R. Kennedy, G. Webb, S. D. Jackson, D. Lennon, Propyne hydrogenation over alumina-supported palladium and platinum catalysts, Appl. Catal. A: Gen. 259 (2004) 109.

[13] A. Borodzinski, A. Cybulski, The kinetic model of hydrogenation of acetylene-ethylene mixtures over palladium surface covered by carbonaceous deposits, Appl. Catal. A: Gen. 198 (2000) 51.

[14] M. J. Vincent, R. D. Gonzalez, A Langmuir-Hinshelwood model for a hydrogen transfer mechanism in the selective hydrogenation of acetylene over a Pd/gamma-Al_2O_3 catalyst prepared by the sol-gel method, Appl. Catal. A: Gen. 217 (2001) 143.

[15] R. Marshall, G. Webb, S. D. Jackson, D. Lennon, Propyne hydrogenation: characteristics of a carbon-supported palladium catalyst that exhibits a kinetic discontinuity effect, J. Mol. Catal. A: Chem. 226 (2005) 227.

[16] H. Molero, B. F. Bartlett, W. T. Tysoe, The hydrogenation of acetylene catalyzed by palladium: hydrogen pressure dependence, J. Catal. 181 (1999) 49.

[17] H. S. Fogler, Elements of Chemical Reaction Engineering, 3rd ed., Chapter 6, Prentice-Hall International, Inc., New Jersey, 1999.

[18] D. D. Do, Adsorption Analysis: Equilibria and Kinetics, Series on Chemical Engineering, Vol. 2, Chapter 5, Imperial College Press, London, UK, 1998.

[19] S. D. Jackson, G. Kelly, Hydrogenation of propyne to propene over platinum silica, J. Mol. Cat. 87 (1994) 275.

[20] G. C. Bond, J. Sheridan, Studies in heterogeneous catalysis. 1. The hydrogenation of methylacetylene, T. Faraday Soc. 48 (1952) 651.

[21] G. C. Bond, P. B. Wells, Hydrogenation of acetylene. 2. Reaction of acetylene with hydrogen catalyzed by alumina-supported palladium, J. Catal. 5 (1965) 65.

[22] Bronkhorst® High-Tech-B.V., Fluidat® on the Net, Gas Conversion Factor Calculations, http://www.fluidat.com/ (Accessed: July 2006).

Part V

7. Conclusions and future work

7.1 Conclusions

This work dealt with the study of the propylene and propyne hydrogenations in a polymeric catalytic membrane reactor (pCMR). As catalytic membrane, a poly(dimethylsiloxane) (PDMS) membrane with embedded palladium nanoclusters was used. A model of the pCMR was then developed and experimentally validated. However, to access to the parameters governing the separation and the chemical reaction kinetics, independent experiments were performed.

First, the kinetics of propylene hydrogenation was determined over palladium nanoclusters stabilized by a surfactant shell that prevents cluster agglomeration, in the absence of mass transfer resistances. Different initial total pressures and initial hydrogen/propylene molar ratios, in a batch reactor, were used at 308 K. A kinetic rate equation was obtained using the method of initial rates and it was found that experimental rate data agrees with a Langmuir-Hinshelwood (L-H) mechanism. The kinetics evidenced a competitive adsorption of hydrogen and propylene with dissociation of hydrogen on the catalyst surface and where surface reaction is the limiting step.

The determination of the kinetics for propyne hydrogenation over the same surfactant-stabilized palladium clusters, in its turn, indicated a L-H mechanism described by a non-competitive adsorption of the propyne and hydrogen for the catalyst active sites, where hydrogen addition in the surface reaction(s) is the limiting step. The results indicated, yet, that the adsorption constant of propyne is much higher than the corresponding one for hydrogen. This leads to a simplification of the kinetic rate equation, thus becoming well represented by a first order dependence on the hydrogen partial pressure and by a negative to zero order in propyne

partial pressure (power-law rate equation). The propyne negative order (zero to negative value) and the hydrogen positive order show that the former is more strongly adsorbed and then the catalyst surface coverage by this species is high, whereas hydrogen is weakly adsorbed by comparison and the catalyst surface coverage by this gas is correspondingly low.

The time-lag and sorption methods were then employed to determine the kinetic and equilibrium relevant mass transport parameters. The permeation characteristics of the composite and of the unfilled PDMS membranes towards argon, hydrogen, propane, propylene and propyne were studied, using ca. 300 μm-thick membranes, at 308 K. The sorption-diffusion model was used to fit the experimental results and the sorption, diffusion and permeability coefficients for the unfilled and palladium-filled (5 wt. %) PDMS membranes determined. From this study, it was concluded that mass transport in a PDMS composite membrane differs from that in the corresponding plain membrane mainly during the transient regime, when the concentration profile is being settling down across the membrane thickness. The presence of the palladium nanoclusters modifies the mass transport during the transient regime, not only because the nanoclusters can act as adsorption wells, but also because they lead to a tortuosity increase. At steady-state conditions, the relevant parameters are the sorption and diffusion coefficients in the polymeric matrix, the volume fraction of the catalyst and the tortuosity.

The previous mass transport and reaction kinetic experiments were used to obtain the relevant parameters necessary to model the hydrogenations in the lab pCMR. These parameters were then inserted in the developed model and simulations performed for the same operating conditions as those employed during the experimental runs. In particularly, the pCMRs were always operated at 308 K.

The model developed for the pCMR includes the mass balances to the retentate and permeate chambers as well as the mass balance to the catalytic membrane, which comprises the transport kinetics and the reaction kinetics. In the case of propylene hydrogenation, the previously determined kinetic parameters over palladium nanoclusters stabilized with the surfactant showed not to describe accurately such hydrogenation experiments in the pCMR. This should be related with a steric hindrance at the catalyst surface because the surfactant interferes strongly with the L-H adsorption constant of especially large molecules. The reaction kinetic parameter as well as the propylene L-H adsorption parameter were then fitted to experimental results using the catalytic membrane. It was, however, assumed that the hydrogen L-H adsorption parameter obtained using the surfactant-stabilized palladium still holds for the catalytic membrane. After this, it was concluded that the pCMR model proposed predicts quite well the experimental data regarding the flow rates and mixture compositions in both chambers, using transport parameters as well the hydrogen L-H adsorption constant in the kinetic equation obtained from independent experiments.

The pCMR performance was mainly studied as a function of the feed hydrogen/propylene molar ratio. It was observed that high concentrations of propane are observed in the permeate chamber when the feed hydrogen/propylene molar ratio ranged between 5 and 6. The proposed model allowed understanding this behaviour, which is mainly related to the reaction kinetics and to the diffusion selectivity.

For propyne hydrogenation, the pCMR model proposed considers a reaction rate equation composed by two terms: the propyne to propylene and the propylene to propane hydrogenations. The selectivity between these two reactions is mainly governed by the bicomponent adsorption of propyne and propylene, which was obtained by the IAST model (thermodynamic selectivity),

being the corresponding parameters obtained from independent experiments (monocomponent sorption equilibrium isotherms). The propyne hydrogenation kinetics previously determined over the surfactant-stabilized palladium nanoclusters did not represent the experimental data owing to the above-described steric hindrance effect towards the hydrocarbons of the surfactant used. This way, the power-law kinetic parameters were obtained by fitting the model to experimental reaction data using the catalytic membrane in the continuous reactors. On the other hand, the propylene rate equation and the mass transport parameters of the reaction species in the membrane were obtained from independent experiments.

The performance of the pCMR was studied experimentally as a function of the feed hydrogen/propyne molar ratio. It was observed that high propylene concentrations could be attained for high feed hydrogen/propyne molar ratios, ca. 12-15. With these conditions the formation of propylene is highly favoured and propylene hydrogenation is hindered. At higher hydrogen/propyne molar ratios, the propyne molar fraction becomes so low that propylene production starts to decrease. At that point, the deeper hydrogenation to propane starts increasing, and then propylene molar fraction in the permeate chamber also decreases. Moreover, the PDMS membrane is more selective towards propyne in terms of permeability, when compared to propylene, leading to the permeation of significant amounts of unreacted propyne to the permeate chamber. This makes the PDMS unsuitable for being used in a pCMR flow through contactor arrangement if high purity propylene is to be obtained.

The proposed pCMR model predicts quite well the experimental data regarding the flow rates and mixture compositions in permeate and retentate chambers, as well as the general performance of the membrane reactor. Though, the model showed some difficulties to predict the propylene hydrogenation at low/intermediate molar ratios of hydrogen/propyne in the feed.

The mass transport of reagents and products through the catalytic membrane depends mostly on the permeability characteristics of the polymeric phase towards these species. It is then possible to use the permeability parameters obtained from independent experiments to model a pCMR. In the same way, it is possible to use, in the developed pCMR model, the reaction kinetics parameters obtained from independent experiments, where the catalyst contacts directly the gas phase. The proposed model assumes that, if $C_i^m = K_i^{mg} p_i$, then:

$$K_i^{L-H} p_i = K_i^{L-H} \frac{C_i^m}{K_i^{mg}} = K_i'^{L-H} C_i^m \tag{7.1}$$

where K_i^{L-H} is the Langmuir-Hinshelwood constant of species *i* obtained with the reactants in gas phase contacting directly the catalyst, C_i^m is the sorbed concentration of species *i* in the membrane, p_i is the partial pressure of species *i* in the gas phase and K_i^{mg} is the partition Henry's constant between the gas and the membrane phases. Finally, $K_i'^{L-H}$ is the L-H constant of species *i* with reactants in the membrane phase, which contains the catalyst. Only the partial validation of this cascade equilibrium of reactants and products for the reaction occurring inside the membrane was observed, because of the different kinetics observed over the surfactant- and the PDMS-stabilized palladium nanoclusters.

7.2 Suggestions for future work

Polymeric catalytic membrane reactors have a lot of potentialities; the flexibility of operation and the possibility to produce a wide variety of polymeric membranes, suitable to such reactors, is a great advantage to accept the challenge that its research implies.

In the immediate future, it would be interesting to investigate further the hydrogenation kinetics studied in this work. For that, the method of initial rates could be used as it still shows to be a useful tool in kinetic modelling. But other methods allowing a deeper understanding of the rather complicated mechanisms behind alkene and alkyne hydrogenations are open.

Apart from the methodology employed to investigate the kinetics, the material supporting the catalyst seems to be very important because, depending on its nature, an influence on the kinetics may be observed. In a first and easier approach, the kinetic parameters for the hydrogenations studied could be obtained performing gas phase experiments using supported catalysts once assured that the mass transfer resistance is negligible, the support does not catalyse the reaction or elemental reaction steps and the catalyst has a similar size as compared to its size when occluded in the polymeric membrane. However, the reaction kinetic parameters should be obtained directly using the palladium stabilized in PDMS. The mass transfer resistance might be made negligible by using more diluted PDMS precursor solutions – PDMS permeability will be higher – or by producing very small composite PDMS particles, e.g. by emulsion. Stabilization techniques allowing negligible mass transport resistances, for the reaction species to reach the surface of the palladium nanoclusters stabilized with PDMS, is a topic of interesting research.

The reaction kinetics then determined would be inserted in the proposed model and compared with the pCMR results reported in this work. Besides, the kinetic parameters obtained using the PDMS polymer as stabilizing agent should be compared with the kinetic parameters obtained for other supported catalysts to analyse the influence of the PDMS polymer on the reaction kinetics. Moreover, a comparison with the kinetic parameters proposed in the present work could also be made.

In addition, it would be also of interest to extend the approach herein developed for other reaction temperatures and the model for other reactor configurations. The effect of temperature in both mass transport and reaction kinetic parameters should be first carefully analyzed, and then experiments performed in the pCMR at different temperatures.

The model developed could also be used to select the best membrane support for a targeted reaction and catalyst. Transport parameters are available for many different species and membranes making a simulation pre-screening possible for various systems. On the other hand, depending on the reaction and transport properties, the distribution of the catalyst throughout the membrane thickness could be optimized. Finally, one could perform a more elaborated optimization taking into account real requirements (in terms of conversion, selectivity, purity, etc.).